THE ROLE OF SODIUM HYDROGEN EXCHANGER ISOFORM 5 (NHE5) IN INTEGRIN β1 TRAFFICKING

by

Vinotheni Rajendran

B.Sc., The University of British Columbia, 2015

A THESIS SUBMITTED IN PARTIAL FULFILLMENT OF

THE REQUIREMENTS FOR THE DEGREE OF

MASTER OF SCIENCE

in

THE FACULTY OF GRADUATE AND POSTDOCTORAL STUDIES

(Biochemistry and Molecular Biology)

THE UNIVERSITY OF BRITISH COLUMBIA

(Vancouver)

October 2018

Committee Page

The following individuals certify that they have read, and recommend to the Faculty of Graduate and Postdoctoral Studies for acceptance, a thesis/dissertation entitled:

The Role of Sodium Hydrogen Exchanger Isoform 5 (NHE5) in Integrin β1 Trafficking

submitted by Vinotheni Rajendran in partial fulfillment of the requirements for

the degree of Master of Science

in Biochemistry and Molecular Biology

Examining Committee:

Dr. Masayuki Numata, Department of Biochemistry and Molecular Biology

Supervisor

Dr. Calvin Roskelley, Department of Cellular and Physiological Sciences, Cell and Development Biology

Supervisory Committee Member

Dr. Shoukat Dedhar, Department of Biochemistry and Molecular Biology

Supervisory Committee Member

Dr. Elizabeth Conibear, Department of Medical Genetics, Department of Biochemistry and Molecular Biology

External Examiner

Abstract

Proper targeting of the receptors to their cellular compartments is essential for their function. This is achieved by vesicular trafficking, which is a highly regulated cellular process. One of the key determinants for this process is organellar pH, which is regulated by various ion transporters. In this thesis, I showed that sodium hydrogen exchanger isoform 5 (NHE5), a neuron-enriched ion transporter that is aberrantly expressed in recycling endosomes of C6 rat glioma cells and acidifies the lumen, regulates the trafficking of integrin β1 (Intβ1), a major class of cell adhesion receptors. Depletion of NHE5 expression in C6 glioma cells resulted in impaired integrin-mediated cell adhesion and spreading. Using various biochemical and immunofluorescence assays, I found that NHE5 influences endocytic recycling and degradation of Intβ1. Interestingly, a reduction in the apparent molecular weight of Intβ1 was observed in NHE5-knockdown cells. Through various enzymatic and lectin pull-down assays, I showed that NHE5 affects the sialylation of Intβ1. Using biochemical assays, I, further demonstrated that Intβ1 is further sialylated ('extra-sialylated') during retrograde trafficking through the *trans*-Golgi Network, in addition to their canonical sialylation in the secretory pathway and this process is mediated by NHE5. Results from this thesis and previous studies led me to propose that NHE5 to be forming a distinct and previously unidentified endosomal compartment, where it sorts and recycles a subset of receptors. By doing so, NHE5 modulates cell attachment, spreading, polarity and migration. Future studies will elucidate how NHE5 modulates retrograde trafficking and sialylation of Intβ1, and influences cell migration, tumor invasion and metastasis of gliomas and other cancers. In summary, this work provides insight into the role of NHE5 in mediating important cellular processes such as cell adhesion, spreading, polarity and migration of C6 glioma.

Lay Summary

Glioma is a type of aggressive brain cancer. This study explores whether the activity of a cell protein called NHE5 within rat glioma cells may lead to further spread of the cancer. NHE5 activity has a significant effect on the fate and behaviour of cell receptors (proteins found on the cell surface). Specifically, we found that the presence of NHE5 within the cell increases the population of a particular type of cell receptor called integrin β1. Integrin β1 plays a major role in cell attachment by its ability to interact simultaneously with both inside the cell and within the extra-cellular environment. As such, its increased activity within glioma cells may lead to further invasion of the glioma. Our study provides an insight on the relationship between NHE5 and glioma cell invasion and malignancy.

Preface

The research presented in the thesis was a collaborative effort between myself, my supervisor, Dr. Masayuki Numata, and the members of Numata lab. The experiments performed in this thesis were designed through collaborative discussions between myself and my supervisor, Dr. Masayuki Numata, with valuable inputs from members of Numata lab, and my supervisory committee members, Dr. Calvin Roskelley and Dr. Shoukat Dedhar.

The oligonucleotides used in making HA-tagged human Intβ1 and some of the oligonucleotides used in making HA-tagged shRNA resistant rat NHE5 were designed by myself, whereas the rest of them are designed by my supervisor, Dr. Numata. The parental NHE5-knockdown and NHE1-knockdown glioma cells were established by Steven Fan (Numata lab) and I generated the rest of the cell lines used in this thesis. Some of the constructs used in this study, such as tetracycline-inducible GFP-tagged Vps29 mishRNA (Figure 4.4 C-D, see section 2.2.2), U6 promoter based anti-Vps29 shRNA (Figure 4.4 F, see section 2.2.3) and Flag-tagged human ST6Gal-I (Figure 4.6 C-D, see section 2.2.5) were made by Dr. Yuka Numata (Numata lab). The rest of the materials used in this study were prepared collaboratively by the members of Numata lab.

I performed all the experiments presented in this thesis, except for the images acquired using TIRF microscopy (Figure 3.1 C), which was done by Dr. Libin Abraham (Gold Lab). I performed the data analysis: densitometric analysis, colocalization analysis and the statistical analysis, with the training and technical guidance from Dr.Yuka Numata, Dr. Libin Abraham and Steven Fan, with the exception for statistical analysis done on cell spreading assay (Figure 3.1A), which was performed by Dr.Yuka Numata. Throughout this study, I received numerous mentorship, training and technical support from many colleagues, especially my supervisor, Dr. Numata, Dr. Yuka Numata, Steven Fan and Dr. Libin Abraham. The first draft of the thesis was revised by my supervisor, Dr. Numata, Dr Yuka Numata and my friends, William Tham Wai Liang and John Young. The writing of lay summary was helped by my aunt, Thora Gislason.

I finished the Biological Safety Training Course, provided by Risk Management Services (Certificate ID: 2014-jqZvx) as required for this research work.

Table of Contents

Abstract ... iii
Lay Summary ... iv
Preface ... v
Table of Contents ... vi
List of Tables ... ix
List of Figures ... x
List of Abbreviations ... xi
Acknowledgements ... xiv
Chapter 1: Introduction ... 1
1.1 The importance of vesicular trafficking ... 1
1.2 Regulators of cellular pH ... 2
1.2.1 Vacuolar type H^+-ATP hydrolases (V-ATPases) ... 2
1.2.2 Anion transporters ... 5
1.2.3 Sodium hydrogen exchangers (NHEs) ... 5
1.2.3.1 NHE classification, structure, expression, and cation selectivity ... 5
1.2.3.2 NHE5 ... 9
1.3 Integrins – cell adhesion receptors ... 11
1.3.1 Integrins structure and subunits ... 11
1.3.2 Integrins conformations and activation ... 14
1.3.3 Integrins glycosylation ... 15
1.4 Trafficking of integrins ... 18
1.4.1 Endocytosis of integrins ... 18
1.4.1.1 Clathrin-dependent endocytosis ... 19
1.4.1.2 Caveolin-mediated endocytosis ... 20
1.4.1.3 Clathrin- and caveolin- independent pathways ... 20
1.4.1.4 Macropinocytosis ... 21
1.4.2 Endocytic recycling and degradation of integrins ... 21
1.4.3 Retrograde trafficking of integrins ... 23
1.5 Thesis investigation ... 26
Chapter 2: Materials and methods ... 28
2.1 Antibodies and Reagents ... 28
2.1.1 Antibodies ... 28
2.1.2 Reagents ... 30
2.2 DNA constructs ... 30
2.2.1 N-terminus and C-terminus tagged human Intβ1 ... 30

2.2.2 Vps29 shRNA construct 31
2.2.3 Tetracycline-inducible Vps29 shRNA 31
2.2.4 Inducible HA-tagged rat NHE5 32
2.2.5 Flag-tagged human ST6Gal-I 33
2.3 Transfection 33
2.3.1 Electroporation 33
2.3.2 Lipofectamine 34
2.4 Cell Culture 34
2.4.1 C6WT, NHE5 and NHE1 knockdown cell lines 34
2.4.2 C6WT and N5KD glioma cells expressing inducible HA-tagged hITGB1 35
2.4.3 C6WT and N5KD glioma cells expressing inducible miRNA-shRNA targeting Vps29 35
2.4.4 C6WT and N5KD glioma cells that concomitantly express inducible HA-hITGB1 and constitutive shRNA targeting Vps29 35
2.4.5 N5KD glioma cells expressing inducible HA-tagged rat NHE5 36
2.4.6 C6WT and N5KD glioma cells expressing Flag-tagged human ST6Gal-I 36
2.5 Immunoblotting 36
2.6 Immunofluorescence and colocalization assays 37
2.6.1 Colocalization between N-terminally tagged and C-terminally tagged hITGB1 37
2.6.2 Colocalization between HA-hITGB1 and vinculin 37
2.6.3 Antibody-feeding assay and colocalization between EEA1 and HA-hITGB1 38
2.7 Cell spreading assay 39
2.8 Total Internal Reflection Fluorescence (TIRF) microscopy 40
2.9 Cell-surface biotinylation assay 40
2.10 Internalization assay 41
2.11 Recycling assays 42
2.11.1 Short-incubation recycling assay 42
2.11.2 Long-incubation recycling assay 43
2.12 Cell-surface biotinylation-based degradation assay 43
2.13 Enzymatic digestion assays 44
2.13.1 PNGase F digestion assay 44
2.13.2 Neuraminidase/Sialydase assay 45
2.14 Lectin pull-down assay 45
2.15 Pulse and chase assay 45

2.16 Synchronized protein trafficking assay 46
2.17 Drug treatment assays 46
2.18 Statistical analysis 47
Chapter 3: NHE5 modulates cell spreading by influencing the trafficking of Intβ1 48
3.1 Introduction 48
3.2 Spreading of C6 glioma cells is affected by NHE5 knockdown 48
3.3 Intβ1 expression at the cell surface is reduced in NHE5-knockdown cells 52
3.4 NHE5 knockdown results in accumulation of internalized receptors 52
3.5 Recycling of Intβ1 is reduced by NHE5 knockdown 60
3.6 Degradation of surface-labelled Intβ1 is increased in NHE5-depleted cells 64
Chapter 4: The role of NHE5 in the sialylation of Intβ1 66
4.1 Introduction 66
4.2 Knockdown of NHE5 affects Intβ1 sialylation 67
4.3 Exogenously expressed HA-hITGB1 in C6WT and NHE5-knockdown cells has sialylation and degradation patterns similar to the endogenous rat Intβ1 70
4.4 Characterization of Intβ1 (HA-hITGB1) sialylation by synchronized trafficking assays in the presence of Brefeldin A 74
4.5 Retrograde trafficking from early endosomes to the TGN influences the sialylation of Intβ1 76
4.6 A possible role of pH in 'extra-sialylation' of Intβ1 80
4.7 Re-expression of rat NHE5 or overexpression of human ST6Gal-I did not rescue the molecular weight of Intβ1 in NHE5-knockdown cells. 82
Chapter 5: Discussion 86
5.1 Summary 86
5.2 Intβ1 trafficking and sialylation regulate cell adhesion, spreading and migration 86
5.3 Sialylation influences Intβ1 activity 88
5.4 Involvement of NHE5 in retrograde trafficking of Intβ1 89
5.5 Endosomal pH regulates Intβ1 trafficking 91
5.6 NHE5 regulates the recycling of Intβ1 and TfR 93
5.7 Future directions 96
5.8 Conclusion/ Model 97
Bibliography 101

List of Tables

Table 1.1 Tissue expression and subcellular localization of NHE1-NHE9. Modified from (Fuster and Alexander, 2014; Orlowski and Grinstein, 2011) 6

Table 2.1 Dilutions of the primary antibodies used in immunoblotting and immunofluorescence experiments 29

Table 2.2 Dilutions of the secondary antibodies used in the immunoblotting and immunofluorescence experiments 29

Table 2.3 Fluorescent probes used in the immunofluorescence experiments 29

List of Figures

Figure 1.1 The pH of different organelles in the cell and the structure of vacuolar-type H^+-ATPase. 3

Figure 1.2 Predicted structure of mammalian sodium hydrogen exchangers. 8

Figure 1.3 A schematic representation of integrin heterodimers and their conformations. 13

Figure 1.4 A diagram depicting the formation of complex N-glycan. 17

Figure 1.5 NHE5 knockdown affects integrin-mediated cell adhesion. 27

Figure 3.1 Spreading of C6 glioma cells on Col IV is affected by NHE5 knockdown. 51

Figure 3.2 The surface population of Intβ1 is lower in NHE5-knockdown cells compared to WT cells at steady state. 53

Figure 3.3 A schematic diagram of the internalization and recycling assays. 54

Figure 3.4 The internalized population of Intβ1 is higher in NHE5-knockdown cells than in C6WT cells. 56

Figure 3.5 Human Intβ1 with HA-tag at its N-terminus is targeted to proper subcellular localization. 59

Figure 3.6 Intβ1 recycling to the cell surface is reduced by NHE5 knockdown. 63

Figure 3.7 The degradation of Intβ1 is enhanced by NHE5 knockdown. 65

Figure 4.1 Knockdown of NHE5 affects the sialylation of Intβ1. 69

Figure 4.2 Sialylation and stability of exogenously expressed HA-tagged hITGB1 in C6WT and NHE5-knockdown cells. 73

Figure 4.3 Synchronized trafficking of HA-hITGB1 in C6WT and NHE5-knockdown cells. 75

Figure 4.4 The effect of Retro-2 treatment and knockdown of Vps29 on the size of Intβ1. 79

Figure 4.5 The decrease in the size of Intβ1 results from the knockdown of NHE5 and inhibition of retrograde trafficking. 81

Figure 4.6 Re-expression of rat NHE5 or overexpression of human ST6Gal-I did not increase the molecular weight of Intβ1 in NHE5-knockdown cells. 85

Figure 5.1 A model of the role of NHE5 in the retrograde trafficking and 'extra-sialylation' of Intβ1. 100

List of Abbreviations

AICAR – 5-aminoimidazole-4-carboxamide-1-β-D-ribofuranoside
ARF – ADP-ribosylation factor
ATP – Adenosine triphosphate
Baf – Bafilomycin A1
BFA – Brefeldin A
BSA – Bovine serum albumin
$CaCl_2$ – Calcium chloride
Cav-1 – Caveolin-1
CFTR – Cytis fibrosis transmembrane conductance regulators
Chlq – Chloroquine
CIC – intracellular chloride channels
CLIC/GEEC -Clathrin-independent carriers/GPI-enriched early endosomal compartment
CLIC3 – Chloride Intracellular Channel Protein 3
CM – Complete media
c-Met – Hepatocyte growth factor/ scatter factor receptor
CO_2 – Carbon dioxide
Col IV – Collagen IV
CPA – Monovalent cation proton antiporter
DMEM – Dulbecco's Modified Eagle Medium
Doxy – Doxycycline
DTT – Dithiothreitol
ECL – Enhanced chemiluminescence
ECM – Extracellular matrix
EEA1 – Early endosome antigen 1
EGFR – Epidermal Growth Factor Receptor
EPS 15 – EGFR pathway substrate 15
ER – Endoplasmic reticulum
ERK – Extracellular signal regulated kinase
ESCRT – Endosomal sorting complex required for transport
FBS – Fetal Bovine Serum
FCHo – FCH domain only
FERM – Four point one Ezrin Radixin Moesin
FN – Fibronectin
G418 – Geneticin
Gal3 – Galectin-3
GalNAc – N-acetylgalactosamine
GalT – Galactose-1-phosphate uridylyltransferase
GFP – Green Fluorescence Protein
GGA3 – Golgi-localized gamma ear-containing ARF-binding protein 3
GlcNAc – N-acteylglucosamine
GnT – N-acetylglucosaminyltransferase
GnT-III – N-acetylglucosaminyltransferase III
GnT V – N-acetylglucosaminyltransferase V
GOLPH3 – Golgi phosphoprotein 3

GPI-AP – GPI-anchored protein
GSL – Glycosphingolipid
GT – Glycosyltransferases
HA – Human influenza hemagglutinin
hITGB1 – Human integrin β1
HRP – Horse Radish Peroxidase
HyD – Hybrid
Hrs – Hours
Intβ1 – Integrin β1
KD – Knockdown
KO – Knockout
MAL II -Maackia Amurensis Lectin II
$MgCl_2$ – Magnesium chloride
Min – Minutes
MIDAS – Metal ion-dependent adhesion sites
N5KD – NHE5 knockdown
NA – Numerical Aperture
NaCl – Sodium chloride
NEM – N-ethylmaleimide
NGF – Nerve growth factor
NHA – Sodium hydrogen antiporter
NHE – Sodium hydrogen exchanger
NHE5 – Sodium hydrogen exchanger isoform 5
NKA – Sodium Potassium ATPase
NMDA – N-methyl-D-aspartate
NP-40 – Nonidet P40
NSF – NEM-sensitive fusion factor
PBS – Phosphate buffered saline
PBS-CM – Phosphate buffered saline containing 1mM of magnesium chloride and 0.1mM of calcium chloride
PC12 – Rat adrenal pheochromocytoma cells
PCR – Polymerase chain reaction
PD – Pulldown
PEI – Polyethyleneimine
PFA – Paraformaldehyde
PI – Protease inhibitor
PI(3)-K – Phosphoinositide 3-kinase
PIP – Phosphatidylinositolphosphate
PKA – Protein kinase A
PKC – Protein kinase C
PM – Plasma membrane
PNRC – Perinuclear recycling compartment
PtdIns3P – Phosphatidylinositol-3-phosphate
PVDF – Polyvinylidene difluoride
R2 – Retro-2
RAVE – Regulator of H^+-ATPase of vacuolar and endosomal membranes

RGD – Arg-Gly-Asp tripeptide
RT – Room temperature
RTK – Receptor Tyrosine Kinases
SCAMP – Secretory carrier membrane proteins
SDS – Sodium dodecyl sulfate
SDS-PAGE – Sodium dodecyl sulfate polyacrylamide gel electrophoresis
SEM – Standard error of mean
shRNA – short hairpin RNA
SL – Surface labelled
SLC – Solute carrier
SNA – Sambucus Nigra (Elderberry) Bark Lectin
SNARE – Small N-ethylmaleimide (NEM)-sensitive fusion factor (NSF) attachment protein (SNAP) receptors
SNX – Sorting nexin
ST3Gal – β-galactoside α2,3-sialyltransferase
ST6Gal – β-galactoside α2,6-sialyltransferase
ST6GalNAc – GalNAc α2,6-sialyltransferase
ST8Sia – α2,8-sialyltransferase
TC – Tissue Culture
TfR – Transferrin receptor
TGN – *Trans*-Golgi Network
TIRF – Total internal reflection fluorescence microscopy
TL – Total lysate
TM – Transmembrane
TrkA – Tropomyosin receptor kinase A or nerve growth factor receptor
V-ATPase – Vacuolar type H^+ -ATPase
Vps – Vacuolar protein sorting-associated protein
WASH – Wiskott-Aldrich syndrome protein and SCAR homology

Acknowledgements

I would like to acknowledge that all the work I have done for this thesis took place on the unceded territory of the Musqueam people. I thank them for the space they have provided for this learning to take place.

The journey of graduate school would not have been possible without my supervisor, Dr. Masayuki Numata. I express my deepest gratitude and appreciation to Dr. Numata for believing in me and dedicating so much energy, time, and resources for me to work on this project. He gave me all the freedom and guidance to explore this project in many directions before settling on what I have presented here. His enthusiasm in science is infectious and fueled my learning and curiosity to keep exploring. I would not have been able to complete this thesis without his mentorship, technical support, and encouragement. I, also would like to thank my committee members, Dr. Calvin Roskelley and Dr. Shoukat Dedhar for their valuable input, constructive feedback and inspiration throughout my study.

I would like to thank past and present members of Numata lab for their help with my project, in preparing communal materials in the lab, and their companionship. Special thanks to Dr. Yuka Numata and Steven Fan for enormous technical help, inspirational discussions, and emotional support. They are two pillars of the lab. I am very grateful to Dr. Libin Abraham from the Gold lab for his friendship, mentorship, support, and expertise. Although he has a busy schedule, he always makes time to train and help me with taking and analyzing microscopic images (and for the pep talks too!). Many thanks to members from Cullis lab, Roberge lab, Duong lab, and Jan lab especially, Dr. Sam Chen, Aruna Balgi, and John Young for their kindness in sharing reagents, protocols and equipment, as well as training me use them.

I am eternally grateful to my family in Vancouver, United States of America and Malaysia for all their unconditional love, support and endless motivation. Without them, I would not have achieved what I have now. They are my greatest strength and helped me get through all the difficulties. Lastly, I would like to thank my friends and fellow graduate students for their generosity, continuous support, and encouragement.

I would like to acknowledge Natural Science and Engineering Research Council of Canada for providing the financial support for this project.

Chapter 1: Introduction

1.1 The importance of vesicular trafficking

Vesicular trafficking plays a major role in trafficking proteins and lipids to the right cellular compartments at the right time for proper cellular functions. For example, during cell migration, various proteins including cell surface receptors, cytoskeleton monomers, signaling molecules, and enzymes are trafficked in a spatiotemporal regulated manner to maintain the polarity and direction of the migrating cells. Given that cell migration is essential for various biological processes, ranging from embryogenesis, to wound-healing, and progression of diseases such as cancer and chronic inflammatory diseases (Lauffenburger and Horwitz, 1996; Ridley et al., 2003), any abnormality in vesicular trafficking will have serious implications on the development and/or disease progression.

One factor that regulates vesicular trafficking is organellar pH, and changes in organellar pH influence transport of proteins and affect cell physiology (Diering et al., 2011, 2013; Maeda et al., 2008; van der Poel et al., 2011). For example, alkalinization of the Golgi apparatus leads to delayed trafficking and mislocalization of glycosyltransferases, resulting in improper glycosylation of glycoproteins (Axelsson et al., 2001; Maeda et al., 2008). In other cases, alterations in endosomal pH lead to aberrant trafficking of growth factor receptors and cell adhesion receptors, thus affecting cancer cell invasion (Fan et al., 2016; Kharitidi et al., 2015; Kondapalli et al., 2015). Therefore, maintaining organellar pH in the physiological range is important for proper vesicular trafficking.

1.2 Regulators of cellular pH

Cells establish a pH gradient along the secretory as well as endocytic pathways for proper cellular physiology (Figure 1.1). The lumen of the endoplasmic reticulum (ER) has a neutral pH around 7.02 – 7.2, which is similar to the cytosolic and the nuclear pH (Casey et al., 2010; Kim et al., 1998). Along the secretory pathway, the pH drops from 6.7 in the lumen of *cis* cisternae of Golgi apparatus to 6.0 in the lumen of the *trans*-Golgi Network (TGN) (Demaurex et al., 1998; Wu et al., 2001). Secretory vesicles have a luminal pH of 5.5 (Wu et al., 2001). In the endocytic pathway, early endosomes have a pH of 6.3, and the pH becomes progressively acidic, *i.e.* 5.0-5.4 in late endosomes and goes as low as 4.6 in lysosomes (Tycko and Maxfield, 1982; Yamashiro and Maxfield, 1987). Typically, recycling endosomal pH is 6.2-6.4 (Diering et al., 2013; Yamashiro et al., 1984).

Various ion transporters and channels fine-tune the distinct pH of different subcellular compartments. Their differential subcellular localizations and regulated activities determine the balance between the influx and efflux of protons and other ions that maintain organelle pH in the cell. The following sections will discuss some of the major transporters involved in pH regulation and homeostasis.

1.2.1 Vacuolar type H^+-ATP hydrolases (V-ATPases)

V-ATPase is a multisubunit protein complex that pumps protons into either the lumen of organelles or the extracellular space against the concentration gradient of protons, using energy from ATP hydrolysis (Figure 1.1). This protein complex is composed of two domains: a peripheral V_1 domain that hydrolyzes ATP, and a transmembrane V_0 domain that facilitates translocation of protons (Forgac, 2007; Marshansky and Futai, 2008). These two domains are connected by central and peripheral stalks. The central stalk (made of subunits D and F from the V_1 domain and subunit d from the V_0 domain) acts as a rotor, where it rotates the proteolipid ring of V_0 domain upon ATP hydrolysis. The peripheral stalk (made of subunits E, G, H from the V_1 domain and N-terminal of subunit a from the V_0 domain) acts as a stator that prevents the rotation of the A_3B_3 hexamer of V_1 domain during ATP hydrolysis (Forgac, 2007).

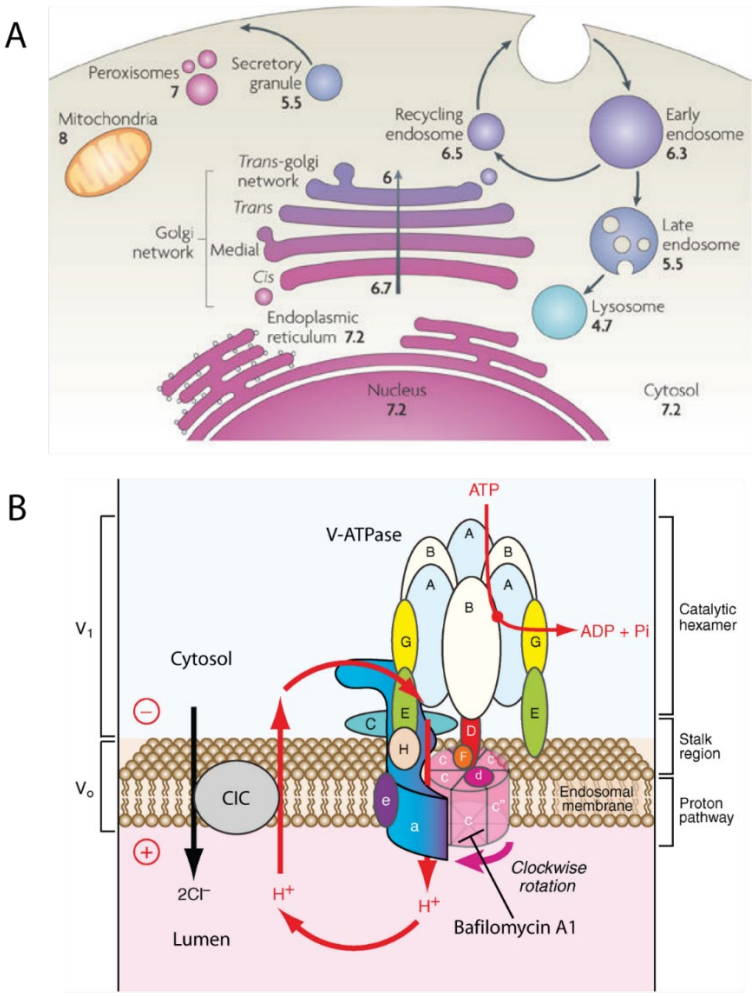

Figure 1.1 The pH of different organelles in the cell and the structure of vacuolar-type H^+-ATPase.

(A) The pH of different subcellular compartments in a mammalian cell is shown in black. The pH of mitochondria refers to the pH of their matrix and the pH of early endosomes refers to the luminal pH of sorting endosomes. Adapted from Casey et al. (2010).

(B) A schematic showing the structure of vacuolar-type H^+-ATPase (V-ATPase). The peripheral V_1 domain contains a hexamer catalytic domain (subunit A and B) for ATP hydrolysis. The transmembrane V_0 domain contains the subunit a (dark blue), subunit d (dark pink), subunit e (purple), and the proteolipid ring (light pink) and translocates protons. Upon ATP hydrolysis (red arrow), the rotator stalk rotates the subunits of the proteolipid ring in a clockwise direction (pink arrow). During rotation, protons from the cytosol translocate into the lumen of the organelle through the acidic residues and arginine residue in the transmembrane helices of proteolipid ring subunits and the subunit a, respectively. The action of V-ATPase is coupled with the action of intracellular chloride channel (CIC), which functions as a proton leak and anion transporter. The black arrow indicates the target site of V-ATPase inhibitor, bafilomycin A1. The image is adapted from Marshansky and Futai (2008).

The ATP-driven translocation of protons from the cytoplasm to the organellar lumen (or the extracellular space) is facilitated by acidic residues in the transmembrane (TM) helices of the proteolipid ring subunits, and an arginine residue in the TM7 of the subunit a of V_0 domain (Kawasaki-Nishi et al., 2001a; Nishi and Forgac, 2002). Protonation and deprotonation of these residues form a route for protons to move from the cytosol into the lumen (Forgac, 2007). In short, multiple subunits of V-ATPase work together and use the energy from ATP hydrolysis to pump hydrogen ions across the membrane.

Varying pH in different subcellular compartments is established in part by differentially regulating the density and activity of V-ATPases. The controlled and reversible assembly and disassembly of V-ATPase modulates its distribution in subcellular compartments. One of the factors that regulates this reversible association is the presence of glucose in the cell. When glucose is depleted, the complex dissociates and this dissociation is likely to be mediated by a glycolytic enzyme aldolase (Forgac, 2007; Lu et al., 2004; Sautin et al., 2005). The assembly of V-ATPases is mediated by a complex termed regulator of H^+-ATPase of vacuolar and endosomal membranes (RAVE) that is composed of three subunits (Seol et al., 2001; Smardon et al., 2002). In addition, efficiency of V-ATPase activity is regulated by modulating the ratio of H^+ transported per molecule of ATP hydrolyzed. For example, the V-ATPase found on the Golgi membrane has lower ratio of H^+ transported/ATP hydrolysis (less protons are pumped across the membrane) than the V-ATPase found on the lysosomal membrane (Forgac, 2007; Kawasaki-Nishi et al., 2001b). Overall, cells use various mechanisms to differentially control the activity of V-ATPases found in various intracellular membranes to establish a pH gradient.

Based on the number of catalytic ATP-binding sites in the V_1 domain and the number of residues that are protonated in the TM region of V_0 domain, the theoretical ratio of H^+/ATP of V-ATPase is 2-3.3 (Forgac, 2007). Given this calculated ratio and near-neutral pH of the cytoplasm, the luminal pH of organelles can theoretically be as low as 3 due to the activity of V-ATPase alone (Casey et al., 2010). However, this is not the case. Hence, there must be other ion transporters regulating the homeostasis of organelle pH (Casey et al., 2010).

1.2.2 Anion transporters

Another family of ion transporters in pH regulation is anion transporters, such as intracellular chloride channels (CIC) and cystic fibrosis transmembrane conductance regulator (CFTR) (Casey et al., 2010; Edwards and Kahl, 2010; Scott and Gruenberg, 2011). Since the activity of V-ATPase is electrogenic, a continuous influx of protons into the lumen of organelles generates an electrochemical proton gradient and a membrane potential. This could eventually limit the acidification of the lumen. To prevent this, anion transporters facilitate the influx of anions to neutralize the electrical potential and maintain the activity of V-ATPase. Studies have shown that suppressing the activity of CIC, such as CIC-3 and CIC-4 impairs endosomal acidification and trafficking of the transferrin receptors (Hara-Chikuma et al., 2005; Mohammad-Panah et al., 2003). Also, studies revealed that CIC, which was believed to be a chloride channel, is an electrogenic ion exchanger that transports 2 Cl^- anions for 1 H^+ (Picollo and Pusch, 2005; Scott and Gruenberg, 2011). This means that CIC also mediates proton leak from the lumen of the organelle to maintain the luminal pH. Another family of proteins that mediate passive efflux of protons is sodium hydrogen exchangers (NHEs) (discussed in section 1.2.3) (Casey et al., 2010).

1.2.3 Sodium hydrogen exchangers (NHEs)

1.2.3.1 NHE classification, structure, expression, and cation selectivity

Sodium hydrogen exchangers (NHEs) are a family of ion transporters that exchange monovalent cations such as Na^+ and K^+ with protons (H^+) across the cellular and organellar membrane in an electroneutral manner (Donowitz et al., 2013; Orlowski and Grinstein, 2004). They are part of the monovalent cation proton antiporter (CPA) superfamily and are encoded by Solute Carrier 9 (SLC 9) genes (Brett et al., 2005). Thirteen NHE isoforms have been identified and are classified into three subfamilies: SLC9A (NHE subfamily), SLC9B (NHA subfamily), and SLC9C (mammalian sperm-NHE like subfamily) (Donowitz et al., 2013; Fuster and Alexander, 2014). In my thesis, I will focus on the NHE subfamily consisting of NHE1- NHE9. The members of NHE family are found in fungi, plants, and animals, and they share ancestry with prokaryotic NhaP genes that exchange Na^+/Li^+ with H^+ in an electroneutral and pH-

dependent manner (Brett et al., 2005). Thus, NHEs are a family of ion transporters that are evolutionarily conserved across many species.

According to a phylogenetic analysis, mammalian NHEs are divided into two groups: plasmalemmal NHEs (NHE1-5) and intracellular NHEs (NHE6-9). The plasmalemmal NHEs are further classified into resident (NHE1, NHE2, and NHE4) and recycling (NHE3, NHE5) plasmalemmal NHEs. As the name suggests, these isoforms are localized differently in subcellular compartments (Table 1.1). The resident plasmalemmal NHEs are only expressed on the plasma membrane, while the recycling plasmalemmal NHEs are found on both the plasma membrane and in recycling endosomes. The intracellular NHEs are mostly localized to the Golgi apparatus and endosomal membrane depending on the isoform. However, they are occasionally targeted to the cell surface (Donowitz et al., 2013; Fuster and Alexander, 2014; Kagami et al., 2008). NHE1, NHE6, NHE7, NHE8 and NHE9 are ubiquitously expressed in all tissues, whereas the rest of isoforms are only expressed in certain tissues (Table 1.1, see also (Fuster and Alexander, 2014; Orlowski and Grinstein, 2011)). Therefore, multiple isoforms of NHEs are expressed and localized to various subcellular compartments in a cell.

Table 1.1 Tissue expression and subcellular localization of NHE1-NHE9. Modified from (Fuster and Alexander, 2014; Orlowski and Grinstein, 2011)

Protein/*Gene*	Tissue expression	Major subcellular localization
NHE1/ *SLC9A1*	Ubiquitous	Plasma membrane, basolateral surface of epithelia
NHE2/ *SLC9A2*	Stomach, intestinal tract, skeletal muscle, kidney, brain, uterus, testis, heart, lung	Plasma membrane, apical surface of epithelia
NHE3/ *SLC9A3*	Intestinal tract, stomach, kidney, gall bladder, epididymis	Apical plasma membrane of epithelia, recycling endosomes
NHE4/ *SLC9A4*	Stomach, kidney	Plasma membrane, basolateral membrane of epithelia
NHE5/ *SLC9A5*	Brain (neurons), testis, spleen, skeletal muscle	Plasma membrane, recycling endosomes
NHE6/ *SLC9A6*	Ubiquitous	Early/recycling endosomes
NHE7/ *SLC9A7*	Ubiquitous	*trans*- Golgi Network, Golgi cisternae, secretory vesicles
NHE8/ *SLC9A8*	Ubiquitous	mid and trans-Golgi cisternae, late endosomes
NHE9/ *SLC9A9*	Ubiquitous	Recycling endosomes

All NHEs have a conserved N-terminus domain consisting of 12 hydrophobic transmembrane spanning alpha-helices, and a variable cytoplasmic tail at the C-terminus (Figure 1.2). The electroneutral proton/cation exchange occurs at the N-terminus domain, whereas the cytoplasmic tail serves as a platform for various regulatory proteins to bind and modulate the activity of the ion transporter (Donowitz et al., 2013; Orlowski and Grinstein, 2011; Wakabayashi et al., 1997). The amino acid sequence and length of the cytoplasmic tail vary among different isoforms (Brett et al., 2005). The crystal structures of NHEs have not been determined, however, the structure of the transport domain of NHEs was predicted using homology modelling based on the crystal structure of E.*coli* Na^+/H^+ antiporter (NhaA) (Donowitz et al., 2013). Assembly of TM4 and TM11 helices in an anti-parallel orientation forms a pocket of acidic residues in an inverted funnel topology, where Na^+/H^+ binding and ion translocation occurs. This assembly is stabilized by the charged ions of the surrounding TM helices (Hunte et al., 2005; Padan et al., 2009). Furthermore, there is a pH sensor domain in TM9, which is separate from the translocation site (Padan et al., 2009). Changes in pH can induce a long-range conformational changes in the assembly of TM helices, which then allow the ions to access and bind to the translocation site (Donowitz et al., 2013; Hunte et al., 2005; Padan et al., 2009). In addition, these ion transporters form homodimers for stability and for ion transport activities (Hisamitsu et al., 2006; Padan et al., 2009).

NHEs can exchange monovalent cations such as Na^+ and K^+ in exchange for H^+, but the cation specificity varies among different isoforms. In general, the plasmalemmal NHEs selectively transport Na^+ in exchange for H^+, thereby extruding cytosolic protons to either the extracellular space or into the lumen of the organelles (Orlowski and Grinstein, 2011). As a result, the plasmalemmal NHEs alkalinize the cytosol and acidify the organelle lumen. On the other hand, the intracellular NHEs have a higher affinity to K^+ than to Na^+, thus K^+/H^+ exchange is the preferred mode of action. As a result, the intracellular NHEs promote proton leak from the organelles and alkalinize the luminal pH (Orlowski and Grinstein, 2011).

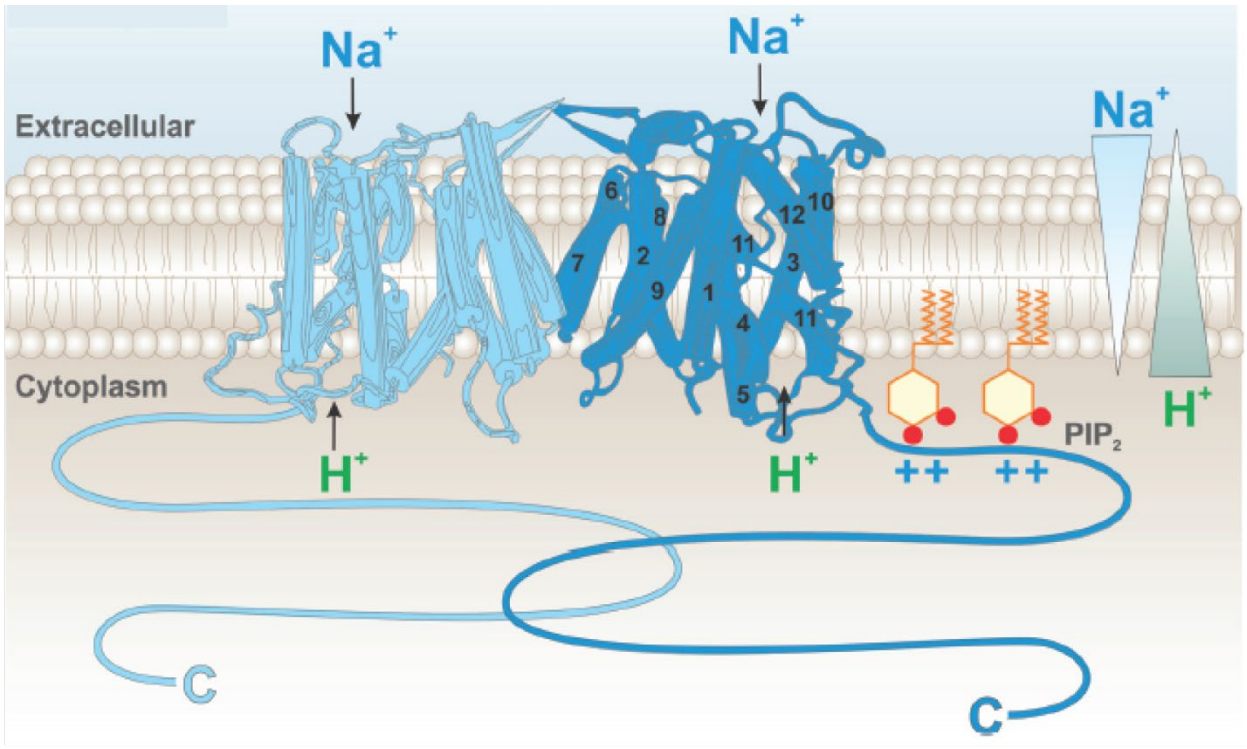

Figure 1.2 Predicted structure of mammalian sodium hydrogen exchangers.

Sodium hydrogen exchangers (NHEs) are predicted to have 12 hydrophobic transmembrane helices at the N-terminus domain and a hydrophilic cytoplasmic tail. The binding sites for Na^+ and H^+ (indicated by the arrows) are predicted based on the crystal structure of bacterial Na^+/H^+ antiporter (NHA). NHEs exist as homodimers on the membrane. The figure is adapted from Orlowski and Grinstein (2011).

1.2.3.2 NHE5

NHE5 was first discovered as an amiloride-insensitive NHE in cultured hippocampal neurons (Klanke et al., 1995; Raley-Susman et al., 1991). The protein expression of NHE5 is enriched in the brain, specifically in neurons (Diering et al., 2011). A northern blot analysis of NHE5 mRNA shows that NHE5 is significantly expressed in neuron-rich brain regions such as the hippocampus, amygdala, caudate nucleus, hypothalamus, subthalamic nucleus, and the thalamus, but not in corpus callosum, which is primarily composed of axons and glial cells (Attaphitaya et al., 1999; Baird et al., 1999). Despite being characterized as neuron-enriched NHE, NHE5 expression was recently found upregulated in C6 glioma cells, but not in rat hippocampal astrocytes (Fan et al., 2016).

Among other isoforms of NHE, NHE5 is most closely related to NHE3. They have about 50% similarity between their amino acid sequences, similar subcellular localizations and regulatory mechanisms (Attaphitaya et al., 2001; Orlowski and Grinstein, 2004; Szászi et al., 2002). In earlier days, heterologous expression of HA-tagged NHE5 was used to characterize the subcellular localization of NHE5. When HA-tagged NHE5 was expressed in non-neuronal cells such as NHE-deficient AP-1 cells and primary culture of hippocampal neurons, NHE5 localized to the cell surfaces as well as intracellular vesicles that were positive for internalized transferrin (Szászi et al., 2002). With the development of NHE5-specific antibodies, subcellular localization of endogenous NHE5 in hippocampal neurons was determined. NHE5 was predominantly found in the intracellular vesicles, but was recruited to the plasma membrane upon external stimulations including glycine-induced N-methyl-D-aspartate (NMDA) receptor activation, the AMP mimetic AICAR, and antimycin-A (Diering et al., 2011; Jinadasa et al., 2014). Like NHE3, NHE5 also shuttles between recycling endosomes and the plasma membrane (D'Souza et al., 1998). Furthermore, Attaphitaya and colleagues found that hyperosmolarity, activation of protein kinase C (PKC), and activation of protein kinase A (PKA) affect the activity of NHE5 to the same extent as NHE3 (Attaphitaya et al., 2001). Although NHE5 and NHE3 are expressed in different tissues, they are considered to have similar cellular trafficking and activities.

Proper targeting of NHE5 to its appropriate cellular localization (the plasma membrane or recycling endosomes) is important for its activity and cellular pH homeostasis (Diering et al.,

2009; Jinadasa et al., 2014; Szabó et al., 2005). Endocytosis of NHE5 from the plasma membrane is mediated by clathrin and β-arrestins (Szabó et al., 2005; Szászi et al., 2002). It was shown that β-arrestin2 binds to an acidic serine/threonine-rich and di-isoleucine motif-containing region in the cytoplasmic tail of NHE5, which is phosphorylated by protein kinase CK2, to internalize the ion-transporter. Upon internalization, the activity of NHE5 at the cell surface was downregulated. Deletion or mutation in the acidic sequence and/or di-isoleucine motif in the cytoplasmic tail inhibited the endocytosis of NHE5 and the downregulation of its activity (Szabó et al., 2005). In addition, recycling of NHE5 from endosomes to the plasma membrane is also important for its activity at the plasma membrane. This step is mediated by secretory carrier membrane protein 2 (SCAMP2) and is dependent on the phosphoinositide 3-kinase (PI3K) activity (Liu et al., 2005; Szászi et al., 2002). SCAMP2 was shown to bind to the cytoplasmic tail of NHE5 and target it to the plasma membrane via the ADP-ribosylation factor 6 (Arf6)-dependent pathway. Overexpression of SCAMP2 increased the cell surface expression of NHE5 and its activity at the cell surface. The SCAMP2-mediated NHE5 activity on the plasma membrane was hampered by the expression of dominant negative Arf6, but not dominant negative Rab11 (Diering et al., 2009). Similarly, when the recycling of NHE5 was inhibited by wortmannin, a PI3K inhibitor, the activity of NHE5 at the plasma membrane of AP-1 cells was reduced (Szászi et al., 2002). These observations collectively indicate that trafficking of NHE5 to and from the cell surface is important since it can influence the activity of the ion transporter at the cell surface.

The role of NHE5 in cellular pH homeostasis is greatly influenced by the selectivity for exchanging Na^+ for H^+ and its intracellular localization. Thus, NHE5 activation leads to either alkalinization of the cytoplasm, or acidification of the lumen of recycling endosomes. NHE5 was shown to negatively regulate the growth of dendritic spines in hippocampal neurons by acidifying the synaptic cleft (Diering et al., 2011). In another study, NHE5 modulated neurite outgrowth in neuroendocrine PC12 cells upon nerve growth factor (NGF) stimulation by acidifying the luminal pH of the recycling endosomes, which promoted the recycling of NGF receptor, TrkA (Diering et al., 2013). These results suggest that NHE5 is involved in neural development and plasticity by regulating the pH in the neurons. NHE5 also rescued neurons

from acidosis during metabolic stress (Jinadasa et al., 2014). Therefore, NHE5 plays a critical role in nervous tissue by maintaining the cellular pH in the normal physiological range.

1.3 Integrins – cell adhesion receptors

Anchorage of cells to the surrounding extracellular matrix (ECM) is important for cell proliferation and migration (Giancotti and Ruoslahti, 1999; Lauffenburger and Horwitz, 1996). Cell adhesion is mediated by a major class of cell adhesion receptors termed integrins. Integrins mediate cell-ECM interactions and cell-cell interactions under certain circumstances (Hynes, 1987, 1992). By linking the ECM and cytoskeleton inside the cell, integrins influence cell shape, spreading, and motility (Gumbiner, 1996; Lauffenburger and Horwitz, 1996). The force generated through the interaction between the ECM and the actin cytoskeleton is transduced for various gene expressions that are required for proper developmental processes including embryogenesis and organogenesis (Mammoto et al., 2012) Also, binding of integrins to their ligands activates multiple signaling pathways including ERK and Akt pathways that promote cell growth (Giancotti and Ruoslahti, 1999; Lee et al., 2010a). In summary, integrin plays crucial role in many cellular processes.

1.3.1 Integrins structure and subunits

Integrins are transmembrane glycoproteins with a large extracellular domain, a single transmembrane domain (TMD) and a short cytoplasmic tail (Hynes, 1987). They exist as heterodimers at the cell surface, consisting of an α and a β subunits (Hynes, 1987). The heterodimerization of α and β subunits of integrins occurs at the ER (Paul et al., 2015). They are held together by non-covalent interactions that occur between their extracellular domains, and a salt bridge that is formed between their cytoplasmic tails (Hynes, 2002). To date, 8 β subunits and 18 α subunits, forming 24 distinct integrin heterodimers have been identified (Figure 1.3) (Hynes, 2002).

A.

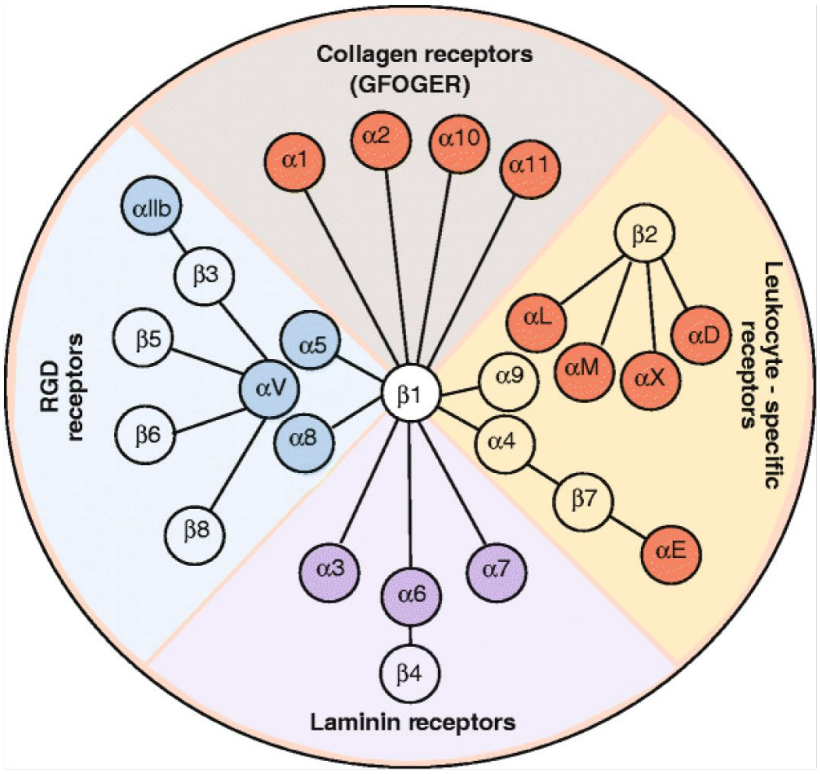
Collagen receptors
(GFOGER)
α1
α2
α10
α11
αIIb
β3
β5
α5
αV
β6
α8
β8
RGD
receptors
β1
α9
α4
β7
αE
β2
αL
αM
αX
αD
Leukocyte - specific
receptors
α3
α6
α7
β4
Laminin receptors

B.

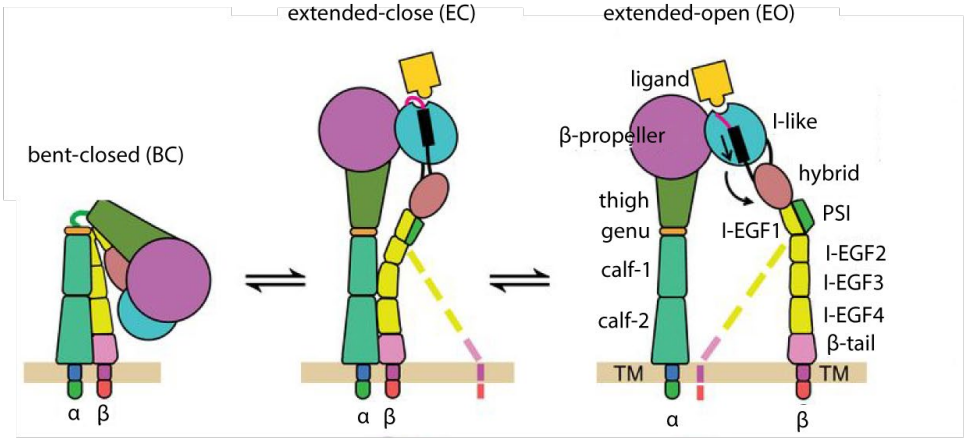
extended-close (EC)
extended-open (EO)
bent-closed (BC)
ligand
β-propeller
I-like
hybrid
PSI
I-EGF1
I-EGF2
I-EGF3
I-EGF4
β-tail
thigh
genu
calf-1
calf-2
TM
TM
α
β
α
β
α
β

Figure 1.3 A schematic representation of integrin heterodimers and their conformations.
(A) Integrin heterodimers and their ligands. The non-covalent association between 8β and 18α subunits forms 24 distinct heterodimers that bind to different ligands. Their ligands and the identified binding motif in the ligand are indicated. The α subunits in red have additional I-domain that contains metal-ion dependent adhesion site (MIDAS). This image is adapted from (Barczyk et al., 2010).
(B) A representation of different conformations of αβ subunits and their extracellular domain. Integrin heterodimer adopts three different conformations: Bent and closed (BC), which is inactive and has low affinity for ligand; Extended and closed (EC), which has intermediate affinity for ligand and called as primed conformation; and Extended and open (EO), which is active and has high affinity for ligand. Binding to ligands is mediated by the β-propeller and the I-like domains of α and β subunits, respectively. The image is adapted from (Li et al., 2017).

Different integrin heterodimers bind to different substrates (Figure 1.3) through β-propeller and I-like domains of α and β subunits, respectively. For example, the arginine residue from the tripeptide Arg-Gly-Asp (RGD) binds to the β-propeller of αV subunit, and the aspartate residue binds to the groove of the I-like domain of β3 subunit (Xiong et al., 2002). Integrins recognize short peptide motifs present in their ligands such as GFOGER (O=hydroxyproline) in collagen and RGD in fibronectin (Barczyk et al., 2010; Emsley et al., 2000). The acidic residues in these motifs are critical for ligand recognition and binding of integrin. This is because acidic residue forms a coordination sphere with divalent cations in the metal-ion dependent adhesion site (MIDAS) that is found in the I-like domain of β subunits and/or in the I-domain of some α subunits. The binding of the acidic residue to MIDAS leads to structural changes in integrin heterodimer, resulting in activation of the receptor (Emsley et al., 2000; Hynes, 2002; Lee et al., 1995; Taniguchi et al., 2017).

1.3.2 Integrins conformations and activation

Integrin heterodimers adopt three different conformations: bent (inactive, low affinity for ligands), extended (intermediate affinity for ligands), and open (active and high affinity for ligands) (Figure 1.3) (Hynes, 2002). Activation of integrin occurs via two mechanisms, namely ‘inside-out’ and ‘outside-in’.

Binding of cytoplasmic proteins such as talin to the cytoplasmic tail of integrin β subunits leads to structural changes in integrin heterodimer and its subsequent activation (Ginsberg, 2014). This is termed ‘inside-out’ activation. Talin, a known activator of integrin, binds to the cytoplasmic tail of integrin β subunits via its head domain (Calderwood et al., 1999). The head domain of talin has four point one, ezrin, radixin, moesin (FERM) domain, consisting of F1, F2 and F3 subdomains. The F2 and F3 subdomains are responsible for the binding to integrin’s cytoplasmic tail (Anthis et al., 2009; Calderwood et al., 2002). The F3 subdomain of talin has a phosphotyrosine binding (PTB) domain that binds to β turns of NPxY motifs on the cytoplasmic tail of integrin β subunits (Calderwood et al., 2002). The F2 subdomain interacts and binds to the negatively charged phospholipids in the plasma membrane via its positively charged residues (Anthis et al., 2009). Binding of talin to the cytoplasmic tail of β subunit disrupts the salt bridge between the heterodimer and tilts the transmembrane domain of β subunit away from the

transmembrane domain α subunit (Anthis et al., 2009). The separation of cytoplasmic domains between α and β subunits activates integrin (Anthis et al., 2009; Ginsberg, 2014).

Binding of ligands to the extracellular domain of integrin also leads to conformational changes and activation of integrin (Takagi et al., 2002). This is known as 'outside-in' activation. Ligand binding or Mn^{2+} activation induces conformational changes in integrin such that the receptor adopts an extended conformation from its initial bent conformation (Takagi et al., 2002). A crystal structure study revealed that upon ligand binding to the I-like domain of β subunit, the C-terminal helix of I-like domain moves downward (Lee et al., 1995), resulting in structural changes that swing the hybrid-domain of the β subunit open and away from the thigh-domain of α subunit. This breaks the interaction between the headpiece of α subunit and the tailpiece of β subunit, leading to a separation between the legs of α and β subunits and thus, activating the integrin (Takagi et al., 2002). The study also showed that integrin is mostly in the bent conformation in the presence of Ca^{2+} or Mg^{2+} alone (Takagi et al., 2002). This indicates that it is likely that integrin is in inactive conformation on the cell surface at steady state and adopts the extended and open confirmation upon activation from 'outside-in' or 'inside-out' signaling or both.

1.3.3 Integrins glycosylation

One of the major post-translation modifications on integrin is glycosylation and integrin has about 26 potential glycosylation sites (both α and β subunits combined) (Janik et al., 2010). Glycosylation of integrin is essential for the heterodimerization of α and β subunits, cell surface targeting, binding to fibronectin, and cell spreading (Isaji et al., 2006, 2009; Zheng et al., 1994). Complete de-glycosylation of α5β1 causes dissociation of the heterodimer and decreased binding to fibronectin (Zheng et al., 1994). Among the 14 and 12 glycosylation sites on α5 and β1 subunits, respectively, three glycosylation sites (S3-5) on the β-propeller domain of α5 and three glycosylation sites (S4-6) on the I-like domain of β1 integrin were shown necessary for α5β1 heterodimerization, surface targeting, and ligand binding (Isaji et al., 2006, 2009).

Glycosylation of integrin is a multi-step process and it begins simultaneously with its polypeptide synthesis in the ER. As polypeptides of integrin subunits enter the ER, a pre-assembled oligosaccharide is transferred from its lipid carrier termed dolichylpyrophosphate to the asparagine residue of the polypeptide with the following consensus sequence: N-X-S/T,

where X can be any amino acid (Aebi, 2013; Janik et al., 2010). A covalent glycosidic bond between the amide group of the side chain of the asparagine residue and N-acetylglucosamine (GlcNAc) of the oligosaccharide is formed. The oligosaccharide is termed N-glycan (Aebi, 2013; Janik et al., 2010). It is further modified by various glycosidases in the ER and the *cis*-Golgi cisternae to hydrolyze glucose and selected mannose, forming a core N-glycan with trimannosyl at the end (Figure 1.4) (Bellis, 2004). As the glycoprotein travels through the Golgi apparatus during biosynthesis, various glycosyltransferases and glycosidases work together to further modify the N-glycan on integrin. (Bellis, 2004).

One of the modifications to the core glycan is the addition of GlcNAc onto mannose by N-acetylglucosaminyltransferases (GnTs). There are two key GnTs that compete for the same substrate but form two different products with contradicting effects on cancer progression. The first one is GnT-III that adds GlcNAc onto mannose to form bisecting GlcNAc linkages, and the second one is GnT-V that forms β1,6-GlcNAc branching linkages (Marsico et al., 2018). The bisecting GlcNAc has tumor suppressing properties, while an elevation in the β1,6-GlcNAc branching on glycoprotein has been correlated with tumor metastasis (Guo et al., 2002; Marsico et al., 2018; Yoshimura et al., 1995). Furthermore, overexpression of GnT-III was shown to decrease the β1,6-GlcNAc branching linkages on α3β1 and resulted in reduced cell migration on laminin (Zhao et al., 2006). The mechanism by which the β1,6-GlcNAc branching linkages contribute to tumor progression is still unknown.

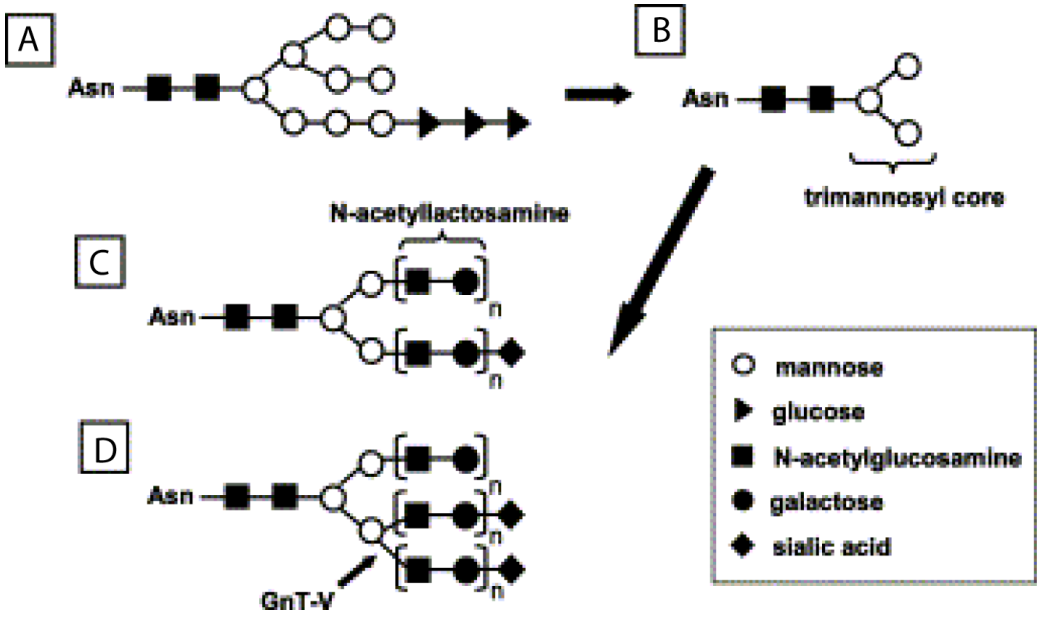

Figure 1.4 A diagram depicting the formation of complex N-glycan.
(A) A representation of the pre-assembled oligosaccharide that is added to the asparagine (Asn) residue of a polypeptide in the endoplasmic reticulum (ER).
(B) The N-glycan is trimmed by various glycosidases in the ER and the *cis*-Golgi cisternae, forming the trimmanosyl core on N-glycan.
(C) The core oligosaccharide is further modified by various glycosyltransferases and glycosidases in the *medial/trans*-Golgi and the *trans*-Golgi Network. One of them is the addition of N-acetylglucosamine onto mannose, followed by addition of galactose. This terminal galactose is recognized by sialyltransferase, ST6Gal-I, and capped with sialic acid.
(D) The action of N-acetylglucosaminyltransferase V (GnT-V) forms β1,6-GlcNAc branching linkages on mannose, which can be further modified by galactose-1-phosphate uridylyltransferase (GalT) and sialyltransferase with galactose and sialic acid, respectively.
This figure is adapted from (Bellis, 2004).

Unlike bisecting GlcNAc, the branching β1,6-GlcNAc linkages can be further processed to form N-acetyllactosamine (Figure 1.4). This is catalyzed by galactose-1-phosphate uridylyltransferase (GalT), which adds galactose to the GlcNAc. The galactose on the N-acetyllactosamine can be capped with sialic acids by sialyltransferases, which is the terminal process of glycosylation (Bellis, 2004). There are at least 20 sialyltransferases classified into four families based on the linkages they form: β-galactoside α2,3-sialyltransferase (ST3Gal), β-galactoside α2,6-sialyltransferase (ST6Gal), GalNAc α2,6-sialyltransferase (ST6GalNAc), and α2,8-sialyltransferase (ST8Sia) (Takashima and Tsuji, 2011). ST3Gal and ST6Gal adds sialic acids onto the 3rd or 6th carbon of the galactose, respectively, forming α2-3 and α2-6 sialylation (Bellis, 2004; Takashima and Tsuji, 2011). Since integrins are α2-6 sialylated, their sialylation are catalyzed by ST6Gal-I (Bellis, 2004; Seales et al., 2005a; Yu et al., 2013). Hypersialylation of integrins has been implicated in cancer progression. Elevated activity of ST6Gal-I and hypersialylated integrin subunits have been observed in various tumors and cancer cell lines (Christie et al., 2008; Isaji et al., 2014; Marsico et al., 2018; Pocheć et al., 2015; Seales et al., 2005a; Wang et al., 2003). Hypersialylation of integrins is also shown to influence adhesion and migration of cancer cells (Isaji et al., 2014; Pocheć et al., 2015; Seales et al., 2005a; Yu et al., 2013).

1.4 Trafficking of integrins

Trafficking of integrin, a key component of cell adhesion and migration, is highly regulated, and any perturbation leads to impaired cell spreading and migration (Ratcliffe et al., 2016; Riggs et al., 2012; Roberts et al., 2001; Shafaq-Zadah et al., 2016). The following section describes steps of integrin trafficking.

1.4.1 Endocytosis of integrins

Both ligand-bound (active) and ligand-unbound (inactive) integrins are endocytosed (Arjonen et al., 2012; Shi and Sottile, 2008). Besides attenuating integrin-mediated signaling, endocytosis of integrins is postulated to increase the pool of intracellular integrin that is used for the formation of new focal adhesions (Paul et al., 2015). Integrins are internalized through four routes; clathrin-dependent, caveolin-dependent, macropinocytosis, and clathrin- and caveolin-independent pathways.

1.4.1.1 Clathrin-dependent endocytosis

Clathrin, a vesicle coat protein, is composed of three heavy and three light chains forming a triskelion, which polymerizes into cages and flat lattices. Nucleation, where the membrane curves and invaginates to form a pit, is the first step in clathrin-mediated endocytosis. This process is initiated by recruiting clathrin adaptor proteins, such as AP-2 or F-BAR domain containing proteins, such as FCH domain only (FCHo) proteins, intersectins and EGFR pathway substrate 15 (EPS15). Binding of these proteins induces membrane curvature and budding. The second step is selection and recruitment of cargoes into the pit. This step involves the recruitment of AP-2 by either directly binding to the cytoplasmic tails of the cargoes, or indirectly through cargo-specific adaptors that link the cargoes to AP-2 and clathrin. Some of these cargo-specific adaptors are Numb that connects Notch to AP-2; Dab2 that recruits LDL receptors; and β-arrestins that mediates recruitment of G protein-coupled receptors (GPCRs) to AP-2. Cargo-containing vesicles mature as accessory proteins and clathrin are recruited to the pits, leading to coat assembly on the vesicle. As clathrin polymerizes, it stabilizes the membrane curvature, which is reinforced by recruiting proteins with BAR domains. Finally, a GTPase dynamin is recruited and mediates membrane scission upon GTP hydrolysis. The clathrin-coated vesicle buds off from the plasma membrane. Upon budding, the vesicle uncoats the clathrin cage through the activity of ATPase heat shock cognate 70 (HSC70) and its cofactor, auxilin or cyclin G-associate kinase (GAK) (McMahon and Boucrot, 2011).

Integrins are recruited into clathrin-coated vesicles through cargo-specific adaptor proteins such as Dab2 and Numb. Dab2 and Numb proteins contain PTB-domains (similar to talin) that bind to the β-turns (NPxY motifs) in the cytoplasmic tail of integrin β subunits (Calderwood et al., 2003). During microtubule-induced focal adhesion disassembly, focal adhesion kinase (FAK) was shown to recruit Dab2, clathrin, and dynamin to the focal adhesions, and mediate the disassembly of focal-adhesions through clathrin-mediated endocytosis of integrin β1 (Intβ1) (Ezratty et al., 2005, 2009). Disruption of clathrin-mediated endocytosis by either genetic perturbation or overexpressing dominant negative dynamin mutants affected the endocytosis of integrin and subsequently impaired cell migration (Arjonen et al., 2012; Ezratty et al., 2009).

1.4.1.2 Caveolin-mediated endocytosis

Caveolae are specialized, detergent-resistant microdomains in the plasma membrane that are enriched in lipids such as cholesterol and sphingolipids, and characterized by the presence of caveolin (Cav-1) (Mayor and Pagano, 2007). Caveolar invagination towards the cytoplasm is induced by the clustering of cargoes to caveolae and their interaction with Cav-1 (Shi and Sottile, 2008; Tagawa et al., 2005; Upla et al., 2004; Wei et al., 1999). Finally, membrane scission is facilitated by dynamin, and the Cav-1-containing vesicles bud off with their cargoes (Mayor and Pagano, 2007). Unlike clathrin, Cav-1 may not disassemble from the vesicles (Tagawa et al., 2005).

Several studies have demonstrated that integrin heterodimers clustered in caveolae and internalized through the Cav-1-dependent pathway (Fabbri et al., 2005; del Pozo et al., 2005; Shi and Sottile, 2008; Upla et al., 2004). In one study, upon chemoattractant activation, leukocyte integrin, αLβ2 accumulated in cholesterol-enriched and detergent-resistant membrane domain at the plasma membrane. The ligand-unbound heterodimers were then rapidly internalized to Rab11 positive compartments using a clathrin-independent mechanism and recycled in a polarized manner (Fabbri et al., 2005). In another study, clustered α2β1 moved laterally to caveolae with the aid of cortical actin microfilaments and got internalized in Cav-1 containing vesicles. This internalization was dependent on the activity of Protein Kinase-C (Upla et al., 2004). Furthermore, depletion of Cav-1 impaired the internalization of α5β1 and affected the endocytosis of fibronectin (Shi and Sottile, 2008).

1.4.1.3 Clathrin- and caveolin- independent pathways

Selected cargoes including integrins are sorted into clathrin-independent carriers (CLICs), a form of clathrin- and caveolin-independent endocytosis. Studies with GPI-anchored proteins (GPI-AP) have shown that GPI-APs are endocytosed through CLICs, a tubular or ring-like structures devoid of clathrin and caveolin (Kirkham et al., 2005). After pinching off from the plasma membrane using a dynamin-independent mechanism, CLICs mature into distinct endosomal compartment termed GPI-AP enriched early endosomal compartments (GEECs). GEECs are not positive for Rab5, Rab4, or Rab7 (Sabharanjak et al., 2002). GEECs are then

targeted to the transferrin receptors-positive recycling endosomes. The formation of CLICs is dependent on CDC42 activity, actin, and cholesterol (Chadda et al., 2007; Kirkham et al., 2005).

In a study, CLIC cargoes were identified and among them were various focal adhesion components including Intβ1, Thy-1, (a GPI-AP that regulates FAK signaling), and CD44 (a hyaluronan receptor) (Howes et al., 2010). Intβ1 was shown to be endocytosed through interaction with galectin-3 (Gal3), a protein that recognizes and binds to carbohydrates (β-galactoside) on glycoproteins (Furtak et al., 2001). Recently, Gal3 was demonstrated to form CLICs in a glycosphingolipid (GSL)-dependent manner and internalize cargoes such as Intβ1 and CD44. Upon binding of Gal3 to the glycoproteins, GSL clustering and oligomerization of Gal3 occurred. This phenomenon later induced membrane bending and formation of CLICs (Lakshminarayan et al., 2014). Moreover, CLIC-mediated endocytosis was shown to occur at the leading edge of migrating cells and found to be required for cell migration during wound-healing process (Howes et al., 2010).

1.4.1.4 Macropinocytosis

Macropinocytosis is a process that uptakes membrane, fluid, and cell surface receptors in bulk through actin polymerization. It is another endocytosis pathway that is independent of clathrin and caveolin. A study showed that a bulk of integrin β3 at the dorsal cell surface to be endocytosed by macropinocytosis upon platelet-derived growth factor (PDGF) stimulation and rapidly recycled to the ventral cell surface through the Rab11 pathway. Actin-dependent circular dorsal ruffle (CDR) was formed during the macropinocytosis and upon internalization, CDR went through early endosomes that were positive for EEA1, Rab4 and Rab5. Within 60 minutes of stimulation, a bulk of integrin β3 were internalized and recycled to the cell surface in a polarized manner to the leading edge (Gu et al., 2011).

1.4.2 Endocytic recycling and degradation of integrins

Recycling of integrin is crucial for cellular processes such as cell adhesion and migration, and accelerated recycling of this receptor is often implicated in cancer progression and invasion (Caswell et al., 2007; Fang et al., 2010; Nguyen et al., 2017; Powelka et al., 2004; Ratcliffe et al., 2016; Roberts et al., 2001, 2004). Approximately 50% of the internalized integrins are recycled within minutes, but the exact kinetics of recycling are dependent on many factors such as the

heterodimer subunits, conformation of integrin (*i.e.* active or inactive), cell-type, and presence of ligand and serum (Arjonen et al., 2012; De Franceschi et al., 2015; Kharitidi et al., 2015; Lobert et al., 2010; Powelka et al., 2004; Roberts et al., 2001).

Endocytosed integrins fuse with either early endosomes or the perinuclear recycling compartment (PNRC) to be recycled back to the plasma membrane via short- or long-loop recycling pathways (Arjonen et al., 2012; Fabbri et al., 2005; Fang et al., 2010; Gu et al., 2011; Sabharanjak et al., 2002). The short-loop or rapid recycling of integrin is mediated by Rab4 recycling endosomes, where the heterodimer is recycled from sorting endosomes to the plasma membrane without passing through the PNRC. The half-life of integrin recycling through this pathway is predicted to be approximately three minutes (Caswell and Norman, 2006; Roberts et al., 2001). It was initially thought that the short-loop pathway was exclusively for αVβ3, not for α5β1. This is because αVβ3, not α5β1, in fibroblasts went through rapid recycling upon PDGF stimulation, and this recycling of αVβ3 was compromised by the expression of dominant negative Rab4 (Roberts et al., 2001). However, recent studies showed that Intβ1 also can undergo rapid recycling via Rab4 pathway (Arjonen et al., 2012; Fang et al., 2010; Ratcliffe et al., 2016). In the long-loop recycling assay, integrin goes from early endosomes to the PNRC before being recycled to the plasma membrane via Rab11-positive recycling endosomes (Arjonen et al., 2012; Powelka et al., 2004; Roberts et al., 2001). The half-life of integrin recycling through this pathway is approximately 10 minutes (Caswell and Norman, 2006).

Another small GTPase that is involved in integrin recycling is ADP-ribosylation factor 6 (Arf6), which localizes to the plasma membrane and tubovesicular structures at the juxtanuclear region (Arjonen et al., 2012; Powelka et al., 2004; Radhakrishna and Donaldson, 1997; Ratcliffe et al., 2016). Arf6 regulates both short- and long-loop recycling of integrin and targets integrin to the protrusions at the plasma membrane in an F-actin dependent manner (Arjonen et al., 2012; Powelka et al., 2004; Ratcliffe et al., 2016). In the short-loop recycling, Arf6 was shown to interact with one of its effectors, Golgi-localized gamma ear-containing Arf-binding protein 3 (GGA3) to recruit Intβ1 to Rab4-positive recycling endosomes (Ratcliffe et al., 2016). In another study, Arf6 was shown to bind preferentially to inactive Intβ1, which had been shown to undergo fast recycling, and target it to the protrusions at the plasma membrane (Arjonen et al., 2012). In the long-loop recycling, Arf6 was shown to recruit Intβ1 from Rab11-positive PNRC

to the protrusions at the plasma membrane upon acute EGF stimulation (Powelka et al., 2004). Therefore, the activity of Arf6 on Intβ1 trafficking via short- and long-loop recycling pathways may be spatially restricted to specific domains on the plasma membrane.

Besides these canonical short- and long loop recycling pathways, integrin is shown to be recycled from early and late endosomes through sorting nexins (SNXs) and Rab25, respectively (Böttcher et al., 2012; Caswell et al., 2007; Dozynkiewicz et al., 2012; Steinberg et al., 2012; Tseng et al., 2014). SNX17 and SNX31 were shown to bind to the membrane-distal NPxY motif in the cytoplasmic tail of Intβ1 through their FERM domains to divert the receptor from lysosomal degradation and recycle Intβ1 back to the cell surface (Böttcher et al., 2012; Steinberg et al., 2012; Tseng et al., 2014). Recently, the molecular mechanisms behind SNX17-dependent recycling of Intβ1 was elucidated. SNX17 associates with a newly discovered complex termed retriever to recycle Intβ1 to the plasma membrane (McNally et al., 2017). Another study showed that Rab25 binds to fibronectin-bound α5β1 and recycles the heterodimer from late endosomes to the plasma membrane in a polarized manner (from the rear to the front of migrating cells) only in the presence of Chloride Intracellular Channel Protein 3 (CLIC3) (Dozynkiewicz et al., 2012).

The degradation of integrin is also an important process to remove any damaged and/or ligand-bound integrins that cannot form new focal adhesions with the ECM. Indeed, cell migration was impaired when the degradation of ligand-bound integrin was inhibited (Lobert et al., 2010). Ubiquitinated integrins is shown to be degraded through the lysosomal pathway in endosomal sorting complex required for transport (ESCRT) machineries-dependent manner (Böttcher et al., 2012; Kharitidi et al., 2015; Lobert et al., 2010).

1.4.3 Retrograde trafficking of integrins

Retrograde trafficking is a mode of transporting cargoes from the endocytic recycling compartments back to the biosynthetic/secretory compartments, including the TGN and the ER (Johannes and Popoff, 2008). This trafficking is important for the retrieval of receptors and enzymes that function in the biosynthetic pathway. For example, retrieval of mannose-6-phosphate receptor, a receptor that binds and sorts mannose-6-phophate hydrolases, to the TGN is required for proper trafficking of the hydrolase (Braulke and Bonifacino, 2009; Lu and Hong, 2014). Additionally, cell surface receptors such as TGN38 and transferrin receptors are also targeted back to the TGN through retrograde trafficking (Chapman and Munro, 1994; Shi et al.,

2012). Furthermore, a recent proteomic study revealed that integrin heterodimers and many protein transporters use this trafficking as well (Shi, 2011; Shi et al., 2012).

One of the sorting complexes involved in retrograde trafficking from early endosomes to the TGN is called retromer. It is a hetero-pentameric complex that is conserved from yeast to human (Bonifacino and Rojas, 2006; Lu and Hong, 2014). There are two sub-complexes in retromer, where one is involved in cargo selection and the other one is involved in membrane binding and membrane modelling (Lu and Hong, 2014). Cargo selection and sorting is performed by a trimer composed of Vps26, Vps29, and Vps35 (Lu and Hong, 2014). Vps35 is recruited to the endosomal membrane to bind to the cytoplasmic tail of the cargoes through its interaction with Vps26 via N-terminal PRLYL motif, and it simultaneously interacts with Vps29 via its C-terminal PRLYL for the assembly of the retromer complex (Collins et al., 2005; Haft et al., 2000; Priya et al., 2015; Shi et al., 2006). The cargo-recognizing sub-complex (Vps26-Vps35-Vps29 trimer) interacts with the membrane binding SNX sub-complex consists of SNX1 and SNX2 (Bonifacino and Rojas, 2006). SNX1/2 dimerize and bind to the curved endosomal membrane, which is enriched in PtdIns3P via their PX domains, while their BAR domains stabilize the curvature and bend the membrane further to form a tubular structure (Lu and Hong, 2014). To bud off from the tubular structure, retromers recruit Wiskott-Aldrich syndrome protein and SCAR homology (WASH) and dynein complex, which connects the retromer complex to both microtubule network and actin cytoskeleton. Then, using the force from actin polymerization, retromer containing tubular membrane undergoes scission and the resulting vesicle is targeted to the TGN through the microtubule network (Gomez and Billadeau, 2009; Lu and Hong, 2014). Besides retromer, clathrin and its adaptor protein, EpsinR mediate the formation of vesicles for retrograde trafficking from early endosomes to the TGN (Saint-Pol et al., 2004).

Another crucial step in retrograde trafficking is the fusion of vesicles derived from early endosomes with the TGN membrane. This process is mediated by two key proteins: tethering factors and small N-ethylmaleimide (NEM)-sensitive fusion factor (NSF) attachment protein (SNAP) receptors (SNAREs). Tethering factors are a class of proteins that are involved in the long- (approximately 200 nm) or short-range (approximately 30 nm) interaction with vesicles, mostly via small GTPases such Rab or Arf proteins, to facilitate the capture, docking and fusion

of vesicles with their target membrane (Bröcker et al., 2010; Hong and Lev, 2014). The tethering protein complex involved in retrograde trafficking is termed GARP, consisting four subunits: Vps51, Vps52, Vps53, and Vps54 (Conibear and Stevens, 2000; Conibear et al., 2003). GARP mediates the interaction between Rab6 containing vesicles and the syntaxin 6/16 SNARE complex at the TGN (Bonifacino and Hierro, 2011; Conibear et al., 2003).

SNAREs are a class of membrane-bound proteins that have a hydrophobic transmembrane domain at the C-terminus, one or two SNARE motifs made up of approximately 70 amino acids with heptad repeats and an N-terminal regulatory sequence (Bock et al., 2001; Hong and Lev, 2014). Generally, SNARE proteins on the membrane of the vesicle are termed v-SNAREs and the ones on the membranes of target organelle are termed t-SNAREs. The pairing of v-SNAREs and t-SNAREs forms a *trans*-SNARE complex, consisting of four SNARE motifs that are twisted in a parallel four-helix bundle (Chen and Scheller, 2001). This interaction brings the vesicle closer in proximity to the target organelle and facilitates membrane fusion. After a successful fusion, the v-t SNARE complex is disassembled by ATPase N-ethylmaleimide-sensitive fusion protein (NSF) and its cofactor soluble NSF attachment protein (SNAP) in the presence of ATP (Chen and Scheller, 2001; Söllner et al., 1993). There are four SNARE complexes involved in retrograde trafficking from early endosomes to the TGN. They are Vamp3/syntaxin 6/ syntaxin 16/ Vti1a, Vamp3/syntaxin 10/ syntaxin 16/ Vti1a, Vamp4/ syntaxin 6/ syntaxin 16/ Vti1a, and GS15/syntaxin 5/GS28/ Ykt6 (Ganley et al., 2008; Mallard et al., 2002; Tai et al., 2004). The v-SNAREs on the vesicular membranes from early endosomes are Vamp3, Vamp4 and GS15, while the rest of the SNARE proteins are t-SNAREs on the TGN membrane.

Integrins were found to be transported from recycling endosomes to the TGN by Riggs and colleagues when the endocytosed integrin α3β1 accumulated in vesicles containing syntaxin 6 and VAMP3 (Riggs et al., 2012). Retrograde trafficking of integrin was further confirmed through proteomic study that analyzed populations of cell surface proteins that were transported from the plasma membrane to the TGN (Shi, 2011; Shi et al., 2012). To date, retrograde trafficking of Intβ1 was shown to be mediated by the retromer complex, VAMP3, Rab6, syntaxin 16 and syntaxin 6 (Riggs et al., 2012; Shafaq-Zadah et al., 2016). Moreover, inhibition of retrograde trafficking of Intβ1 impaired polarized trafficking of this receptor during directional

cell migration (Shafaq-Zadah et al., 2016). The discovery of retrograde trafficking of integrin is relatively recent and more studies are needed to better understand the molecular mechanisms involved in this trafficking.

1.5 Thesis investigation

Recent discovery of aberrant expression of NHE5, which was thought as a neuron-specific NHE, in C6 glioma cells (Figure 1.5 A) led to the question: What is the role of NHE5 in C6 glioma cells? By suppressing the expression of NHE5 using shRNAs, our lab previously found that C6 glioma cells exhibit reduced cell adhesion on collagen IV, but not on polyethyleneimine (PEI) (Figure 1.5 B). Similar results were observed with cell adhesion on fibronectin and collagen I (unpublished observation). These results together suggested that NHE5 is likely to affect integrin-mediated cell adhesion. Given that heterologously-expressed HA-tagged human NHE5 in AP-1 cells was shown to exhibit integrin-induced activation and interact with Intβ1 (Onishi et al., 2007), and that Intβ1 is highly expressed in C6 glioma cells (Malek-Hedayat and Rome, 1992), we immunoblotted for Intβ1 in the lysates from C6WT and NHE5 depleted cells. Strikingly, we observed a difference in the molecular weight of Intβ1 between these cell lines (see chapter 4). During my directed studies project, I previously, characterized that the molecular weight difference is mostly caused by a defect in α2-6 sialylation of Intβ1 in N5KD cells.

The objective of my thesis is to investigate the role of NHE5 in integrin-mediated cell adhesion and Intβ1 sialylation. I hypothesized that NHE5, by modulating the pH of recycling endosomes, influences the trafficking of Intβ1 and affects Intβ1 sialylation and cell adhesion. Hence, using C6 glioma cells as my model system, I performed various biochemical and immunofluorescence assays to understand the relationship between NHE5 and Intβ1.

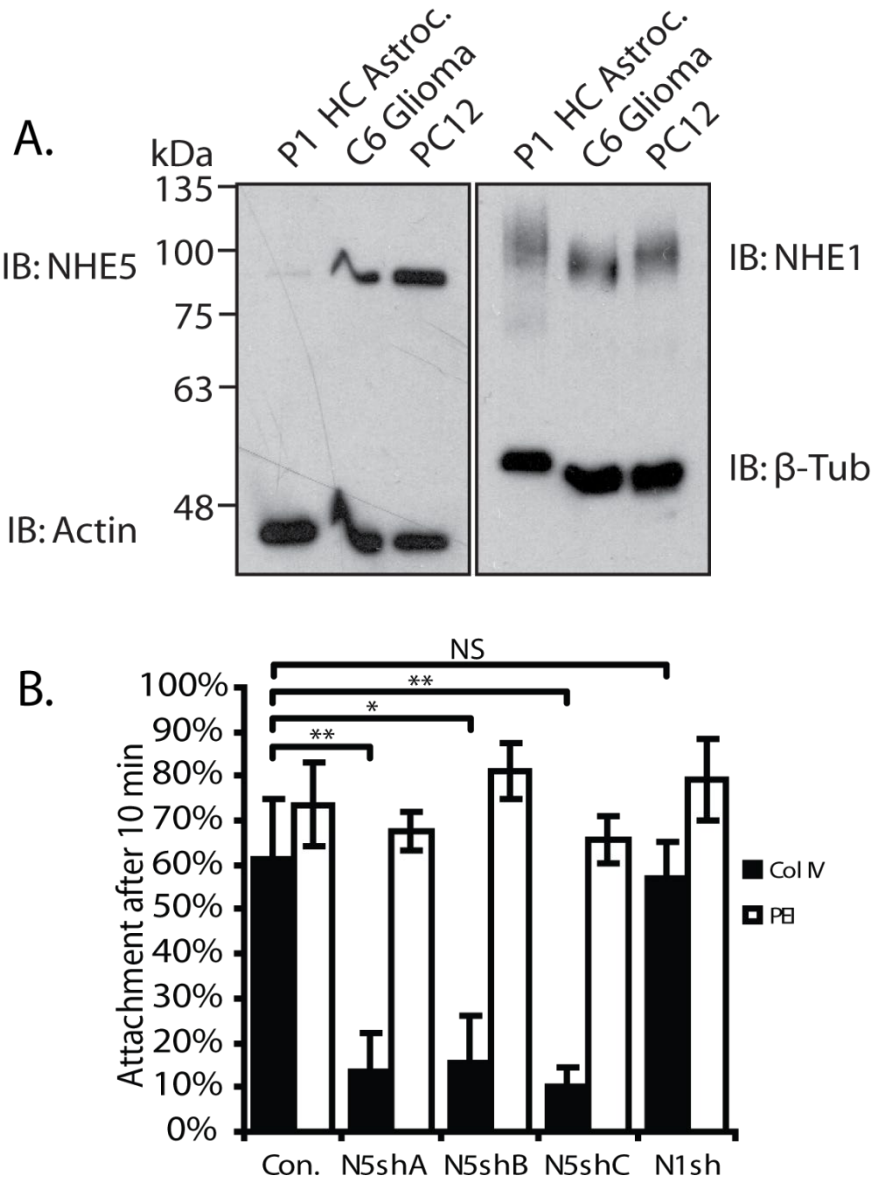

Figure 1.5 NHE5 knockdown affects integrin-mediated cell adhesion.
(A) Aberrant expression of NHE5 in C6 glioma cells. Proteins from post-natal day 1 rat hippocampal astrocytes (P1 HC Astroc.), C6 rat glioma, and PC12 neuroendocrine cells were subjected to immunoblotting and probed for the expression of NHE5, NHE1, actin, and β-tubulin.
(B) NHE5 knockdown affects cell attachment on integrin substrate. Cells were seeded and incubated on polyethyleneimine (PEI) or collagen IV (Col IV) coated wells for 10 and 90 minutes (min). The number of cells attached at 10 minutes were normalized to that of 90 minutes and plotted as attachment percentage. Student's unpaired t-tests. (*$p<0.05$; **$p<0.01$, NS= not significant)
This figure is adapted from (Fan, 2015).

Chapter 2: Materials and methods

2.1 Antibodies and Reagents

2.1.1 Antibodies

Rabbit polyclonal anti-rat NHE5 was custom made (GenScript, Piscataway, NJ, USA) as previously described (Diering et al., 2011). The mouse monoclonal antibodies against β-tubulin (clone E7) and α1 subunit of Na^+/K^+ ATPase (NKA) (clone a6F), which were developed by Micheal Klymkowsky and D.M Fambrough, respectively, were obtained from the Developmental Studies Hybridoma Bank, created by NICHD of the NIH and maintained at The University of Iowa, Department of Biology, Iowa City, IA 52242, USA. The purified mouse monoclonal anti-EEA1 (clone 14/EEA1, #610456) antibody was obtained from BD Bioscience (Mississauga, ON, Canada). Mouse monoclonal anti-HA (clone 16B12) antibody was obtained from Covance (Princeton, NJ, USA). Rabbit monoclonal anti-HA (clone C29F4, #3724) antibody was purchased from Cell Signaling Technology (Danvers, MA, USA).

Rabbit polyclonal anti-integrin β1 (M-106, #sc-8978), mouse monoclonal anti-GAPDH (6C5, #sc-32233) and mouse monoclonal anti-VPS29 (D1, #sc3988) antibodies were purchased from Santa Cruz Biotechnology (Dallas, TX, USA). Mouse monoclonal anti-vinculin antibody in ascites fluid (clone hVIN-1) and mouse monoclonal anti-Flag® (M2, #F3165) were purchased from Sigma Aldrich (St. Louis, MO, USA). Mouse monoclonal anti-transferrin receptor (clone H68.4, #13-6800) antibody, Alexa-Fluor conjugated phalloidin (#A-12379), Alexa-Fluor conjugated goat anti-mouse (#A-11004) and goat anti-rabbit (#A-21210) secondary antibodies and DRAQ5^{TM} (#62254) were obtained from Thermo Fisher Scientific (Waltham, MA, USA). The HRP-conjugated secondary goat anti-mouse and goat anti-rabbit antibodies were purchased from Jackson ImmunoResearch Laboratories, Inc. (West Grove, PA, USA).

Table 2.1 Dilutions of the primary antibodies used in immunoblotting and immunofluorescence experiments

Primary antibody	Immunoblotting	Immunofluorescence
Anti-β-tubulin (mouse)	1:10 000 – 1:50 000	-
Anti-EEA1 (mouse)	-	1:200
Anti-Flag	1:50 000	1:1000
Anti-GAPDH	1:100 000	-
Anti-HA (mouse)	1:8 000 – 1:10 000	1:1000
Anti-HA (rabbit)	-	1:1000
Anti- integrin β1 (rabbit)	1:5 000 -10 000	-
Anti- rat NHE5 (rabbit)	1:5000	-
Anti-NKA (mouse)	1:3000	-
Anti- transferrin receptor (mouse)	1:8000 – 1:50 000	-
Anti-vinculin (mouse)	-	1:400
Anti-Vps29 (mouse)	1:2000	-

Unless otherwise stated, the dilutions were made from the laboratory or manufacturer's stock.

Table 2.2 Dilutions of the secondary antibodies used in the immunoblotting and immunofluorescence experiments

Antibody	Immunoblotting	Immunofluorescence
Alexa 488-goat anti-rabbit	-	1:500
Alexa 568-goat anti-mouse	-	1:1000
HRP-conjugated goat anti-mouse	1:20 000	-
HRP-conjugated goat anti-mouse	1:20 000	-

Unless otherwise stated, the dilutions were made from the laboratory or manufacturer's stock.

Table 2.3 Fluorescent probes used in the immunofluorescence experiments

Antibody	Dilution
Draq5™	1:1000
Alexa 488-Phalloidin	1:250

Unless otherwise stated, the dilutions were made from the laboratory or manufacturer's stock.

2.1.2 Reagents

The EDTA-free protease inhibitor (PI) cocktail was obtained from Roche Diagnostic Corporation (Indianapolis, IN, USA). Fibronectin (#F1141), collagen type IV (#C0543), polyethyleneimine (PEI) solution (#P3143), L- Gluthathione reduced (#G4251), Retro-2 (#SML-1085), and Brefeldin A (#B6542) were purchased from Sigma Aldrich. Sulfo-NHS-SS-Biotin (#A8005) was purchased from Apex Biotechnology Inc (Hsinchu City, Taiwan). EZ-Link™ Sulfo-NHS-SS-Biotin (#21331) and Pierce™ NeutrAvidin™ Agarose resins (#29200) were obtained from Thermo Fisher Scientific. Doxycycline hyclate (#DOX444) was purchased from BioShop Canada Inc (Burlington, Ontario, Canada). Bafilomycin A1 (#B-1080) was purchased from LC Laboratories (Woburn, MA, USA). The α2-3,6,8 neuraminidase (P0720S) and PNGase F (P0704S) were bought from New England Biolabs, NEB (Ipswich, MA, USA). Biotinylated *Sambucus Nigra* (Elderberry) Bark (SNA) lectin (#B-1305) and *Maackia Amurensis* lectin II, MAL II (#B-1265) were purchased from Vector Laboratories (Burlingame, CA, USA).

Chloroquine diphosphate salt (#6628, Sigma Aldrich) was a generous gift from Roberge Lab (Department of Biochemistry and Molecular Biology, The University of British Columbia).

2.2 DNA constructs

2.2.1 N-terminus and C-terminus tagged human Intβ1

Human integrin β1 (hITGB1) cDNA was amplified from pMD-ITGB1 (#HG10587-M, Sino Biological, Beijing, China) using the following primers: sense- 5'-CCTCGAAAGGCCTCTGAGGCCATGAATTTACAACCAATTTTCTGG-3' and antisense – 5'- GGAAGCTTGGCCTGACAGGCCTCATTTTCCCTCATACTTCGG-3'. The PCR amplicon was then ligated into a mammalian expression vector pSBtet-Pur made by Kowarz, Löscher, & Marschalek (2015) (# 60507, Addgene plasmid, Cambridge, MA, USA). The sequence of the hITGB1 insert was verified and site-directed mutagenesis, modified from Klock & Lesley (2009) and Liu & Naismith (2008), was carried out to insert HA-tag after the 24th amino acid residue of hITGB1 using the following primers: sense -5'-CCATATGACGTGCCCGACTACGCCGGAGAAAATAGATGTTTAAAAGCAAATGCC-3' (sense) and 5'-

GGCGTAGTCGGGCACGTCATATGGGTATTCATCTGTTTGAGCAAACAC-3' (antisense). Inducible HA-tagged hITGB1 (HA-hITGB1) was generated.

C-terminus GFP tagged human integrinβ1 (hITGB1-GFP) was a generous gift from Roskelley lab (Department of Cellular and Physiological Sciences, The University of British Columbia).

2.2.2 Vps29 shRNA construct

Short-hairpin RNA construct targeting rat VPS29 was made by ligating synthetic double stranded oligonucleotides into pRNAT-U.6-Hygro. The following synthetic oligonucleotides were annealed to generate Vps29 shRNA A – 5'-GATCCC**GGTGATGTCCACATCGTAAGA**TTGATATCCG**TCTTACGATGTGGACATCACC**TTTTTTCCAAA-3' (sense) and 5'-AGCTTTTGGAAAAAA**GGTGATGTCCACATCGTAAGA**CGGATATCAA**TCTTACGATGTGGACATCACC**GG-3' (antisense). The bold type is the sequence targeting rat Vps29.

2.2.3 Tetracycline-inducible Vps29 shRNA

Vps29 miRNA-shRNA hybrid expressed under tetracycline-inducible was generated through multiple steps. First, our lab generated a tetracycline inducible miRNA backbone by incorporating miR30-pricursor arms (Lebbink et al., 2011) into pSBtet-Pur (# 60507, Addgene plasmid, Cambridge, MA, USA). This was done by ligating the following annealed synthetic double-stranded oligonucleotides flanking *SfiI* sites into the plasmid: 5'-AGGCCTCGAG**AAGAAGGTATATTGCTGTTGACAGTGAGCG**TC**TGCCTACTGCCTCGGACTTCAAGGGG**CCTGTC – 3' (sense); 5'-AGG**CCCCTTGAAGTCCGAGGCAGTAGGCA**GA**CGCTCACTGTCAACAGCAATATACCTTCTT**CTCGAGGCCTCAG -3' (antisense). The bold type indicates the sequence of the miR30-pricursor arms. Then, a site-directed mutagenesis was performed as described (Klock and Lesley, 2009) to convert the miR30-based shRNA backbone to a more potent miR-E-based shRNA backbone (Fellmann et al., 2013) and to insert a *NotI* site downstream of the promoter. The following primers were used for the site-directed mutagenesis to introduce these modifications: 5'-*GCGGCCGC*TCTA**GACTTCTTAACCCAACAGAAGG*CTCGAG*AAGG**TATATTGCTGTT

GACAGTGAGC- 3’ (sense); 5’-
GTTAAGAAGTCTAGA*GCGGCCGC*GGCCTCAGAGGCCTTTCGAG -3’ (antisense). The sequence in bold represents the additional sequence inserted to make miR-E-based shRNA, while the *NotI* and *XhoI* restriction sites are in italics and underlined, respectively. Following this round of mutagenesis, another site-directed mutagenesis was performed with the following primers to introduce the sequence targeting rat Vps29 shRNA and the miR30_loop into the miR-E-based shRNA backbone: 5’-
TAGTGAAGCCACAGATGTA**GGTGATGTCCACATCGTAAGA**CTGCCTACTGCCTCG
GACTTCAAGG -3’ (sense); 5’-
TACATCTGTGGCTTCACTA**GGTGATGTCCACATCGTAAGA**ACGCTCACTGTCAACA
GCAATATACC -3’ (antisense). The underlined sequence represents the miR30-loop and the bold-type is the target sequence for rat Vps29. Lastly, EGFP was added to the backbone as a marker. For this purpose, EGFP cDNA was amplified from pEGFP-N1 as a template. The following primers were used: 5’-
AAGGAAAAAAGCGGCCGCATATGGTGAGCAAGGGCGAGG – 3’ (sense); 5’ –
AAGGAAAAAAGCGGCCGCCTTGTACAGCTCGTCCATGCC – 3’ (antisense). The *NotI* flanking amplicon was ligated between the promoter and Vps29 shRNA. GFP-tagged Vps29 shRNA with an enhanced miR30 system expressed under tetracycline-inducible promoter was generated.

2.2.4 Inducible HA-tagged rat NHE5

A site-directed mutagenesis was first performed using rat NHE5 cDNA as template (a generous gift from Dr. John Church, Department of Cellular and Physiological Sciences, The University of British Columbia) to modify the intrinsic *SfiI* restriction site using the following primers: sense – 5’- CTGTGGATTCTGGTCGCCAGCTTGGCCAAAATCGTG -3’ and antisense – 5’- CTGGCGACCAGAATCCACAGGGCCACCAG- 3’. After verifying that the internal *SfiI* site in rat NHE5 had been modified, PCR amplification was performed to amplify the gene. The following primers were used: sense – 5’-
CCCAAGCTTGGCCTCTGAGGCCATGCTGCGCGTCGCACTGCTTC- 3’ and antisense – 5’– GCTCTAGAGGCCTGACAGGCCTACAGCCTGCCTCCTCTGTTGAAC- 3’. The PCR amplicon was then ligated into a mammalian expression vector pSBtet-Pur made by Kowarz,

Löscher, & Marschalek (2015) (# 60507, Addgene plasmid, Cambridge, MA, USA) and the sequence of the insert was verified.

Following this, another round of site-directed mutagenesis was performed to introduce unmatched sequence into the shRNA A region to make rat NHE5 resistant to shRNA A using the following primers: sense- 5'- GTTTCACAAAATCTAAACCTCGACCCCGCAAGACC-3' and antisense – 5'- CGAGGTTTAGATTTTGTGAAACAGATGTTATGTTTGG-3'. Final round of site-directed mutagenesis was conducted to add HA-tag after Leu38 of the protein, which is predicted to be the first extracellular loop of NHE5. Hence, the protein encoded by this NHE5 construct is expected to have the HA-tag facing the extracellular space, which should be recognized by extracellularly treated anti-HA antibodies. The following primers were used for the site-directed mutagenesis: sense- 5'-GTACCCCTACGACGTGCCCGACTACGCCTTCCGCTGGCAGTGGCAC-3' and antisense-5'-GGCACGTCGTAGGGGTACGCGGCCGCGAGCGCCAAGCCTGGAGG-3'. Inducible HA-tagged rat NHE5 resistant to shRNA A was generated.

2.2.5 Flag-tagged human ST6Gal-I

Human ST6Gal-I (hST6Gal-I) cDNA was amplified from pMD-ITGB1 (#HG11590-M, Sino Biological, Beijing, China) using the following primers: sense – 5'-GGACCAGGCCTCTGAGGCCATGATTCACACCAACCTGAAG - 3' and antisense – 5'-AAGGCTGGCCTGACAGGCCTTACTTGTCGTCATCGTCTTTGTAGTCGCAGTGAATGG TCCGGAAGCC – 3'. The underlined sequence corresponds to the FLAG-tag sequence. The PCR amplicon is then ligated into a mammalian expression vector pSBbi-Pur made by Kowarz, Löscher, & Marschalek (2015) (# 60523, Addgene plasmid, Cambridge, MA, USA). The sequence of the hST6Gal-I with FLAG-tag insert was verified by sequencing.

2.3 Transfection

2.3.1 Electroporation

DNA was introduced to cells via electroporation using the BioRad GenePulser Xcell electroporation system (BioRad, Hercules, CA, USA). Approximately $1x10^5$ cells were collected after trypsinization and resuspended in ice-cold electroporation buffer containing 1M HEPES and 6 mM of D-glucose, and 5 μg of plasmid DNA into electroporation cuvettes with 0.1 cm gap

(#1652083, BioRad). Then, they were subjected to an electric pulse (250V, 200μF) and were transferred immediately into culture plate containing conditioned prewarmed Dulbecco's Modified Eagle Medium (DMEM) (#12800-082, Thermo Fisher Scientific) supplemented with 10% fetal bovine serum (FBS). The culture medium was replaced with DMEM supplemented with 10% FBS the following day.

2.3.2 Lipofectamine

Approximately $3x10^4$ cells were seeded and grown on a coverslip in a 24-well plate for five hours at 37 °C prior to transfection. The culture medium was then replaced with serum-free DMEM. 0.8 μg of LipofectAMINE PLUS reagent (#10964-013, Life Technologies) and 0.5 μg of plasmid DNA were mixed in 100 μL OPTI-MEM (#31985-062, Gibco by Thermo Scientific Fisher). Then, 100 μL of transfection mix was added slowly to a 24-well containing 400 μL of serum-free DMEM and incubated overnight. The culture medium was replaced with DMEM supplemented with 10% fetal bovine serum (FBS) on the following day.

2.4 Cell Culture

2.4.1 C6WT, NHE5 and NHE1 knockdown cell lines

All cell lines were cultured at 37°C in a humidified atmosphere containing 5% CO_2, unless otherwise stated. The C6 rat glioma cells, a generous gift from the Naus Lab (Department of Cellular and Physiological Sciences, University of British Columbia), were cultured in DMEM supplemented with 10% FBS (complete medium).

The C6 rat glioma cells stably expressing shRNA targeting NHE5 were generated as previously described in Fan et al. (2016). In brief, the C6 glioma cells were transfected using electroporation (see section 2.3.1) with pRNAT-U.6-based shRNA plasmids with the following target sequence for NHE5 (Diering et al., 2013): **GTTTGCTCTTGGTGAAACAGATGTTA** (shRNA A); **ATAGTGGTGGCCACAAAGTAGTCCT** (shRNA B); and **TTTGTGGTAATCACTCCTCTTCACC** (shRNA C). The NHE5 knockdown (N5KD) cells were selected in complete medium containing 1000 μg/mL of G418 and maintained in medium containing 500 μg/mL of G418.

C6 rat glioma cells stably expressing shRNA against NHE1 were previously generated in Numata lab by transfecting C6 glioma cells using electroporation (see section 2.3.1) with

pRNAT-U.6 based shRNA plasmid with the following target sequence for NHE1: **GGACATTGACTACTTACATGT**. The N1KD cells were selected in complete medium containing 500 μg/mL of hygromycin and maintained in medium containing 250 μg/mL of hygromycin.

2.4.2 C6WT and N5KD glioma cells expressing inducible HA-tagged hITGB1

C6 glioma cells stably expressing tetracycline-inducible HA-hITGB1 were generated by transfecting C6WT and N5KD (expressing shRNA A) glioma cells with HA-tagged hITGB1 (described in 2.2.1) using electroporation (see section 2.3.1). The pool of transfected WT and N5KD were selected and maintained in culture medium containing 1.5 μg/ml and 4.0 μg/ml of puromycin, respectively for two weeks. Expression and subcellular localization of the HA-hITGB1 were determined by immunoblotting and immunofluorescence.

2.4.3 C6WT and N5KD glioma cells expressing inducible miRNA-shRNA targeting Vps29

C6WT and N5KD (expressing shRNA A) glioma cells stably expressing tetracycline-inducible GFP-tagged Vps29 miRNA-shRNA were generated. Cells were transfected with the inducible miRNA-shRNA against Vps29 construct (see section 2.2.3) using electroporation (see section 2.3.1). The pool of transfected C6WT and N5KD cells were selected with 12.5 μg/mL and 15 μg/mL of puromycin, respectively for two weeks. Then, the cells were maintained in culture medium containing 6.25 μg/mL and 7.5 μg/mL of puromycin for WT and N5KD cells, respectively. Expression level of Vps29 before and after induction was determined by immunoblotting.

2.4.4 C6WT and N5KD glioma cells that concomitantly express inducible HA-hITGB1 and constitutive shRNA targeting Vps29

C6WT and N5KD (expressing shRNA A) glioma cells stably expressing inducible HA-hITGB1 were further transfected with the plasmid encoding shRNA against Vps29 (see section 2.2.2) using electroporation (see section 2.3.1). The transfected C6WT and N5KD glioma cells were selected using 1000 μg/mL and 1500 μg/mL of hygromycin respectively for two weeks. After that, C6WT cells were maintained in complete medium containing 6.25 μg/mL of puromycin and 250 μg/mL of hygromycin, whereas N5KD were maintained in complete medium

containing 7.5 μg/mL of puromycin, 500 μg/mL of G418 and 250 μg/mL of hygromycin. Expression level of Vps29 was determined by immunoblotting.

2.4.5 N5KD glioma cells expressing inducible HA-tagged rat NHE5

N5KD (expressing shRNA A) glioma cells were transfected with inducible HA-tagged rat NHE5 (section 2.2.4) using electroporation (see section 2.3.1). The transfected N5KD glioma cells were selected with 4 μg/mL of puromycin for two weeks. Then, the cells were maintained in culture medium containing 2 μg/mL of puromycin. Expression level of HA-tagged rat NHE5 with and without induction was determined by immunoblotting.

2.4.6 C6WT and N5KD glioma cells expressing Flag-tagged human ST6Gal-I

C6WT and N5KD (expressing shRNA A) glioma cells were transfected with Flag-tagged human ST6Gal-I (Flag-hST6Gal-I) (section 2.2.5) using electroporation (section 2.3.1). The pool of transfected WT and N5KD were selected in culture medium containing 12.5 μg/ml and 15 μg/ml of puromycin, respectively for two weeks. Then, the cells were maintained in culture medium containing 6.25 μg/mL and 7.5 μg/mL of puromycin for WT and N5KD cells respectively. Expression and subcellular localization of the Flag-hST6Gal-I were determined by immunoblotting and immunofluorescence.

2.5 Immunoblotting

C6 glioma cells were lysed on ice in either Radioimmunoprecipitation Assay (RIPA) buffer (0.5% sodium deoxycholate, 150 mM NaCl, 0.1% SDS, and 50 mM Tris-HCl, pH 7.2) or 1% NP-40 in Phosphate Buffered Saline (PBS, pH 7.4), which are freshly supplemented with protease inhibitor (PI) cocktails. The insoluble cellular debris was removed by centrifugation at 16,100 x g for 20 minutes at 4 ºC and the total protein concentration in the lysate was quantified using Bradford Assay. Protein samples were prepared in Laemmli sample buffer (125 mM Tris-HCl pH 6.8, 20% glycerol, 4% SDS, 0.2% bromophenol blue, and 100 mM dithiothreitol, DTT) and resolved in either 6% or 12% SDS-PAGE depending on the protein of interest. The resolved proteins were then electrotransfered onto polyvinylidene difluoride (PVDF) membranes. The blot was blocked with 5% skimmed milk for 60-120 minutes and incubated with primary antibodies overnight at 4ºC. The dilution conditions of primary antibodies used are shown in Table 2.1. After extensive washing with 1xPBS-T (PBS with 0.075% Tween-20), the blot was

incubated at room temperature (RT) for 45-60 minutes in 1xPBS-T containing 0.5% milk and appropriate secondary antibody (see dilution conditions in Table 2.2). The blot was washed extensively for 45-60 minutes with 1xPBS-T and treated with enhanced chemiluminescence (Millipore, Danvers, MA). The signal was detected by autoradiography and the intensity of the band was quantitated using built-in "gel analyze" plugin in Fiji Is Just ImageJ (Fiji) software version 1.52 (NIH, Bethesda, MD, USA).

2.6 Immunofluorescence and colocalization assays

2.6.1 Colocalization between N-terminally tagged and C-terminally tagged hITGB1

C6WT and N5KD (expressing shRNA A) glioma cells stably expressing inducible HA-tagged hITGB1 were transfected with hITGB1-GFP using lipofectamine (see section 2.3.2). The cells were grown on coverslips (#12-545-82, Fisher Scientific, Pittsburgh, PA, USA) at 37°C for 16 hours in the presence of 200 ng/mL of doxycycline and fixed with 3% paraformaldehyde (PFA) for 15 minutes at RT. All the subsequent steps were performed at RT unless stated otherwise. The cells were permeabilized with 0.1% Triton X-100 in PBS for 15 minutes and blocked with 3% BSA-PBS solution for 60 minutes. After blocking, the cells were incubated for two hours in anti-HA (mouse) primary antibody diluted in 0.1% BSA-PBS containing 0.01% Triton X-100. The dilution conditions for different antibodies are listed in Table 2.1. The coverslips were briefly washed with 0.01% Triton X-100 in PBS prior to a 60-minute incubation of Alexa Fluor-568 conjugated goat anti-mouse secondary antibody and Draq5 (nucleus staining) diluted in 0.1% BSA-PBS containing 0.01% Triton X-100. Their dilutions conditions are shown in Table 2.2 and Table 2.3. After extensive washing with 0.01% Triton X-100 in PBS and a rinse with distilled water, the coverslips were mounted using ProLong Diamond Antifade Reagent (#P36970, ThermoFisher Scientific). The images were acquired using Leica TCS-SP8 laser scanning confocal microscope equipped with 63x/NA 1.40 oil objectives, Diode/Argon/HeNe lasers, and HyD™ hybrid detectors (Wetzlar, Germany).

2.6.2 Colocalization between HA-hITGB1 and vinculin

C6WT and N5KD (expressing shRNA A) glioma cells stably expressing HA-hITGB1 were grown on a coverslip overnight in the presence of 200 ng/mL of doxycycline. All the subsequent steps were performed at RT unless stated otherwise. The cells were fixed with 3%

PFA for 15 minutes, permeabilized with 0.1% Triton X-100 in PBS for 15 minutes and incubated with 3% BSA-PBS solution for 60 minutes to block non-specific binding of antibodies. Cells were then incubated for 2 hours with primary antibodies that were diluted in 0.1% BSA-PBS containing 0.01% Triton X-100: anti-HA (rabbit) and anti-vinculin (mouse), their dilution condition is indicated in Table 2.1. The samples were briefly washed with 0.01% Triton X-100 in PBS and incubated for 60 minutes with Alexa Fluor-568 conjugated goat anti-mouse, Alexa Fluor-488 conjugated goat anti-rabbit secondary antibodies, and Draq5 (nucleus staining) that were diluted in 0.1% BSA-PBS containing 0.01% Triton X-100. The dilution conditions are indicated in Table 2.2 and Table 2.3. After extensive washing with 0.01% Triton X-100 in PBS and a rinse with distilled water, the coverslips were mounted using ProLong Diamond Antifade Reagent. The images were acquired using a Leica TCS-SP8 laser scanning confocal microscope equipped with 63x/NA 1.40 oil objectives, Diode/Argon/HeNe lasers, and HyD™ hybrid detectors.

2.6.3 Antibody-feeding assay and colocalization between EEA1 and HA-hITGB1

The coverslips were coated with 0.88 μg/cm^2 of fibronectin (FN) at 37°C for 60 minutes. C6WT and N5KD (expressing shRNA A) glioma cells stably expressing inducible HA-hITGB1 were grown overnight at 37°C on the precoated coverslip in complete medium containing 200 ng/mL of doxycycline. The cells were rinsed with ice-cold 1xPBS-CM (PBS supplemented with 1 mM $MgCl_2$, and 0.1 mM $CaCl_2$) of pH 7.4 twice and incubated in it for 5 minutes at 4°C. Then, the cells were incubated with 50 μL of rabbit monoclonal anti-HA antibody (dilution 1:100) for 45 minutes at 4°C to label the cell surface HA-hITGB1. After the cold-labelling with anti-HA antibody, the cells were immediately incubated in conditioned complete medium for 10 minutes at 37°C in humidified atmosphere with 5% CO_2. At the end of the incubation, the cells were rinsed with ice-cold 1xPBS pH 7.4 and fixed with 3% PFA for 15 minutes at RT.

All the subsequent steps were performed at room temperature unless stated otherwise. The fixed cells were permeabilized with 0.1% Triton X-100 in PBS for 15 minutes and incubated with 3% BSA-PBS solution for 60 minutes to block non-specific antibody binding. After blocking, the cells were incubated for 2 hours with anti-EEA1 (mouse) diluted in 0.1% BSA-PBS containing 0.01% Triton X-100 (see Table 2.1 for dilution conditions). The samples were briefly washed with 0.01% Triton X-100 in PBS and incubated for 60 minutes with Alexa Fluor-

568 conjugated goat anti-mouse, Alexa Fluor-488 conjugated goat anti-rabbit secondary antibodies, and Draq5 (nucleus staining) diluted in 0.1% BSA-PBS containing 0.01% Triton X-100 (see Table 2.2 and 2.3 for dilution conditions). After extensive washing with 0.01% Triton X-100 in PBS and rinsing with distilled water, the coverslips were mounted using ProLong Diamond Antifade Reagent.

Images were captured with a Leica TCS-SP8 laser scanning confocal microscope equipped with 63x/NA 1.40 oil objectives, Diode/Argon/HeNe lasers, and HyD^{TM} hybrid detectors. Data were analyzed by Just Another Colocalization Plugin (JACoP) in Fiji Is Just ImageJ (Fiji) software to obtain the Pearson's coefficient between the signals from HA-hITGB1 and EEA1.

2.7 Cell spreading assay

The coverslips were coated with either 4.4 μg/cm^2 of polyethyleneimine (PEI) or 2.65 μg/cm^2 of collagen type IV (Col IV) overnight at 4°C. Cells were seeded onto PEI- or Col IV-coated coverslips and incubated at 37°C for 15 minutes, 2 hours or 24 hours. At the end of the incubation, the cells were fixed with 3% PFA at RT for 15 minutes.

All the subsequent steps were performed at RT unless stated otherwise. The cells were permeabilized with 0.1% Triton X-100 in PBS for 15 minutes and blocked with 3% BSA-PBS solution for 60 minutes. After blocking, the cells were incubated for 60 minutes with Alexa-Fluor-488 conjugated phalloidin and Draq5 (nucleus staining) that were diluted in 0.1% BSA-PBS containing 0.01% Triton X-100. The antibody dilutions are shown in Table 2.3. After extensive wash with 0.01% Triton X-100 in PBS and rinsing with distilled water, the coverslips were mounted using ProLong Diamond Antifade Reagent. The images were captured with a Leica TCS-SP8 laser scanning confocal microscope equipped with 20x/NA 0.70 air objectives, Diode/Argon/HeNe lasers, and HyD^{TM} hybrid detectors.

The images (using Alexa 488-phalloidin signal) were processed and analyzed by Fiji Is Just ImageJ (Fiji) software. First, the brightness and contrast of the images were auto adjusted. Then, auto threshold of the signal for these images were applied to generate binary images. The area of the cells was measured using the "measure" plugin in the software.

2.8 Total Internal Reflection Fluorescence (TIRF) microscopy

The coverslips were coated with 2.65 μg/cm^2 of collagen type IV (Col IV) overnight at 4°C. WT and N5KD (expressing shRNA A) glioma cells were seeded on the Col IV-coated coverslips and incubated at 37°C for 4 hours or 16 hours. All the subsequent steps were performed at RT unless stated otherwise. At the end of the incubation, the cells were fixed with 3% PFA for 15 minutes, followed by permeabilization with 0.1% Triton X-100 in PBS for 15 minutes. The cells were then blocked with 3% BSA-PBS solution for 60 minutes and incubated for 2 hours with anti-vinculin (mouse) diluted in 0.1% BSA-PBS containing 0.01% Triton X-100 as indicated in Table 2.1. Next, the cells were briefly washed with 0.01% Triton X-100 in PBS and incubated for 60 minutes with Alexa Fluor-488 conjugated phalloidin and Alexa Fluor-568 conjugated goat anti-mouse secondary antibody diluted in 0.1% BSA-PBS containing 0.01% Triton X-100 (see Table 2.2 and 2.3). After extensive wash with 0.01% Triton X-100 in PBS and rinsing with distilled water, the coverslips were mounted using SlowFade^R Gold Antifade Reagent (#S36936, ThermoFisher Scientific).

The fixed samples were imaged as described previously in Abraham et al. (2017) with some modifications. Briefly, the cell surface was imaged using Olympus TIRFM system with the following components: an inverted microscope (Olympus IX81) equipped with a 100X NA 1.49 TIRFM objective (Olympus), motorized filter wheel (Olympus), high-performance electron multiplier (EM)-charge-coupled device (CCD) camera (Photometrics Evolve), and data acquisition software (Metamorph Version7.8). The 491 nm and 561 nm solid-state diode lasers were used to excite the Alexa-Fluor 488 on phalloidin and Alexa-Fluor 568 on vinculin respectively. The TIRF plane was adjusted to yield a penetration depth of ~65–75 nm from the coverslip and the images were acquired using EMCCD camera (Photometrics Evolve).

2.9 Cell-surface biotinylation assay

The cell-surface biotinylation experiment was performed with some modification from the previously described protocol (Fan et al., 2016). The 60 mm cell culture dishes were coated with either 2.85 μg/cm^2 of Col IV or 0.95 μg/cm^2 of FN overnight at 4°C. Approximately 5.0x10^5 C6WT cells and 5.5x10^5 N5KD (expressing shRNA A) glioma cells were seeded onto uncoated or Col IV- or FN-coated plates and grown in complete medium for 16 hours. The subconfluent cells were rinsed with ice-cold 1xPBS-CM, pH 8.0 twice, followed by a 5-minute

incubation in ice-cold PBS-CM pH 8.0 at 4°C. Then, the cell surface proteins were labelled with 0.3 mg/mL of membrane impermeable biotinylated amino-reactive (NHS ester) solution (Sulfo-NHS-SS-Biotin, #A8005, Apex Biotechnology Inc) in PBS-CM pH 8.0 for 35 minutes at 4°C. After cold-labelling, the unreacted biotinylating agent was removed by rinsing and incubating the cells with quenching buffer (20 mM of glycine in PBS-CM pH 8.0) twice for 7 minutes each at 4°C. Lastly, the cells were rinsed 4-5 times with ice-cold PBS-CM pH 8.0 before being lysed on ice with RIPA buffer containing fresh protease inhibitor cocktail. The protein concentration was determined using Bradford Assay and 25 µg of total protein was incubated with Pierce™ NeutrAvidin™ conjugated agarose beads (#29200, Thermo Fisher Scientific) with rotation overnight at 4°C. On the following day, the beads were washed three times with ice-cold 1% NP-40 in PBS pH 7.4 and the proteins were eluted with 2x Laemelli sample buffer. The eluted protein samples as well as ~5 µg of the total protein that was not subjected to the NeutrAvidin™ agarose beads pulldown were immunoblotted for Intβ1 and sodium potassium ATPase α1 subunit (NKA) as described in section 2.5.

2.10 Internalization assay

Internalization assays were conducted as described in (Fan et al., 2016) with some modifications. The 100 mm cell culture dishes were coated with 0.69 µg/cm^2 of FN overnight at 4°C with a continuous gentle shaking. Approximately 1.3x10^6 of WT cells and 1.5x10^6 of N5KD (expressing shRNA A) glioma cells were seeded onto these FN-coated plates and cultured for 16 hours in complete medium. The subconfluent cells were rinsed with ice-cold 1xPBS-CM, pH 8.0 twice, followed by a 5-minute incubation in ice-cold PBS-CM pH 8.0 at 4°C. Then, the cell surface proteins were labelled with 0.3 mg/mL of biotinylating reagent (EZ-Link™ Sulfo-NHS-SS-Biotin, #21331, Thermo Fisher Scientific) for 35 minutes at 4°C. After quenching the unreacted biotinylating agent, the cells were incubated in conditioned complete medium at 37°C in a humidified atmosphere with 5% CO_2 for 0 or 10 minutes to allow for internalization of the cell surface proteins. Upon internalization, the cells were rinsed and incubated with ice-cold cell-impermeable cleavage buffer (50 mM glutathione, 90 mM NaCl, 1 mM $MgCl_2$, 0.1 mM $CaCl_2$, 0.2% BSA, pH 8.6) three times for 15 minutes each at 4°C to remove the biotin from the non-internalized cell surface proteins. Lastly, the cells were rinsed with ice-cold 1xPBS-CM pH 8.0 few times and lysed with ice-cold RIPA buffer containing 1xPI. Some samples were not

subjected to the cleavage step to determine intrinsic degradation during incubation at 37°C. The protein concentration was quantified and 30 µg and 160 µg of protein from the cell lysates without and with cleavage, respectively were incubated with Pierce™ NeutrAvidin™ conjugated agarose beads overnight with rotation at 4°C. The beads were washed three times with ice-cold 1% NP-40 in PBS pH 7.4 and the proteins were eluted with 2x Laemelli sample buffer. The eluted protein samples as well as ~6 µg of the total protein that was not subjected to the NeutrAvidin™ agarose beads pulldown were immunoblotted for Intβ1 and transferrin receptor (TfR) as described in section 2.5.

Densitometry analysis was performed to obtain the percentage of internalized Intβ1 and TfR. First, the ratio of signal intensity from the NeutrAvidin pulldown samples to their corresponding total lysates was estimated. Then, the following equation was used to determine the internalization percentage: [10' (+) - 0' (+)]/ 10' (-), where 10' (+) and 0' (+) represent the biotinylated proteins that were treated with cleavage buffer after 10 minutes and 0 minutes of post-biotinylation incubations. 10' (-) represents the biotinylated proteins (not treated with cleavage buffer) after 10 minutes of post-biotinylation incubation, which includes both internalized and non-internalized populations. Note: (+) indicates that samples were treated with the cleavage buffer at indicated times whereas (-) that indicates samples were not treated with the cleavage buffer.

2.11 Recycling assays

2.11.1 Short-incubation recycling assay

Recycling assays were performed as described previously (Fan et al., 2016) with some modifications. Approximately $1.3x10^6$ of WT cells and $1.5x10^6$ of N5KD (expressing shRNA A) glioma cells were seeded onto 100 mm plates that were pre-coated with 0.69 µg/cm^2 of FN overnight at 4°C with a continuous gentle shaking. The cells were grown for 16 hours in complete medium, subjected to cell-surface biotinylation, internalization at 37°C for 10 minutes, and a first post-incubation cleavage as described in section 2.10. After the first post-incubation cleavage, the cells were subjected to a second round of incubation at 37°C in humidified atmosphere with 5% CO_2 for 0 and 10 minutes to allow the internalized biotin-labelled proteins to be recycled to the cell surface. The cells were then subjected to a second round of treatment with cleavage buffer at 4°C to remove biotin from the proteins that had recycled to the cell

surface. Recycled proteins on the cell surface are susceptible to the cleavage whereas proteins remaining in endosomes (non-recycled) are protected from the cleavage. The cells were then rinsed with ice-cold 1xPBS-CM pH 8.0 several times and lysed with ice-cold RIPA buffer freshly supplemented with protease inhibitor cocktail. Some samples were not subjected to the second post-incubation cleavage to determine intrinsic degradation during incubation at 37°C. Approximately 450 µg of total protein was incubated overnight with Pierce™ NeutrAvidin™ conjugated agarose beads with rotation at 4°C. The following day, the beads were washed three times with ice-cold 1% NP-40 in PBS pH 7.4 and the proteins were eluted with 2x Laemelli sample buffer. The eluted protein samples as well as ~6 µg of the total protein that was not subjected to the NeutrAvidin™ agarose beads pulldown were immunoblotted for Intβ1 and TfR as described in section 2.5.

Data obtained by densitometric analysis was used to calculate recycling rates of Intβ1 and TfR relative to the control cells. The ratio of signal intensity from the NeutrAvidin pulldown samples to their corresponding total lysate was first estimated. Then it was used in the following equation, which quantified the ratio of recycled proteins after 10 minutes (10') of second incubation at 37°C: 1- (10'(+) / 10'(-)), in which (+) indicates cells treated second post-incubation cleavage while (-) indicates cells without second post-incubation cleavage. Note: 10' (+) represents the non-recycled population of receptors and 10' (-) represents both recycled and non-recycled populations of receptors.

2.11.2 Long-incubation recycling assay

Long-incubation recycling assay was performed similarly to the short-incubation recycling assay (see section 2.11.1), except for few parameters. The incubation time for internalization of the surface-biotinylated proteins was 30 minutes and the incubation time for recycling of the internalized receptors was 20 minutes.

2.12 Cell-surface biotinylation-based degradation assay

Cells were seeded on uncoated plates and grown overnight in complete medium. The cells were subjected to cell-surface biotinylation with Sulfo-NHS-SS-Biotin (#A8005, Apex Biotechnology Inc) (see section 2.9). After quenching, the cells were incubated at 37°C in a humidified atmosphere with 5% CO_2 for indicated times, followed by rinsing twice with 1xPBS

pH 7.4 and lysed with ice-cold RIPA buffer supplemented with proteinase inhibitor cocktails. The protein concentration was quantified using Bradford assay and approximately 50-60 μg of total protein was incubated with Pierce™ NeutrAvidin™ agarose beads overnight at 4°C with rotation. The beads were washed three times with ice-cold 1% NP-40 in PBS pH 7.4 and the proteins were eluted with 2x Laemelli sample buffer. As for the samples from the 24 hours chase, approximately 100-120 μg were incubated with Pierce™ NeutrAvidin™ agarose beads for 150 minutes. The eluted protein samples as well as ~6 μg of the total protein that was not subjected to the NeutrAvidin™ agarose beads pulldown were immunoblotted for Intβ1 as described in section 2.5.

Densitometry analysis was performed to determine the ratio of the remaining surface labelled Intβ1 to its total lysate with chase relative to 0 hours of chase. First, the ratio of signal intensity from NeutrAvidin pulldown samples to their corresponding total lysate was quantified. The relative ratio of the remaining surface labelled Intβ1 to its total lysate was obtained by normalizing the calculated ratio to the one from 0 hours chase time point of the respective cell lines.

2.13 Enzymatic digestion assays

2.13.1 PNGase F digestion assay

PNGase F digestion assay was modified and optimized from Bartik et al. (2008) and Seales et al. (2005). C6WT and N5KD (expressing shRNA A) glioma cells were lysed with RIPA buffer freshly supplemented with protease inhibitor cocktail and the concentration of the total proteins in the cell lysates was quantified using Bradford assay. About 20 μg of the total proteins was denatured at 65ºC for 10 minutes in denaturing buffer (0.5% SDS and 40 mM DTT), followed by the addition of 0.1% NP-40, 1xG7 reaction buffer (50 mM sodium phosphate), and 500U of PNGase F, and incubation at 37ºC for 30 minutes. Instead of PNGase F, dH_2O was added to the control sample. Enzymatic reaction was stopped by adding Laemelli sample buffer. Immunoblotting (see section 2.5) was carried out to detect Intβ1 and β-tubulin in the protein samples.

2.13.2 Neuraminidase/Sialydase assay

Neuraminidase assay was carried out according to Bartik et al. (2008) and Seales et al. (2005) with some modifications. C6WT and N5KD (expressing shRNA A) glioma cells were lysed with RIPA buffer freshly supplemented with protease inhibitor cocktail and the concentration of the total proteins in the cell lysates was quantified using Bradford assay. About 40 µg of the total proteins were incubated with 25U of α2-3, 6, 8-neuraminidase in 1xG1 buffer (50 mM sodium citrate) for 30-60 minutes at 37ºC. Instead of the neuraminidase, dH_2O was added to the control sample. The enzyme was inactivated by heating the reaction at 65ºC for 10 minutes followed by the addition of Laemelli sample buffer to the reaction. Immunoblotting (see section 2.5) was done to detect the protein of interest.

2.14 Lectin pull-down assay

Lectin binding pull-down assays were performed as described in Seales et al. (2005) with some modifications. C6WT and N5KD (expressing shRNA A) glioma cells were lysed using 1% NP-40 in PBS freshly supplemented with protease inhibitor cocktail and the protein concentration was quantified using Bradford assay. Approximately 50 µg of total protein from the cell lysates were incubated with 20 µg/mL of biotinylated *Sambucus Nigra* (Elderberry) Bark lectin (SNA), or *Maackia Amurensis* lectin II, (MAL II) for three hours without rotation at 4ºC. The samples were affinity purified using NeutrAvidin beads by incubating at 4ºC for two hours with rotation. After washing with ice-cold 1% NP-40 in PBS for three times, the glycoproteins were eluted from the beads-lectin-glycoprotein complex with 15 µL of Laemelli sample buffer. The protein samples were immunoblotted for Intβ1 as described in section 2.5.

2.15 Pulse and chase assay

C6WT and N5KD (expressing shRNA A) glioma cells stably expressing inducible HA-hITGB1 were seeded and cultured overnight without doxycycline. Protein expression of HA-hITGB1 was induced (pulsed) with 100 ng/mL of doxycycline for three hours at 37°C in a humidified atmosphere with 5% CO_2. Doxycycline was washed out by changing the culture medium and the cells were chased in doxycycline-free complete medium for 0, 5, 24 and 48 hours. After chase, the cells were collected into cell pellets and stored at -70°C. Later, the cells

pellets were lysed and subjected to immunoblotting (see section 2.5) for HA-hITGB1 using anti-HA (mouse) and anti-β-tub.

Densitometric analysis was conducted to calculate the ratio of induced HA-hITGB1 to β-tub present in the cell lysate over time relative to the ratio at 0 hours chase period. First, the ratio of the signal intensity of HA-hITGB1 to its β-tubulin for each chase period was estimated. Then, these ratios were normalized to the one of 0 hours chase in doxycycline-free complete medium. The normalized ratio of HA-hITGB1 to β-tubulin of C6WT and N5KD cells were plotted against the chase period.

2.16 Synchronized protein trafficking assay

C6WT and N5KD (expressing shRNA A) glioma cells stably expressing inducible HA-hITGB1 were grown overnight in a 12-well plate without doxycycline. The cells were then treated with 5 μg/mL of Brefeldin A (BFA) and 200 ng/ml of doxycycline for three hours at 37°C, followed by a washout, where the culture medium was replaced with fresh medium containing no drugs. The cells were chased in the absence of BFA and doxycycline at 37°C in humidified atmosphere with 5% CO_2 for indicated times. Samples were analyzed by immunoblotting (see section 2.5) to detect the presence and size of HA-hITGB1.

2.17 Drug treatment assays

The experiment was carried out similarly to the one in section 2.16 with some modifications. Five hours after seeding, cells were treated for 16 hours with the following inhibitors at the indicated final concentrations: Retro-2 (40 μM), bafilomycin A1 (100 nM) and chloroquine (400 μM). In the control experiment, the cells were not exposed to any pharmacological drugs. The cells were then treated with 5 μg/mL of Brefeldin A (BFA) and 200 ng/ml of doxycycline for three hours at 37°C in the presence of indicated inhibitor drugs. It is followed by a washout of the medium and chase for indicated times in complete medium with or without the aforementioned pharmacological drugs. Upon the chase period, the cells were collected in pellets and stored at -70°C. The cell pellets were lysed and immunoblotted as described in section 2.5.

2.18 Statistical analysis

For the cell spreading assays, Kruskal-Wallis test was performed to determine whether there is a significant difference in the spread area between the cell lines. Dunn test with Bonferroni corrections were performed for multiple comparisons of the spread area between the control and other cell lines. Stata Statistical Software version 14 (StataCorp, College Station, TX) was used to analyze the data.

For the antibody-feeding and colocalization assays, Mann-Whitney test was performed using GraphPad software version Prism 6 (La Jolla, CA, USA) to determine whether the difference in the Pearson's coefficient between WT and N5KD cells is significant. *p*-values are indicated in the figures as the following: **p*<0.05, ***p*<0.01, ****p*<0.001, NS= not significant.

Chapter 3: NHE5 modulates cell spreading by influencing the trafficking of Intβ1

3.1 Introduction

Efficient trafficking of integrin is a prerequisite for cell adhesion. Studies have shown that the perturbation in integrin endocytosis, endocytic recycling and retrograde trafficking results in defective cell adhesion and spreading (Macia et al., 2006; Ratcliffe et al., 2016; Shafaq-Zadah et al., 2016). Since NHE5 has been shown to regulate the recycling of TrkA (nerve growth factor receptor) and c-Met (hepatocyte growth factor receptor), and to interact with Intβ1 when it is expressed in NHE-deficient AP1 cells, I hypothesize that NHE5 knockdown affects the trafficking of Intβ1 and results in defective cell spreading (Diering et al., 2013; Fan et al., 2016; Onishi et al., 2007).

Therefore, my goal in this chapter is to understand the role of NHE5 in the trafficking of Intβ1. Hence, I performed various biochemical and immunofluorescence assays on C6WT and N5KD glioma cells expressing shRNA A.

3.2 Spreading of C6 glioma cells is affected by NHE5 knockdown

As cells come in contact with integrin substrates during cell attachment, integrins bind to their ligands and cluster, forming focal complexes, which later matures into focal adhesions (Yu et al., 2011; Zaidel-Bar et al., 2003). Subsequently, cells begin to spread outwards through the formation of lamellipodia and new focal contacts, thus increasing their radii (Dubin-Thaler et al., 2004; Yu et al., 2011). Cell adhesion and spreading are important for biological phenomena such as cell survival, migration, and tissue development (Gumbiner, 1996). Since it has been previously found that NHE5 knockdown (KD) affects cells attachment on integrin substrate such as collagen IV (Col IV) (Figure 1.5 B), I performed a cell spreading assay with parental C6WT cells, three different NHE5 knockdown (N5KD) cells and NHE1-knockdown (N1KD) cells on polyethyleneimine (PEI) or Col IV to further define the effect of NHE5 suppression on cell spreading phenotypes.

Figure 3.1 (A, B) shows the cell area after spreading on PEI or Col IV over 15 minutes, 2 hours, and 24 hours. There was no difference in the spread area among the five different cell lines after 15 minutes of spreading on PEI, which is not an integrin substrate. Even after 24 hours of spreading, the cell spread area among these cell lines was still comparable (Figure 3.1 A). However, N5KD cells exhibited a lower cell spread area on Col IV than that of the control and N1KD cells within 15 minutes of spreading. The noticeable decrease in the cell area persisted up to 24 hours of spreading (Figure 3.1 A-B). After 15 minutes of spreading, C6WT and N1KD cells, not N5KD begun to spread on Col IV (Figure 3.1 B). In contrast, the shape of C6WT, N1KD and N5KD cells remained round on PEI after 15 minutes of spreading (Figure 3.1 B). These results indicate that NHE5 knockdown impairs the cell spreading onto Col IV, but not onto PEI. Given that integrins are one of the receptors that bind to collagen and one of its subunit has been shown to interact with NHE5 (Onishi et al., 2007), this observation suggests that NHE5 is likely to play a role in integrin-dependent cell spreading.

The quality and dynamics of focal adhesions formed in cells determine the nature of their spreading (Cleghorn et al., 2015; Kaushik et al., 2014). Therefore, to study the quality of focal adhesions formed after spreading on Col IV, C6WT and N5KD cells were imaged using internal reflection fluorescence (TIRF) microscopy by staining their actin and vinculin. After four hours of spreading, N5KD cells appeared to form a lower number of focal adhesions than C6WT cells. There were also many and smaller focal contacts at the periphery of C6WT cells compared to the periphery of N5KD cells (Figure 3.1 C). Even after 16 hours of spreading, N5KD cells had only mature focal adhesions with stress fibers whereas C6WT cells had both focal adhesions with stress fibers and smaller focal contacts with lamellipodia and transverse arcs (Figure 3.1 C). The presence of clustered and mature focal adhesions at the periphery of N5KD cells suggests that the turnover of focal adhesions is affected by knockdown of NHE5 (Cleghorn et al., 2015; Ilić et al., 1995; Kaushik et al., 2014). Therefore, studying the trafficking of Intβ1, a component of focal adhesions, can provide insight on the dynamics of focal adhesions in C6WT and N5KD cells.

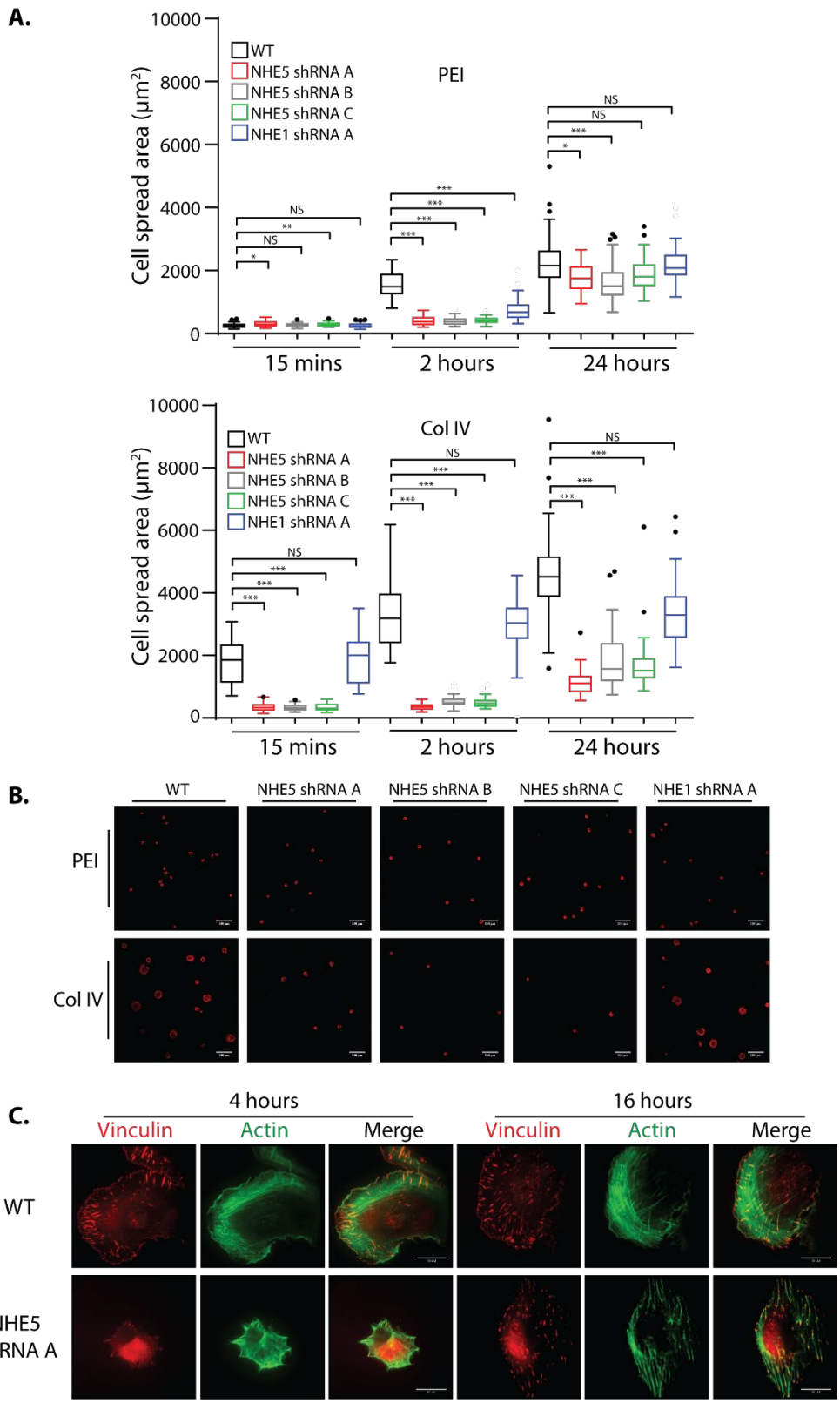
A.
PEI
Col IV
Cell spread area (μm²)
10000
8000
6000
4000
2000
0
WT
NHE5 shRNA A
NHE5 shRNA B
NHE5 shRNA C
NHE1 shRNA A
15 mins
2 hours
24 hours
NS
*
**
***
B.
WT
NHE5 shRNA A
NHE5 shRNA B
NHE5 shRNA C
NHE1 shRNA A
PEI
Col IV
C.
4 hours
16 hours
Vinculin
Actin
Merge
WT
NHE5 shRNA A

Figure 3.1 Spreading of C6 glioma cells on Col IV is affected by NHE5 knockdown.
(A) C6WT, three N5KD cell lines that express three different shRNAs against NHE5 mRNA, and a N1KD cell line that expresses shRNA against NHE1 mRNA were seeded on polyethyleneimine (PEI) (top) or collagen IV (Col IV) (bottom) coated coverslips and incubated for 15 minutes, 2 hours, or 24 hours. The spread area of 40 cells (randomly selected) was analyzed and the distribution is shown as box-and-whisker plots with the ends of the whiskers set at 1.5x interquartile range (IQR) above the third quartile and 1.5x IQR below the first quartile. Kruskal-Wallis tests with Dunn's test with Bonferroni correction for pairwise comparison were performed. (*p<0.05, **p<0.01, ***p<0.001, NS= not significant)
(B) Representative confocal images of C6WT, N5KD and N1KD cells seeded on PEI or Col IV coated coverslips and incubated at 37°C for 15 minutes. Actin is visualized using fluorescence-conjugated phalloidin. Scale bar = 100 μm.
(C) Representative total internal reflection fluorescence images of C6WT and N5KD cells seeded onto Col IV coated coverslips and incubated at 37°C for 4 hours or 16 hours. Vinculin is visualized with red fluorescence and actin is visualized with green fluorescence. Scale bar = 20 μm.

3.3 Intβ1 expression at the cell surface is reduced in NHE5-knockdown cells

The small spread area and small numbers of focal adhesions in N5KD cells raise the question of whether Intβ1 is properly targeted to the cell surface when NHE5 expression is depleted. Therefore, I performed a cell surface biotinylation assay (outlined in Figure 3.2 A) to detect Intβ1 on the plasma membrane. The abundance of protein at the plasma membrane is measured by the signal intensity from the pulldown samples. Thus, N5KD cells had less Intβ1 at the cell surface than C6WT cells (Figure 3.2 B). On the other hand, the cell surface abundance of sodium-potassium ATPase (NKA), a resident protein at the plasma membrane, was found to be similar between C6WT and N5KD cells. This result suggests that at a steady-state, knockdown of NHE5 affects the abundance of Intβ1, but not NKA on the cell surface.

Reduced expression of Intβ1 on the cell surface suggests that the trafficking of Intβ1 to the cell surface is affected by NHE5 knockdown. The defect in the targeting of Intβ1 to the cell surface could be due to a difference in the rate of biosynthesis, endocytosis of Intβ1 from cell surface, recycling of Intβ1 to the cell surface and/or degradation of Intβ1.

3.4 NHE5 knockdown results in accumulation of internalized receptors

The first aim was to investigate whether internalization of Intβ1 is affected by NHE5 knockdown. Because of the large size and fewer focal adhesions at the cell periphery of N5KD cells, I hypothesized that the internalization of Intβ1 in N5KD cells is slower than that of C6WT cells. To test this hypothesis, I performed a cell-surface biotinylation-based internalization assay as described in section 2.10 (see also Figure 3.3). Surprisingly, there was almost twice as much internalized Intβ1 in N5KD cells than in C6WT cells (Figure 3.4 A-B). A similar result was observed with transferrin receptors, where there was approximately 180% of internalized transferrin receptors (TfR) in N5KD cells relative to the C6WT cells.

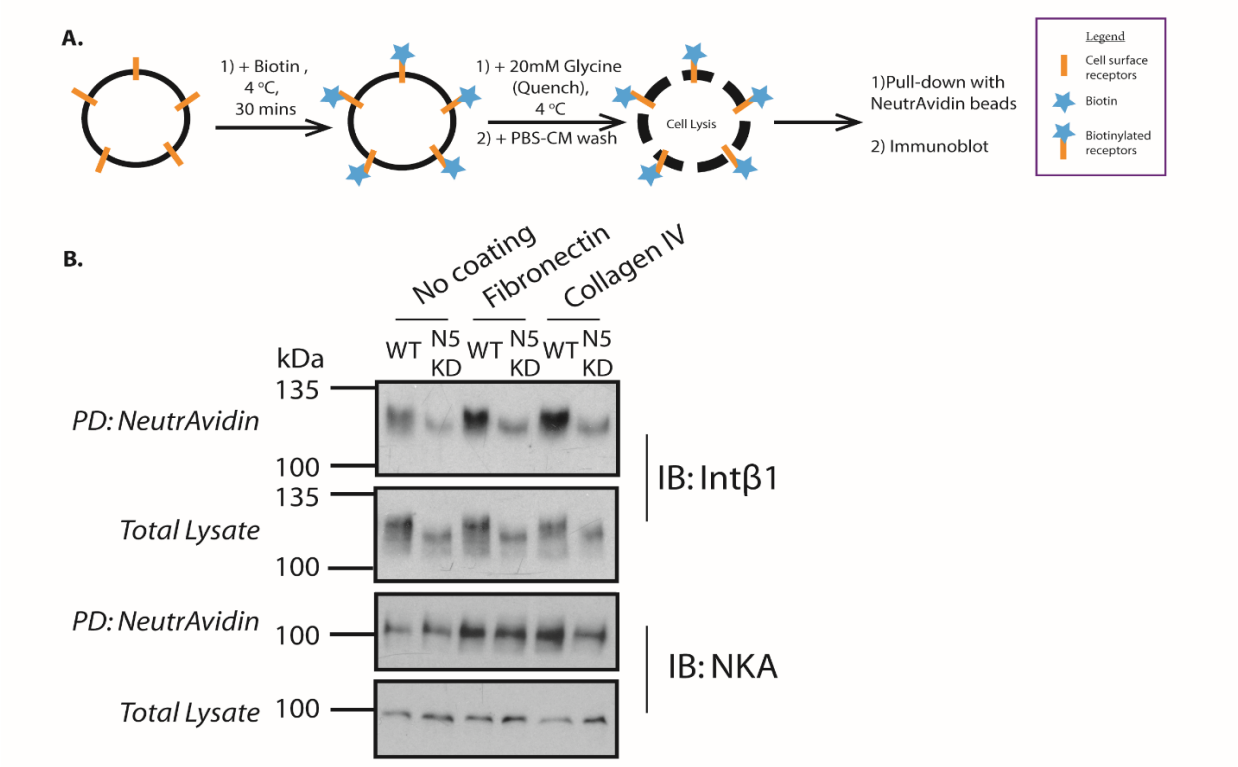

Figure 3.2 The surface population of Intβ1 is lower in NHE5-knockdown cells compared to WT cells at steady state.
(A) A schematic diagram of the cell-surface biotinylation assay (see section 2.9). Cell-surface biotinylation and the following affinity purification by NeutrAvidin agarose beads were used to label and purify the cell surface proteins.
(B) Surface population of integrin β1 (Intβ1) and sodium-potassium ATPase (NKA) in C6 wildtype (WT) and NHE5-knockdown (N5 KD) cells. Cells were grown on uncoated, fibronectin-coated or collagen IV-coated plates. *PD: NeutrAvidin* represents the biotin-labelled proteins that were affinity purified using NeutrAvidin agarose beads and *Total Lysate* represents the 5 µg of the cell lysates that were not subjected to affinity purification. Samples were immunoblotted for Intβ1 and NKA. This is a representative blot of two independent trials.

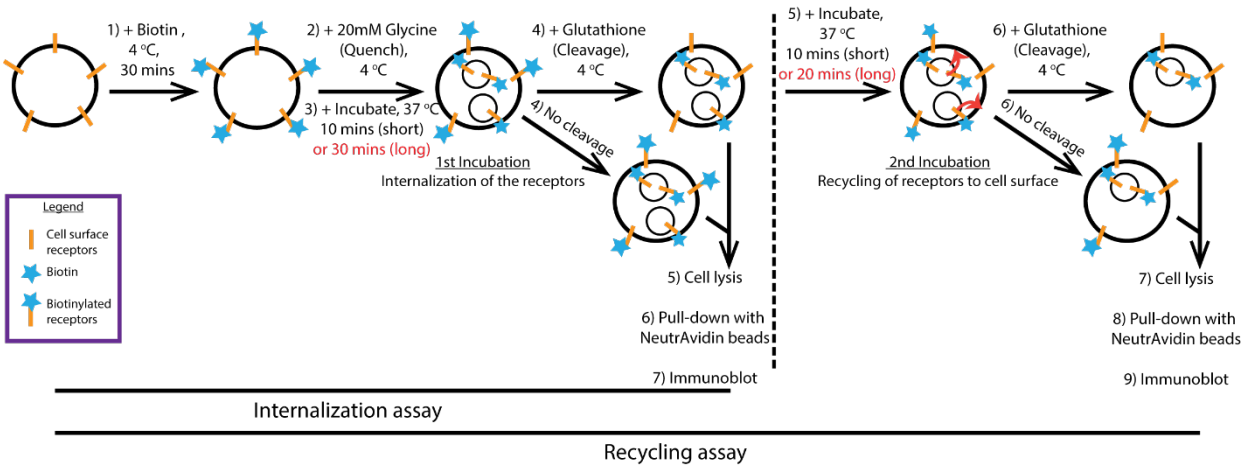

Figure 3.3 A schematic diagram of the internalization and recycling assays.
The experimental procedures of cell-surface biotinylation-based internalization (see section 2.2.10) and recycling assays (see section 2.2.11) are illustrated. The time points in black and red represent the duration used in the short- and long-incubation recycling assays, respectively.

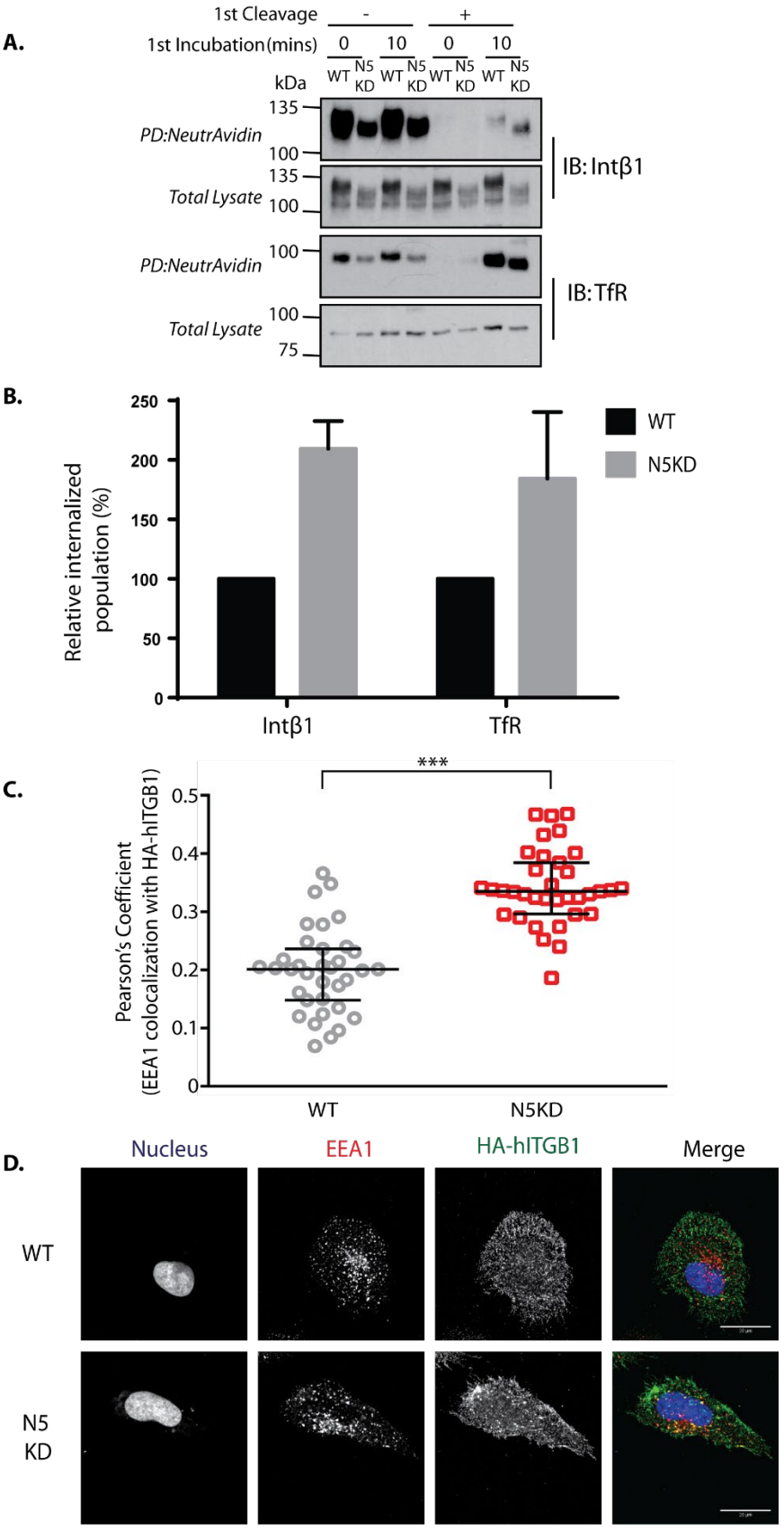
A.
1st Cleavage
-
+
1st Incubation (mins)
0
10
0
10
WT
N5 KD
kDa
135
PD:NeutrAvidin
100
IB: Intβ1
Total Lysate
PD:NeutrAvidin
IB: TfR
Total Lysate
75
B.
Relative internalized population (%)
250
200
150
100
50
0
WT
N5KD
Intβ1
TfR
C.
***
Pearson's Coefficient (EEA1 colocalization with HA-hITGB1)
0.5
0.4
0.3
0.2
0.1
0
WT
N5KD
D.
Nucleus
EEA1
HA-hITGB1
Merge
WT
N5 KD

Figure 3.4 The internalized population of Intβ1 is higher in NHE5-knockdown cells than in C6WT cells.

(A) A representative blot of the internalization assays performed as indicated in Figure 3.3. The semi-confluent C6 wildtype (WT) and NHE5-knockdown (N5KD) cells were grown on fibronectin (FN)-coated plastic plates and incubated with a membrane-impermeable biotinylating agent at 4°C, followed by quenching of unreacted biotinylating agent, and incubation at 37°C for 0 (0') and 10 minutes (10'). The cells were either subjected (+) or not subjected (-) to cell-impermeable cleavage buffer that removes the labelled biotin from the cell surface proteins. The biotin-labelled proteins in the cell lysates that were affinity purified using NeutrAvidin agarose beads (*PD: NeutrAvidin*) and approximately 6 µg of cell lysates that were not subjected to the pulldown (*Total Lysate*) were immunoblotted for integrin β1 (Intβ1) and transferrin receptor (TfR).

(B) Densitometry analysis of the internalization assay. Firstly, the ratio of the signal intensity from *PD: NeutrAvidin* samples to their corresponding total lysate was estimated. This calculated ratio was used in the following equation to calculate the percentage of respective internalized receptors: [10' (+) - 0' (+)]/ 10' (-), in which (+) indicates with cleavage and (-) indicates without cleavage samples. The relative percentage of internalized Intβ1 and TfR were obtained by normalizing the calculated percentage of respective internalized receptors to the values of the control cells (C6WT). The graph shows the mean and SEM of four independent trials.

(C) The graph shows the Pearson's coefficient of colocalization between HA-tagged human integrin β1 (HA-hITGB1) and early endosome antigen 1 (EEA1) in C6WT and N5KD cells. Cells stably expressing inducible HA-hITGB1 were grown overnight on FN-coated coverslips with doxycycline induction, labelled with anti-HA antibody at 4°C for 45 minutes, and incubated at 37°C for 10 minutes prior to fixation with 3% PFA. The cells were stained for anti-EEA1 and anti-HA antibodies. Colocalization between HA-hITGB1 and EEA1 was analyzed in approximately 30 cells and the Pearson's coefficient of each cell is plotted. Median and the interquartile range are shown. (***$p<0.001$; Mann-Whitney test; A representative of two independent experiments).

(D) Representative confocal images of the antibody feeding assay that was quantified in **(C)**. The nucleus, EEA1, and HA-hITGB1 of both C6WT and N5KD cells with inducible HA-hITGB1 were labelled in blue, red, and green, respectively. Scale bars = 20 µm.

Next, I wanted to use immunofluorescence microscopy to further confirm the results from biochemical internalization assays. Toward this goal, I first established C6WT and N5KD cells stably expressing a construct of human Intβ1 with HA-tag at its N-terminus (HA-hITGB1) under a tetracycline-inducible promoter. According to amino acid sequence analysis and crystal structure of the extracellular fragment of α5β1 integrin, the N-terminal position where I inserted the HA-tag falls in the PSI domain of Intβ1 subunit (Hynes, 2002; Nagae et al., 2012). As such, the HA-tag is expected to be exposed to the extracellular space, hence can be used to perform antibody-feeding assays. Interestingly, another study too showed that it is possible to tag at the N-terminus of Intβ1 without disrupting the function of the receptor (Huet-Calderwood et al., 2017).

Prior to using the newly generated cell lines for an antibody-feeding assay, I performed a series of immunofluorescence microscopy to confirm that the subcellular localization of the HA-hITGB1. Firstly, I performed an immunofluorescence experiment to determine the colocalization between HA-hITGB1 and the well-established C-terminus GFP-tagged human Intβ1 (hITGB1-GFP). Although there was a significant staining of HA-hITGB1 inside the cell that looks like the ER, there was a population of HA-hITGB1 at the cell surface which colocalized with hITGB1-GFP in both C6WT and N5KD cells (Figure 3.5 A). To further confirm that HA-hITGB1 is targeted to focal adhesions sites, I performed an immunofluorescence experiment by co-staining HA-hITGB1 with vinculin. There was colocalization between HA-hITGB1 and vinculin, indicating that HA-hITGB1 is indeed being targeted to focal adhesions at the cell surface (Figure 3.5 B). A cell-surface biotinylation assay also was done to confirm that the HA-hITGB1 is targeted to cell surface (see section 4.3, Figure 4.2 C). These results together suggest that the N-terminally HA-tagged hITGB1 is targeted to the correct the subcellular localization.

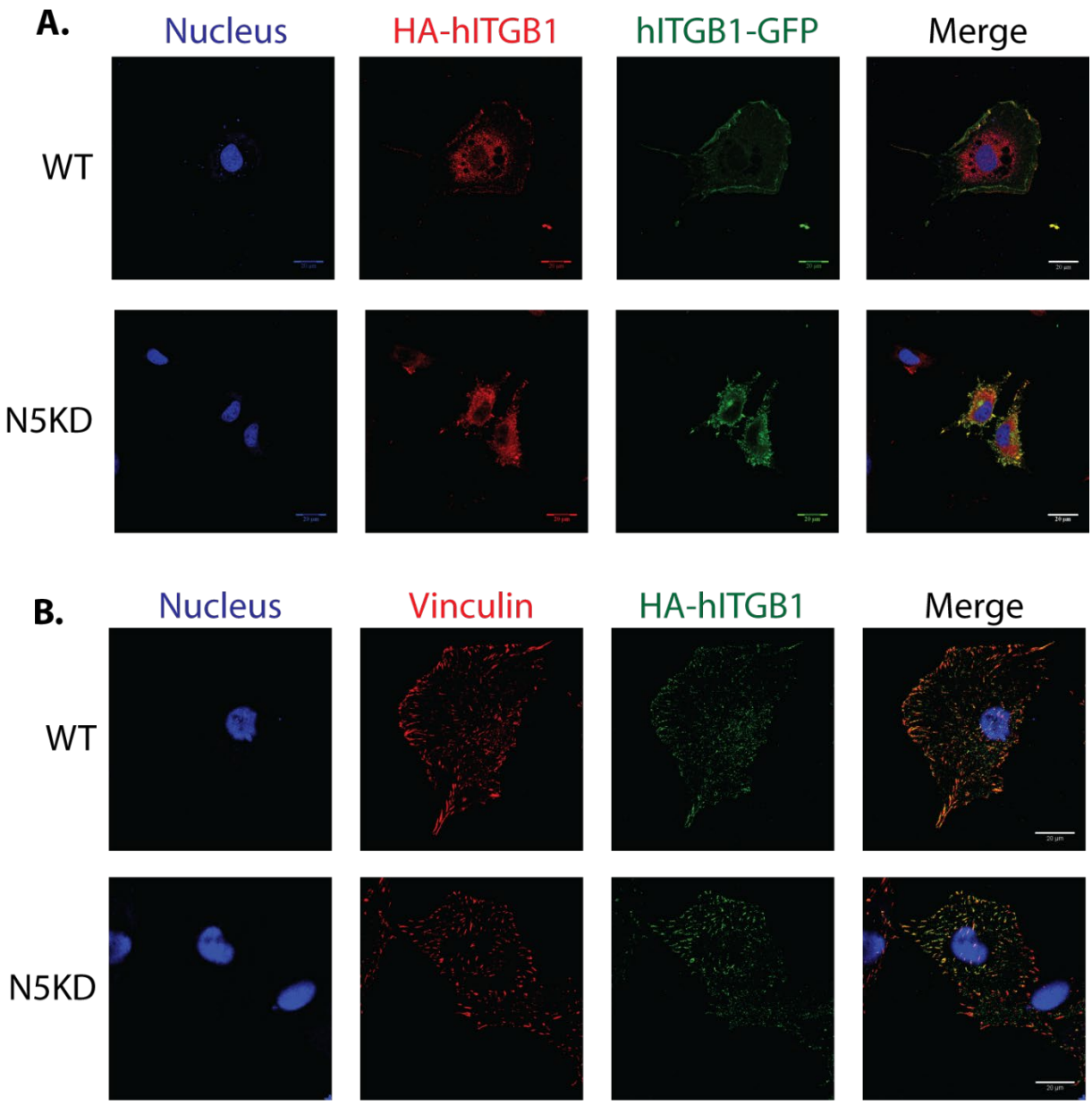
A.
Nucleus
HA-hITGB1
hITGB1-GFP
Merge
WT
N5KD
B.
Nucleus
Vinculin
HA-hITGB1
Merge
WT
N5KD

Figure 3.5 Human Intβ1 with HA-tag at its N-terminus is targeted to proper subcellular localization.
(A) C6 wildtype (WT) and NHE5-knockdown (N5KD) cells stably expressing inducible human Intβ1 with HA-tag at its N-terminus (HA-hITGB1) were transiently transfected with human Intβ1 with C-terminally tagged GFP (hITGB1-GFP). HA-hITGB1 expression was induced by adding 200 ng/mL of doxycycline overnight, followed by fixing with 3% PFA, and staining for the nucleus (blue), HA-hITGB1 (red), and hITGB1-GFP (green). The colocalization between N-terminally tagged HA-hITGB1 and C-terminally tagged hITGB1-GFP in the cells was observed. The presence of yellow colored pixels in the merged panel indicates the colocalization.
(B) HA-hITGB1 expression was induced by adding 200 ng/mL of doxycycline overnight. Cells were fixed and stained for nucleus (blue), vinculin (red), and HA-hITGB1 (green). The colocalization between HA-hITGB1 and vinculin, a marker for focal adhesions, in the cells was determined qualitatively by observing the presence of yellow pixels in the merged panel.

Following this, I performed an antibody-feeding assay (see section 2.6.3) to determine the colocalization between surface-labelled HA-hITGB1 and EEA1, an early endosomal marker, after 10 minutes of internalization at 37°C. I used Pearson's coefficient as a measure of colocalization between these two proteins. The coefficient value, indirectly, indicates the degree of internalization of HA-hITGB1. There was a higher degree of colocalization between HA-hITGB1 and EEA1 after 10 minutes of internalization in N5KD cells than there was in C6WT cells (Figure 3.4 C-D). These microscopic results were consistent with the results obtained from the cell-surface biotinylation-based internalization assay. In brief, both biochemical and immunofluorescence approaches showed that there is a larger internalized population of Intβ1 in N5KD cells comparing to C6WT cells. These results were unexpected and against my initial hypothesis whereby N5KD cells have slower endocytosis of Intβ1.

3.5 Recycling of Intβ1 is reduced by NHE5 knockdown

There are two possibilities for the apparent increase in the internalized populations of Intβ1 and TfR in N5KD cells: (1) internalization of these receptors is enhanced by N5KD or (2) recycling of these receptors to the cell surface is impaired by the depletion of NHE5 expression. I postulated that the second possibility is more likely to be the case because previous studies have shown that when recycling of Intβ1 is inhibited, there is an accumulation of endocytosed Intβ1 in the cells, which is similar to my observation (Arjonen et al., 2012; Nguyen et al., 2017). Moreover, NHE5 was shown to modulate recycling of other receptors such as TrkA and c-Met (Diering et al., 2013; Fan et al., 2016). Therefore, I performed cell-surface biotinylation-based recycling assays as described in section 2.11 (see also Figure 3.3) to test this hypothesis.

After observing that 10 minutes of internalization at 37°C leads to an accumulation of Intβ1 and TfR in the cells, I postulated that 10 minutes is sufficient for the receptors to be recycled. Hence, I performed a short-incubation recycling assay (outlined in Figure 3.3). After internalizing the biotin-labelled receptors for 10 minutes and performing the first post-incubation cleavage to remove biotin from non-internalized receptors, the cells were incubated again for 10 minutes at 37°C to allow recycling of these labelled receptors back to the cell surface. Then, a second post-incubation cleavage was performed to remove biotin from the receptors that had been recycled to the cell surface, leaving only the non-recycled receptors inside the cells labelled with biotin. These biotinylated receptors were pulled down by NeutrAvidin beads upon cell lysis.

Efficient recycling of receptors results in a decreased signal intensity in the pulldown samples after the second post-incubation cleavage. The signal intensity of the biotinylated Intβ1 and TfR in pulldown samples after the second post-incubation cleavage was higher in N5KD cells than in C6WT cells (Figure 3.6 A), indicating that recycling of these receptors is reduced by the knockdown of NHE5. Densitometry analysis in Figure 3.6 B shows that the relative recycling populations of Intβ1 and TfR were markedly diminished in N5KD cells to approximately 54% and 45% of those in C6WT cells, respectively. This observation suggests that increased internalization of Intβ1 and TfR in N5KD cells is due to reduced recycling of these receptors to the plasma membrane.

However, these results were not consistent with previous findings, where recycling of TfR was not influenced by NHE5 knockdown (Diering et al., 2013; Fan et al., 2016). I used 10 minutes periods to internalize and recycle the receptors, whereas previous studies took 30 minutes for internalization and 20 minutes for recycling. Thus, I reasoned that the discrepancy in the recycling results could be due to the difference in the incubation periods used in the assay. I, therefore performed a long-incubation recycling assay (outlined in Figure 3.3) to determine whether different incubation periods in this assay could lead to different results. After the internalization of the receptors for 30 minutes at 37°C, the second incubation was carried out at 37°C for 20 minutes to facilitate recycling of these receptors. The result from long-incubation recycling assays showed that the relative recycling populations of Intβ1 and TfR in N5KD cells to C6WT cells were ~77% and ~76%, respectively (Figure 3.6 C-D). This result demonstrates that the difference in the recycling of Intβ1 and TfR between C6WT and N5KD cells becomes less apparent with longer incubation periods.

A.

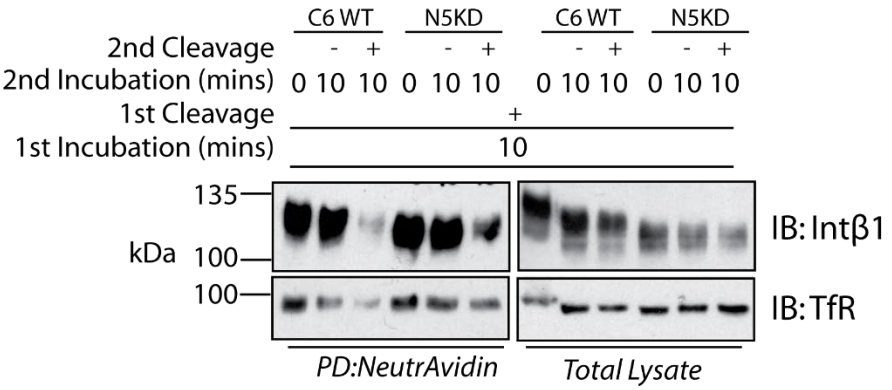
C6 WT
N5KD
C6 WT
N5KD
2nd Cleavage
- + - + - + - +
2nd Incubation (mins)
0 10 10 0 10 10 0 10 10 0 10 10
1st Cleavage
+
1st Incubation (mins)
10
135
kDa
100
100
IB: Intβ1
IB: TfR
PD:NeutrAvidin
Total Lysate

B.

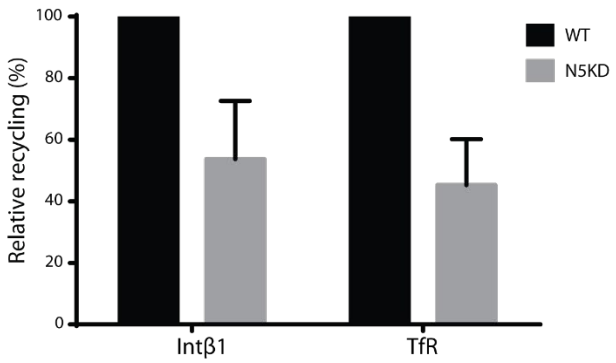
Relative recycling (%)
100
80
60
40
20
0
WT
N5KD
Intβ1
TfR

C.

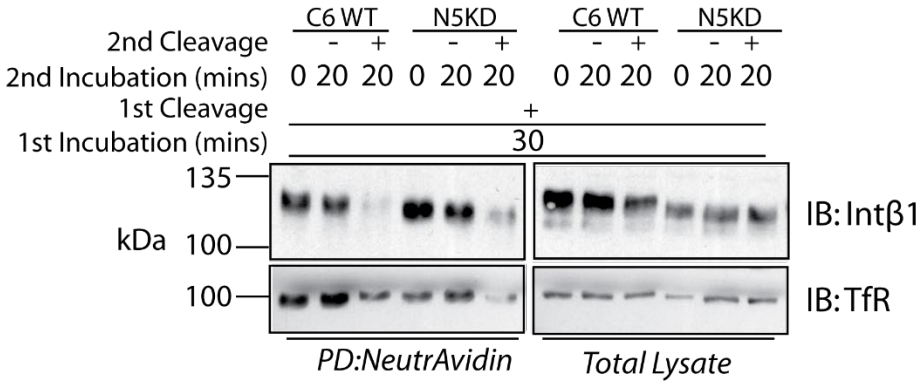
C6 WT
N5KD
C6 WT
N5KD
2nd Cleavage
- + - + - + - +
2nd Incubation (mins)
0 20 20 0 20 20 0 20 20 0 20 20
1st Cleavage
+
1st Incubation (mins)
30
135
kDa
100
100
IB: Intβ1
IB: TfR
PD:NeutrAvidin
Total Lysate

D.

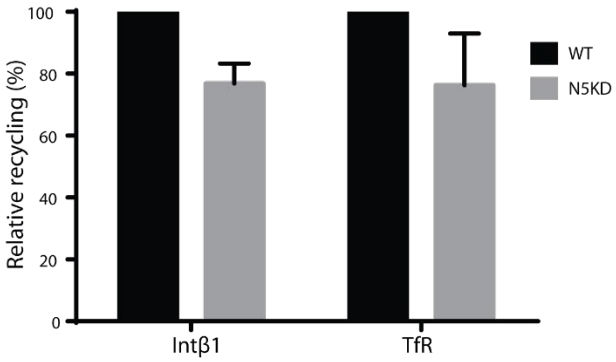
Relative recycling (%)
100
80
60
40
20
0
WT
N5KD
Intβ1
TfR

Figure 3.6 Intβ1 recycling to the cell surface is reduced by NHE5 knockdown.
(A) A representative blot of the short-incubation recycling assays that were performed as illustrated in Figure 3.3. C6 wildtype (WT) and NHE5-knockdown (N5KD) cells were grown on FN-coated plates, labelled with a membrane-impermeable biotinylating reagent, incubated at 37°C for 10 minutes (10') for internalization, and treated with cleavage buffer to remove biotin from the non-internalized cell surface proteins. A second incubation at 37°C was conducted for 0 (0') and 10 minutes (10'), followed by either a cell lysis (-) or second post-incubation cleavage (+) to strip biotin from the proteins that had recycled to cell surface prior to cell lysis. Biotin-labelled proteins in the cell lysates that were affinity purified using NeutrAvidin agarose beads (*PD: NeutrAvidin*) and approximately 6 µg of cell lysates that were not subjected to the pulldown (*Total Lysate*) were immunoblotted for integrin β1 (Intβ1) and transferrin receptor (TfR).
(B) Densitometric analysis of short-incubation recycling assays. First, the ratio of the signal intensity of pulldown samples (*PD: NeutrAvidin)* to that of the corresponding total lysate was calculated. The calculated value was used in the following equation to quantify the ratio of the recycled Intβ1 and TfR: [1- (10' (+)/ 10' (-))], in which (+) indicates the samples with the second post-incubation cleavage and (-) indicates the samples without the second post-incubation cleavage. The relative recycling percentage of Intβ1 and TfR was obtained by normalizing their recycled ratio to the values of the C6WT cells. The graph shows the mean and SEM of four independent trials.
(C) A representative blot of the long-incubation recycling assays that were performed as illustrated in Figure 3.3. It was conducted similar to short-incubation recycling assays in **(A)** except that the first and second incubations at 37°C were done for 30 minutes (30') and 20 minutes (20'), respectively. See details in section 2.11.2.
(D) Densitometric analysis of long-incubation recycling assays was conducted as in (B) and the ratios of the recycled Intβ1 and TfR were calculated as the following equation: [1- (20' (+)/ 20' (-))]. The graph shows the mean and SEM of three independent trials.

3.6 Degradation of surface-labelled Intβ1 is increased in NHE5-depleted cells

Internalized receptors are generally either recycled back to the plasma membrane or degraded via lysosomal pathway. Böttcher et al. (2012) demonstrated that when the recycling of Intβ1 was reduced, its stability also decreased. Hence, I wanted to investigate whether the degradation of Intβ1 is influenced by NHE5. To study the degradation rate of surface-biotinylated Intβ1 between C6WT and N5KD cells, I performed cell-surface biotinylation-based degradation assay (illustrated in Figure 3.7 A). The degradation of cell surface-biotinylated Intβ1 was enhanced in N5KD cells and the half-life of Intβ1 in N5KD cells and C6WT cells was about 6 hours and 18 hours, respectively (Figure 3.7 B-C). This observation suggests that the depletion of NHE5 accelerates the degradation of Intβ1, possibly by decreasing the recycling of this receptor. The decrease in the cell surface abundance of Intβ1 in N5KD cells is possibly due to the increased degradation of Intβ1 in N5KD cells.

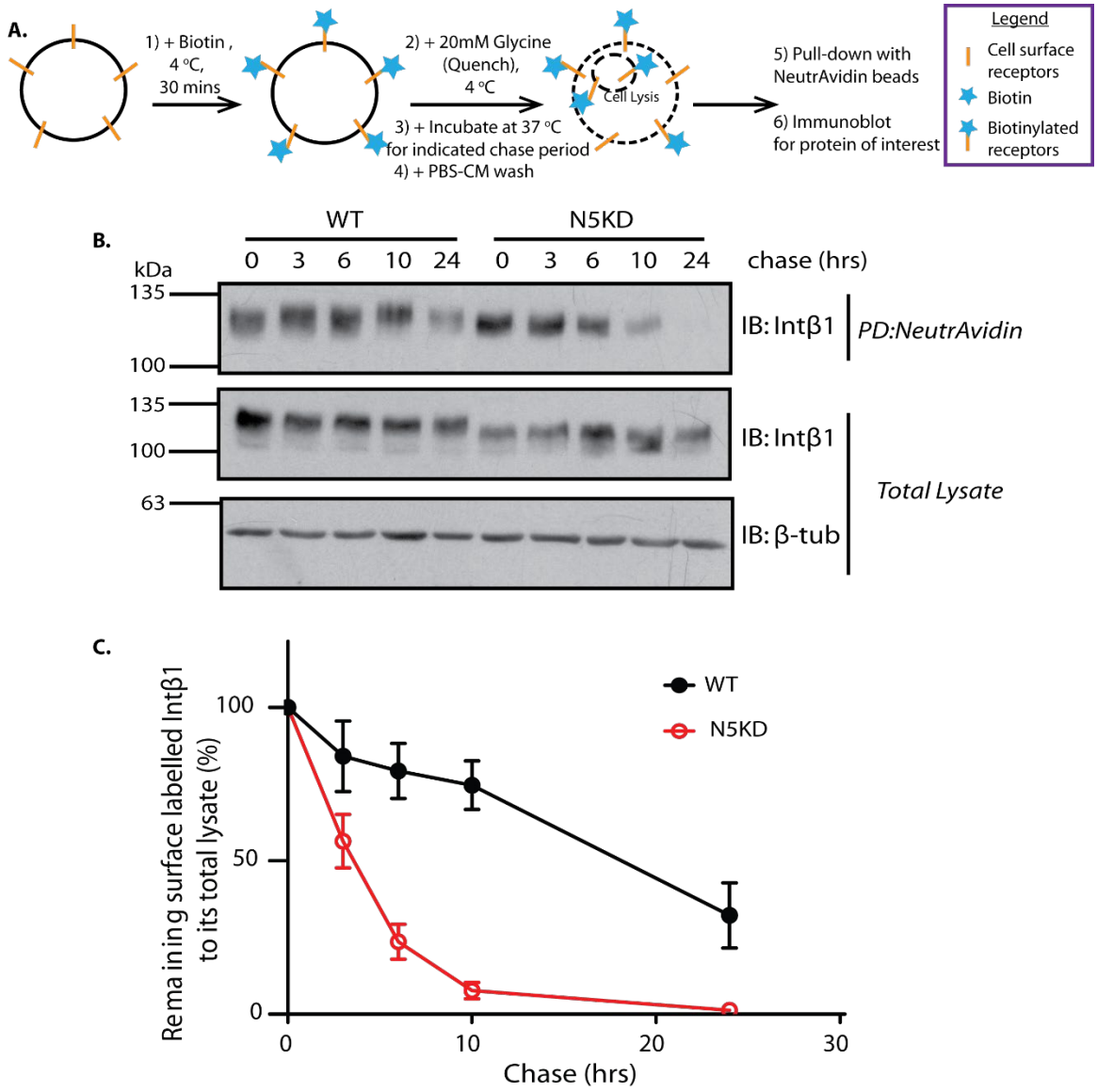

Figure 3.7 The degradation of Intβ1 is enhanced by NHE5 knockdown.
(A) A schematic illustration of the cell-surface biotinylation-based degradation assay (see section 2.12) to study the stability of the biotin-labelled integrin β1 (Intβ1).
(B) A representative blot of degradation assays. The biotin-labelled proteins in the cell lysates were affinity purified using NeutrAvidin agarose beads (*PD: Neutravidin*) and immunoblotted for Intβ1. Approximately 6 µg of cell lysates that were not subjected to pulldown (*Total Lysate*) was immunoblotted separately for Intβ1 and beta tubulin (β tub).
(C) Densitometric analysis of the degradation assays of the surface-labelled Intβ1. First, the ratio between the signal intensity of the pulldown samples (*PD: Neutravidin)* and its corresponding total lysate was calculated. The calculated ratio was plotted as the percentage of the remaining surface-labelled Intβ1 to its total lysate relative to the values of the ratio at chase time of 0 hours. The graph shows the mean and SEM of seven independent experiments.

Chapter 4: The role of NHE5 in the sialylation of Intβ1

4.1 Introduction

In addition to the defect in cell adhesion, we observed a decrease in the apparent molecular weight of Intβ1 when NHE5 was knocked down in C6 glioma cells. Using various enzymatic digestion assays, we found that NHE5 influences the sialylation of Intβ1. In this chapter, my aim is to investigate the role of NHE5 in Intβ1 sialylation.

Sialylation is the last step in glycosylation and it occurs in the TGN during protein biosynthesis. Interestingly, a study showed that desialylated transferrin receptor from the plasma membrane is resialylated during its endocytic recycling (Snider and Rogers, 1985). This observation is the first to indicate that sialylation of certain cell surface proteins can occur during their recycling. Moreover, we identified Vps29 as a potential NHE5 binding partner through screening a human brain cDNA library by a yeast two-hybrid assay and preliminarily verified by Co-IP experiments (unpublished observations). Vps29 is a component of the retromer complex that retrieves cargoes from endosomes to the TGN (Burd and Cullen, 2014; Haft et al., 2000). A recent study showed that cell-surface Intβ1 undergoes retrograde trafficking to the TGN, before being recycled back to the plasma membrane (Shafaq-Zadah et al., 2016).

Taken together, I hypothesize that the sialylation of Intβ1 occurs via two pathways, the canonical secretory pathway and the retrograde trafficking, and propose that, NHE5 regulates Intβ1 sialylation by regulating the retrograde trafficking of Intβ1. I termed the sialylation of Intβ1 during the retrograde trafficking ‘extra-sialylation’ to distinguish it from the sialylation occuring during *de novo* synthesis.

4.2 Knockdown of NHE5 affects Intβ1 sialylation

When C6WT, N5KD cells and N1KD cell lysates were immunoblotted for Intβ1, the apparent molecular weight of Intβ1 was found to be smaller in all three N5KD cells than C6WT and N1KD cells (Figure 4.1 A). I postulated that NHE5 regulates the size of Intβ1 by influencing the glycosylation of the protein. This is because glycosylation is a pH-dependent process and is one of the major post-translational modifications of Intβ1 since it was shown to be glycosylated at least 10 N-glycosylation acceptor sites (Axelsson et al., 2001; Maeda et al., 2008; Seales et al., 2005b). Since oligosaccharides are added to asparagine residues of Intβ1 (Janik et al., 2010), and thus to determine whether glycosylation is affected by NHE5 knockdown, I treated the cell lysates with PNGase F, an enzyme that hydrolyzes all the sugar chains added to the asparagine residues of the glycoproteins, and examined the effect on the apparent molecular weight of Intβ1 (Tarentino and Plummer Jr, 1993). Upon PNGase F digestion, the differences between the apparent molecular weight of Intβ1 from both C6WT and N5KD cells disappeared and they shifted to about 85kDa, the predicted molecular weight of Intβ1 based on its amino-acid sequence (Figure 4.1 B) (Seales et al., 2003). Since the molecular weight of de-glycosylated Intβ1 is the same between WT and N5KD cells, it suggests that N-glycosylation of Intβ1 is affected by NHE5 knockdown. The next question is which step(s) of glycosylation is (are) affected by NHE5 depletion since glycosylation of Intβ1 is a diverse and multi-step process (Janik et al., 2010).

I began testing a hypothesis wherein the sialylation of Intβ1 is regulated by NHE5. This is because Intβ1 sialylation occurs in the TGN, which is in the close proximity of recycling endosomes where NHE5 localizes, and the activity of sialyltransferase is pH-dependent (Condon et al., 2013; Kitazume, 2014; Snider and Rogers, 1985). Moreover, there is evidence suggesting that hypersialylation of Intβ1 enhances adhesion and motility of cancer cells (Isaji et al., 2014; Seales et al., 2003, 2005a). This is in agreement with our previous finding, where knockdown of NHE5 decreased adhesion and migration of C6 glioma cells (Fan et al., 2016).

A.

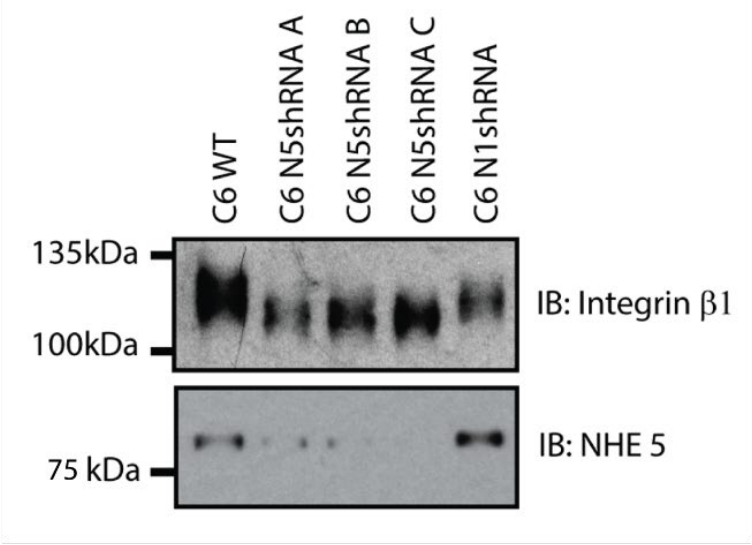
C6 WT
C6 N5shRNA A
C6 N5shRNA B
C6 N5shRNA C
C6 N1shRNA
135kDa
100kDa
IB: Integrin β1
75 kDa
IB: NHE 5

B.

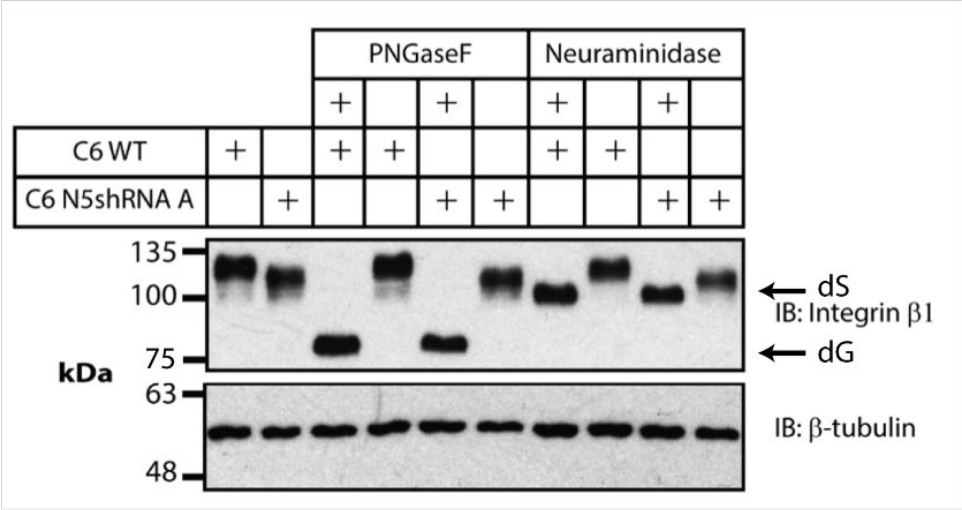
PNGaseF
Neuraminidase
C6 WT
C6 N5shRNA A
135
100
75
kDa
63
48
dS
IB: Integrin β1
dG
IB: β-tubulin

C.

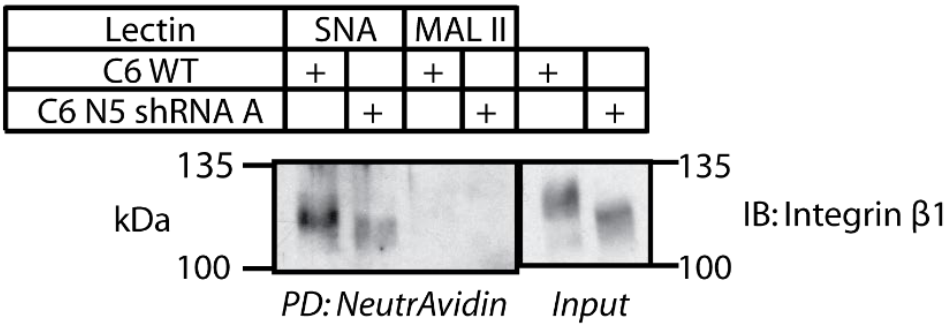
Lectin
SNA
MAL II
C6 WT
C6 N5 shRNA A
135
kDa
100
135
100
IB: Integrin β1
PD: NeutrAvidin
Input

Figure 4.1 Knockdown of NHE5 affects the sialylation of Intβ1.
(A) Immunoblot of Intβ1 and NHE5. Lysates were extracted from C6WT, three different N5KD cells (C6 N5 shRNA), and N1KD cells (C6 N1 shRNA) and probed with anti-Intβ1 and NHE5 antibodies. This is a representative blot of three independent experiments.
(B) Lysates isolated from C6WT and N5KD cells were treated with or without PNGase F and neuraminidase for 30 minutes at 37°C and Intβ1 and β-tubulin were characterized by immunoblot. This is a representative blot of three independent experiments. dG: Deglycosylated; dS: Desialylated.
(C) Lysates isolated from C6WT and N5KD cells were treated with either biotinylated *Sambucus Nigra* (Elderberry Bark) lectin (SNA), or biotinylated *Maackia Amurensis* lectin II (MAL II), followed by pulldown with NeutrAvidin agarose beads at 4°C (*PD:NeutrAvidin*). Approximately 6 μg of the cell lysates that were not subjected to the incubation with biotinylated lectins and the following pulldown were included as *(Input)*. Samples were resolved in SDS-PAGE and immunoblotted for Intβ1. This is a representative blot of three independent experiments.

To test whether the sialylation of Intβ1 is affected by NHE5 knockdown, cell lysates isolated from C6WT and N5KD were treated with neuraminidase, an enzyme that hydrolyzes sialic acids from glycoproteins. Upon neuraminidase treatment, the apparent molecular weight of Intβ1 in C6WT and N5KD cells reduced to about 100 kDa (Figure 4.1 B), coinciding with the predicted size of desialylated Intβ1 (Isaji et al., 2014). This result suggests that NHE5 influences the sialylation of Intβ1.

Sialic acids are added either to the 3rd or 6th carbon of the terminal galactose of the N-glycans of glycoproteins, forming α2-3 or α2-6 linkages, respectively (Bellis, 2004; Schultz et al., 2012). To distinguish between these two types of sialylation, a class of proteins called lectins can be used. Lectins are capable of recognizing and binding to specific mono- and oligosaccharides on glycoproteins in a highly specific manner (Lis and Sharon, 1998). In the current experiment, I used the following biotinylated lectins: *Sambucus Nigra* (Elderberry) Bark (SNA) and *Maackia Amurensis* lectin II (MAL II), that recognize α2-6 and α2-3 sialylation, respectively, and performed lectin pull-down assays on the lysates extracted from C6 WT and N5KD cells. As predicted, Intβ1 was detected only when pulled down with SNA lectin, but not with MAL II since Intβ1 is known to be α2-6 sialylated (Figure 4.1 C) (Lee et al., 2010b; Seales et al., 2003). The lower intensity of α2-6 sialylated Intβ1 in N5KD cells compared to C6WT cells (Figure 4.1 C) further suggests that the knockdown of NHE5 affects α2-6 sialylation of Intβ1.

4.3 Exogenously expressed HA-hITGB1 in C6WT and NHE5-knockdown cells has sialylation and degradation patterns similar to the endogenous rat Intβ1

My next aim is to investigate the role of NHE5 in Intβ1 sialylation during its trafficking *i.e.* as it goes through the secretory and recycling pathways. For this purpose, inducible HA-hITGB1 cell lines (described in section 3.4) were established, which allowed us to synchronize the protein synthesis and trafficking of Intβ1 in C6WT and N5KD cells.

To ensure that the inducible system does not have leaky expression, I performed immunoblotting to detect the expression of HA-hITGB1 in C6WT and N5KD cells that were grown with and without doxycycline (Doxy). HA-hITGB1 was only expressed in the presence of the inducer, Doxy in both C6WT and N5KD cells (Figure 4.2 A), confirming that the inducible system is not leaky. The level of HA-hITGB1 expression increased with the increasing time of induction (Figure 4.2 A). Heterologously expressed HA-hITGB1 contains two bands, where the

upper band represents mature, sialylated HA-hITGB1 and the lower band represents immature, non-sialylated HA-hITGB1 (Figure 4.2 A-B). When HA-hITGB1 expression was induced for four and eight hours, followed by a chase-incubation in Doxy-free complete medium for 16 hours, the lower immature band was not detectable. This suggests that during chase-incubation, there is no *de novo* protein synthesis, and that the immature HA-hITGB1 has completely maturated (Figure 4.2 A). This result further suggests that the induced expression is tightly regulated by the inducer and leaky expression is negligible.

Moreover, the molecular weight of upper band, but not that of lower band of HA-hITGB1 was smaller in N5KD cells. Upon neuraminidase treatment, the upper band of HA-hITGB1 in both cell lines shifted down to the same position as the lower band (Figure 4.2 B). This result, similar to endogenous Intβ1, suggest that sialylation of HA-hITGB1 is a predominant step regulated by NHE5. To define the cell-surface targeting of HA-hITGB1, HA-hITGB1 expression was induced for various times (0-8 hours) and cell-surface biotinylation experiments were conducted (see Figure 3.2 A). After three hours of induction, HA-hITGB1 was detected on the cell surface (Figure 4.2 C), suggesting that three hours is sufficient for newly synthesized HA-hITGB1 to be targeted to the plasma membrane along the secretory pathway.

Furthermore, I evaluated the stability of HA-hITGB1 in C6WT and N5KD cells through pulse-chase experiments. Expression of HA-hITGB1 was first induced by Doxy for three hours, followed by chase incubation for indicated periods in Doxy-free medium, and the amount of HA-hITGB1 was detected by immunoblotting. The intensity of HA-hITGB1 band dissipated faster in N5KD cells than in C6WT cells during the chase period (Figure 4.2 D-E). This result suggests that the stability of HA-hITGB1 is decreased by the depletion of NHE5, similar to the endogenous rat Intβ1. Higher expression of HA-hITGB1 after five hours of chase compared to 0 hours of chase may be due to the lagging effect of protein synthesis after the removal of Doxy. The similar stability and sialylation pattern of heterologously expressed HA-hITGB1 with endogenous rat Intβ1 suggests that the inducible HA-hITGB1 expression system is suitable for investigating the role of NHE5 on Intβ1 sialylation and trafficking.

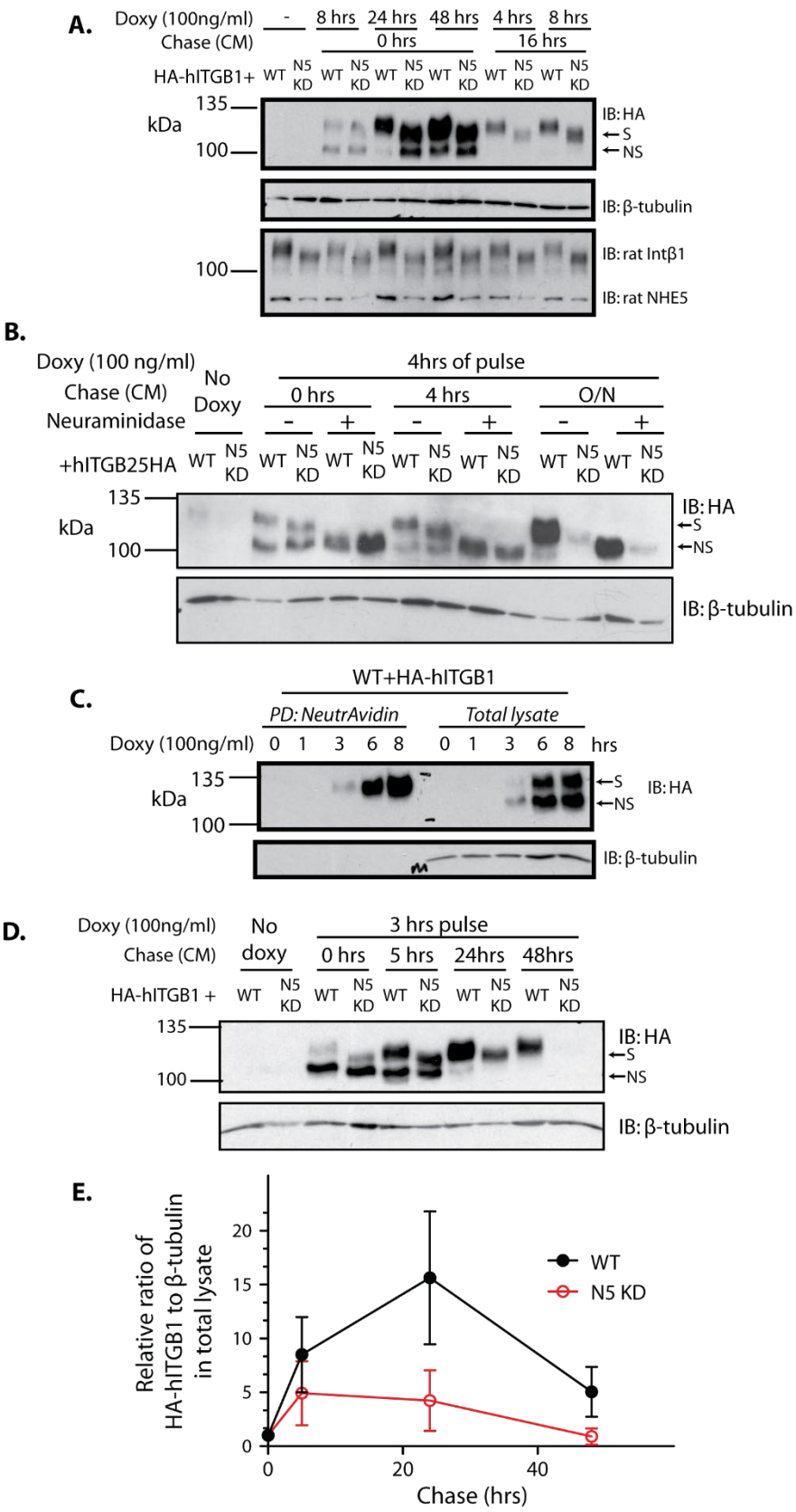
A.
Doxy (100ng/ml)
Chase (CM)
HA-hITGB1+
WT
N5 KD
8 hrs
24 hrs
48 hrs
4 hrs
8 hrs
0 hrs
16 hrs
135
100
kDa
IB: HA
S
NS
IB: β-tubulin
IB: rat Intβ1
IB: rat NHE5
B.
Doxy (100 ng/ml)
Chase (CM)
Neuraminidase
No Doxy
4hrs of pulse
0 hrs
4 hrs
O/N
+hITGB25HA
C.
WT+HA-hITGB1
PD: NeutrAvidin
Total lysate
0 1 3 6 8 0 1 3 6 8 hrs
D.
No doxy
3 hrs pulse
0 hrs
5 hrs
24hrs
48hrs
E.
Relative ratio of HA-hITGB1 to β-tubulin in total lysate
Chase (hrs)
WT
N5 KD

Figure 4.2 Sialylation and stability of exogenously expressed HA-tagged hITGB1 in C6WT and NHE5-knockdown cells.
(A) HA-hITGB1 expression was induced in C6 wildtype (C6WT) and NHE5-knockdown (N5KD) cells by adding 100 ng/mL of doxycycline (Doxy) to culture medium for indicated times and chased in Doxy-free complete medium (CM) for either 0 or 16 hours (hrs). Cells cultured in the absence of Doxy served as a negative control. Expression of HA-hITGB1, β-tubulin, endogenous rat Intβ1 and NHE5 were detected using immunoblotting. A preliminary result of one-time experiment is presented.
(B) HA-hITGB1 expression was induced in C6WT and N5KD cells by 100 ng/mL of Doxy for four hours, and the cells were subjected to chase incubation in the absence of Doxy for indicated times. The cell lysates were subjected to neuraminidase digestion for 60 minutes at 37°C prior to immunoblotting to detect HA-hITGB1 and β-tubulin. This is a representative blot of two experiments.
(C) HA-hITGB1 expression was induced in C6WT cells by 100 ng/mL of Doxy for indicated periods, and the cells were subjected to cell-surface biotinylation (see Figure 3.2 A). HA-hITGB1 and β-tubulin in biotinylated proteins (*PD:NeutrAvidin*) and approximately 5 µg of total cell lysates *(Total lysate)* were analyzed by immunoblotting. A preliminary result of one-time experiment is presented.
(D) HA-hITGB1 expression in C6WT and N5KD cells was induced in the presence of Doxy for three hours and then chased in Doxy-free complete medium for indicated times. The cell lysates were then immunoblotted to characterize HA-hITGB1 and β-tubulin. A representative result of three independent experiments is shown.
(E) Densitometry analysis of the pulse-chase experiment that was conducted as in **(D)**. First, the ratio of the signal intensity of HA-hITGB1 (both mature and immature bands) to its β-tubulin was calculated. These ratios were then normalized to the one at 0 hours chase.
NS: Non-sialylated; S: Sialylated.

4.4 Characterization of Intβ1 (HA-hITGB1) sialylation by synchronized trafficking assays in the presence of Brefeldin A

Brefeldin A (BFA) inhibits the transport of proteins from the ER to the Golgi apparatus (Lippincott-Schwartz et al., 1989), and serves as a useful tool to block the trafficking of newly synthesized HA-hITGB1 along the secretory pathway. Since the effect of BFA is reversible, upon BFA and Doxy washout, the trafficking of HA-hITGB1 in C6WT and N5KD cells beyond the ER to the rest of the secretory pathways can be synchronized. Thus, any changes in the apparent molecular weight of mature HA-hITGB1 in C6WT and N5KD cells can be traced during the chase.

My hypothesis is that NHE5 regulates 'extra-sialylation' of HA-hITGB1 that occurs during retrograde trafficking from early endosomes to the TGN. If this hypothesis is correct, then during the chase after BFA and Doxy treatment, the bands of mature HA-hITGB1 between these two cell lines should be briefly identical before it keeps increasing in C6WT cells (due to 'extra-sialylation'). However, this was not the case. Rather, a difference in the apparent molecular weight of mature HA-hITGB1 between C6WT and N5KD cells was observed as early as two hours of chase (Figure 4.3 A). In the presence of BFA (0 hours of chase), HA-hITGB1 was not sialylated as predicted and had the same apparent molecular weight in both C6WT and N5KD cells. After two hours of chase, mature and sialylated HA- hITGB1 was detected in both C6WT and N5KD cells (Figure 4.3 A-B). However, the apparent molecular weight of mature HA-hITGB1 in C6WT cells kept increasing from two hours to 24 hours of chase. Meanwhile, the apparent molecular weight of mature HA-hITGB1 in N5KD cells appeared relatively similar between two hours and 24 hours of chase (Figure 4.3 A). The use of BFA during induction of HA-hITGB1 expression is able to synchronize the trafficking of HA-hITB1 in C6WT and N5KD cells.

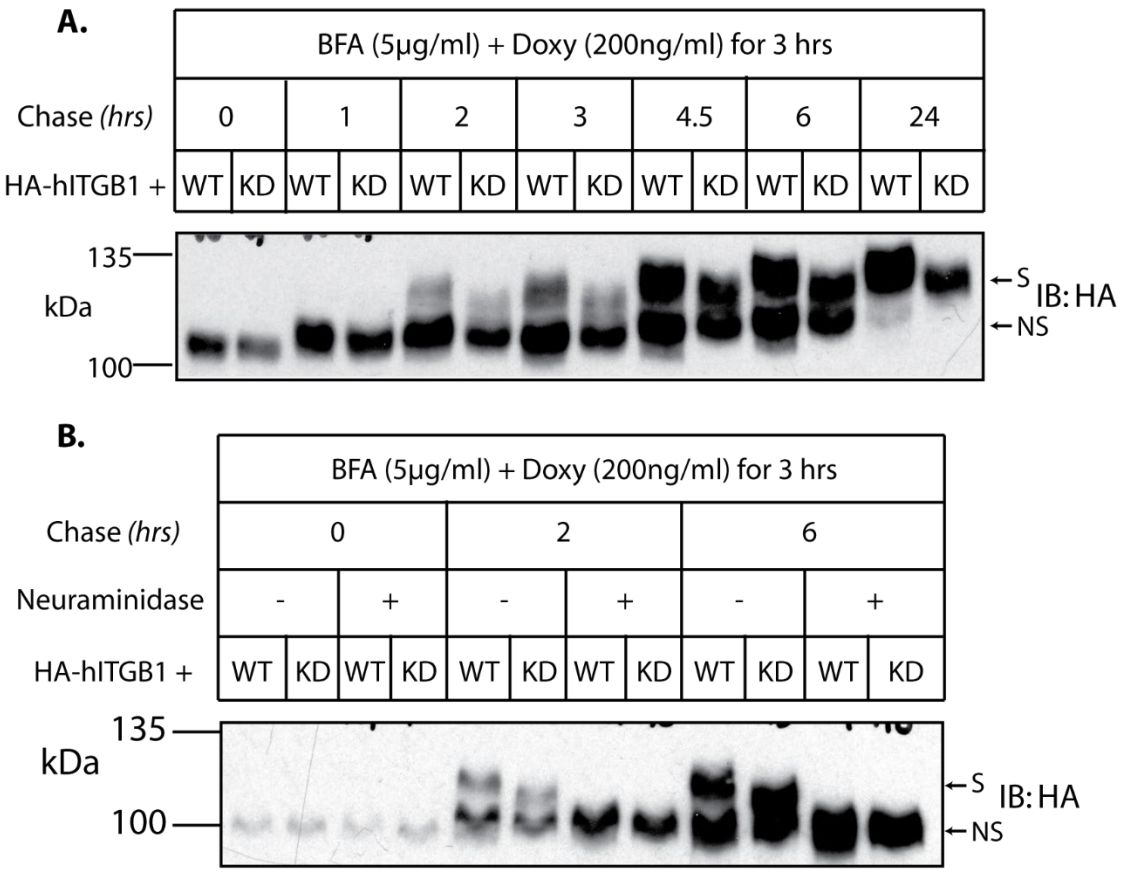

Figure 4.3 Synchronized trafficking of HA-hITGB1 in C6WT and NHE5-knockdown cells.
(A) HA-hITGB1 expression was induced in C6WT (WT) and N5KD (KD) cells by 200 ng/mL of doxycycline (Doxy) in the presence of 5 µg/mL of Brefeldin A (BFA) for three hours (hrs). The drugs were then washed out and the cells were chased in Doxy- and BFA-free complete medium for indicated periods. The presence and size of HA-hITGB1 were detected by immunoblotting. A representative blot of three independent experiments is shown.
(B) Experiment was carried out as in **(A)**. Cell lysates were digested with neuraminidase for 60 minutes at 37°C prior to immunoblotting for HA-hITGB1. A representative blot of three independent experiments is shown.
NS: Non-sialylated; S: Sialylated.

4.5 Retrograde trafficking from early endosomes to the TGN influences the sialylation of Intβ1

Although my previous experiment did not support the hypothesis that NHE5 regulates HA-hITGB1 'extra-sialylation', I designed another experiment to further test the involvement of NHE5 in the retrograde trafficking and 'extra-sialylation' of HA-hITGB1 by using (±)-2-(((5-methylthiophen-2-yl)-3-phenyl-2,3-dihydroquinazolin-4(1H)-one (Retro-2), a pharmacological inhibitor of retrograde trafficking (Park et al., 2012; Stechmann et al., 2010). Retro-2 mislocalizes syntaxin 5, syntaxin 6 and syntaxin 16, all of which are t-SNARE complexes at the TGN, and thus inhibits retrograde trafficking by preventing the fusion of vesicles from early endosomes to the TGN (Bock et al., 1997; Hay et al., 1998; Mallard et al., 2002; Stechmann et al., 2010; Tai et al., 2004). It is shown to be specific to retrograde trafficking because it does not affect the endocytosis of STxB and transferrin, the lysosomal degradation of EGF, the recycling of transferrin, or the anterograde trafficking of vesicular stomatitis virus glycoprotein (VSVG) (Stechmann et al., 2010). If the difference in the apparent molecular weight of mature HA-hITGB1 between C6WT and NHE5KD is due to 'extra-sialylation' of HA-hITGB1, then Retro-2 would prevent the 'extra-sialylation' of HA-hITGB1 by inhibiting the retrograde trafficking of HA-hITGB1. Hence, the difference in the apparent molecular weight of HA-hITGB1 between C6WT and N5KD cells would be abolished.

To investigate whether HA-hITGB1 is 'extra-sialylated', I synchronized the trafficking of HA-hITGB1 in C6WT and N5KD cells as previously described (see section 4.4), with and without Retro-2 treatment. Interestingly, after six hours of chase in the presence of Retro-2, the apparent molecular weights of HA-hITGB1 were similar between C6WT and N5KD cells. However, the apparent molecular weight of HA-hITGB1 in Retro-2 treated N5KD cells was smaller than that of C6WT cells after 24 hours of chase. It is possible that both Retro-2 treatment and the knockdown of NHE5 resulted in an additive inhibitory effect and lowered the apparent molecular weight of HA-hITGB1. Most importantly, the molecular weight of HA-hITGB1 of Retro-2 treated C6WT cells was the same as the molecular weight of HA-hITGB1 in N5KD cells without Retro-2 treatment at both 6 and 24 hours of chase (Figure 4.4 A). Furthermore, the disappearance of mature and upper bands of HA-hITGB1 in both Retro-2 treated C6WT and N5KD cells upon neuraminidase digestion further indicates that it is likely that the HA-hITGB1

from Retro-2 treated cells are still sialylated (Figure 4.4 B). These results together suggest that HA-hITGB1 is 'extra-sialylated' during retrograde trafficking in addition to the canonical sialylation during its biosynthesis. When the retrograde trafficking is inhibited by Retro-2 or in N5KD cells, the 'extra-sialylation' of HA-hITGB1 is blocked, resulting in similar apparent molecular weights of mature HA-hITGB1 between C6WT and N5KD cells.

In addition to the pharmacological inhibition, a genetic approach is used to inhibit retrograde trafficking to investigate the 'extra-sialylation' of HA-hITGB1. Vps29 is a component of the retromer complex (Haft et al., 2000) and identified to interact with NHE5 (unpublished data). Thus, I disrupted the expression of Vps29 using a tetracycline-inducible miRNA-shRNA against Vps29 (Figure 4.4 C). C6WT and N5KD cells stably expressing miRNA-shRNA-Vps29 had reduced expression of Vps29 when (Doxy was added to the culture medium (Figure 4.4 D). The apparent molecular weight of Intβ1 in C6WT and N5KD cells before and after depletion of Vps29 was not much different (Figure 4.4 D). Unexpectedly, NHE5 expression was increased when Vps29 was knocked down (Figure 4.4 D).

It is probable that visualizing the difference in the apparent molecular weight of endogenous rat Intβ1 after conditional knockdown of Vps29 is difficult. Although the exact reason for this is not known, one possible reason is the presence of mixed populations of newly synthesized Intβ1 and fully sialylated Intβ1. To support this hypothesis, I found it difficult to visualize a decrease in the size of endogenous Intβ1 in C6WT cells with Retro-2 treatment even after 24 hours of the treatment (Figure 4.4 E) in contrast with the obvious decrease in the size of HA-hITGB1 after six hours of chase in Retro-2 containing medium (Figure 4.4 A).

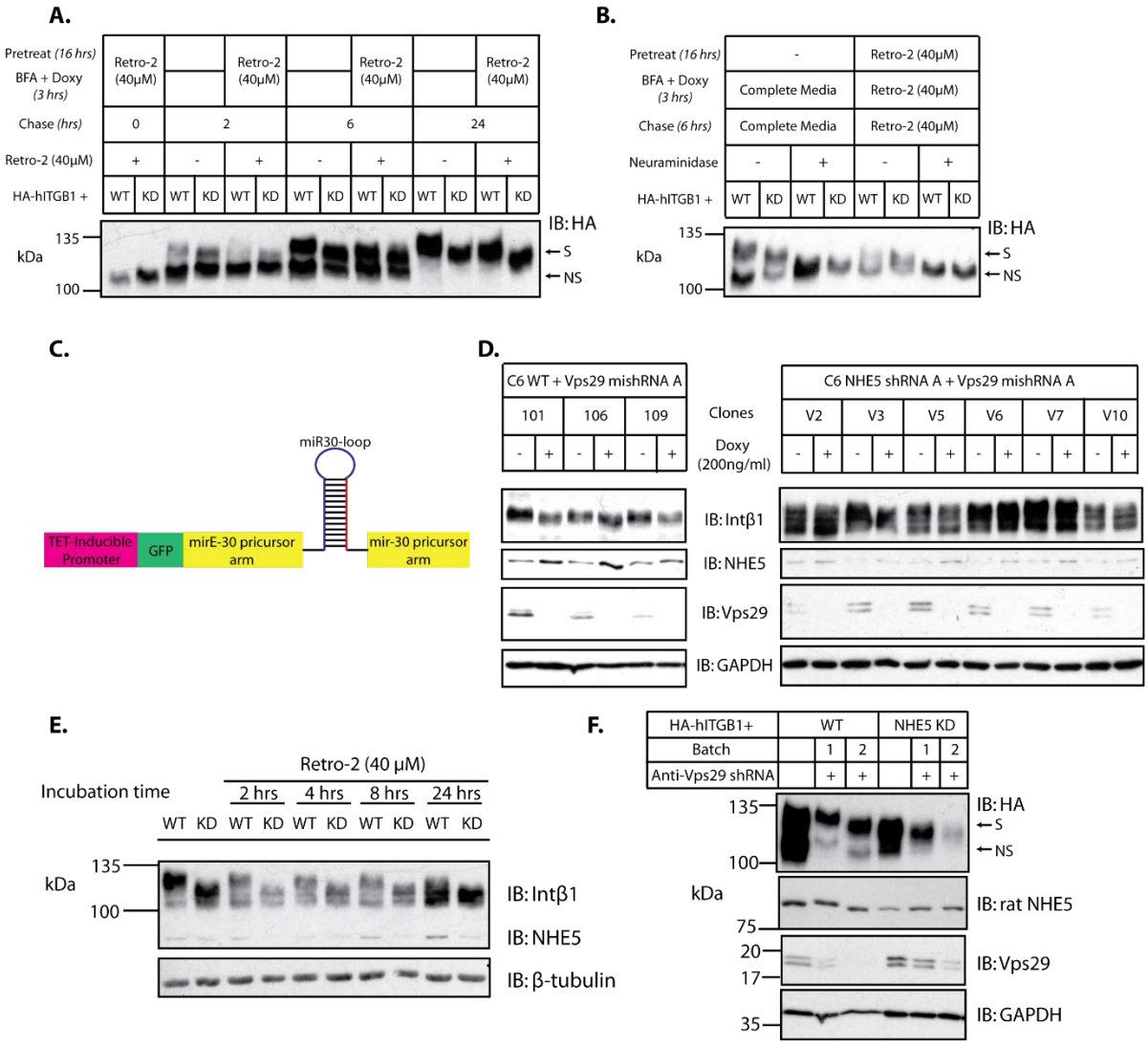
A.
Pretreat (16 hrs)
BFA + Doxy (3 hrs)
Chase (hrs)
Retro-2 (40μM)
HA-hITGB1 +
WT KD
0
2
6
24
IB: HA
S
NS
kDa
135
100
B.
Pretreat (16 hrs)
BFA + Doxy (3 hrs)
Chase (6 hrs)
Neuraminidase
Complete Media
C.
miR30-loop
TET-Inducible Promoter
GFP
mirE-30 pricursor arm
mir-30 pricursor arm
D.
C6 WT + Vps29 mishRNA A
101
106
109
C6 NHE5 shRNA A + Vps29 mishRNA A
Clones
V2
V3
V5
V6
V7
V10
Doxy (200ng/ml)
IB: Intβ1
IB: NHE5
IB: Vps29
IB: GAPDH
E.
Retro-2 (40 μM)
Incubation time
2 hrs
4 hrs
8 hrs
24 hrs
IB: Intβ1
IB: NHE5
IB: β-tubulin
F.
HA-hITGB1+
WT
NHE5 KD
Batch
Anti-Vps29 shRNA
IB: rat NHE5
IB: Vps29
IB: GAPDH
75
20
17
35

Figure 4.4 The effect of Retro-2 treatment and knockdown of Vps29 on the size of Intβ1.
(A) C6 wildtype (WT) and NHE5-knockdown (KD) cells stably expressing inducible HA-hITGB1 were treated with or without 40 μM of Retro-2 for 16 hours (hrs) and then incubated with 200 ng/mL of doxycycline (Doxy) and 5 μg/mL of Brefeldin A (BFA) for three hours in the presence or absence of 40 μM of Retro-2. After washing out the drugs, the cells were chased in complete media with and without 40 μM of Retro-2 for indicated times. HA-hITGB1 in the cell lysates were detected by immunoblotting. This is a representative blot of three independent experiments.
(B) Experiment was conducted as in **(A)**. Cells were chased for six hours in the presence or absence of Retro-2 after BFA and Doxy washout and the cell lysates were subjected to neuraminidase digestion for 60 minutes at 37°C prior to immunoblotting. This is a representative blot of three independent experiments.
(C) A schematic representation of the construct of GFP-tagged anti-Vps29 miRNA-shRNA hybrid that is expressed under RNA polymerase II-dependent tetracycline-inducible promoter.
(D) C6WT and N5KD cells stably expressing inducible anti-Vps29 shRNA shown in **(C)** were grown in complete medium with and without 200 ng/mL of Doxy for 96 hours. The cell lysates were immunoblotted for endogenous rat Intβ1, NHE5, Vps29 and GAPDH. This is a preliminary result of one-time experiment.
(E) C6WT and N5KD cells were incubated with 40 μM of Retro-2 for indicated times and cell lysates were immunoblotted for endogenous rat Intβ1, NHE5 and β-tubulin. This is a representative blot of two independent experiments.
(F) C6WT and N5KD cells concomitantly expressing inducible HA-hITGB1 and constitutive shRNA against Vps29 shRNA were induced with 200 ng/mL of Doxy overnight and immunoblotted for HA-hITGB1, Vps29 and GAPDH. This is a preliminary result of one-time experiment.
NS: Non-sialylated; S: Sialylated.

To examine the involvement of Vps29 in HA-hITGB1 retrograde trafficking and 'extra-sialylation', I generated C6WT and N5KD cells expressing inducible HA-hITGB1 and Vps29 shRNA driven by the constitutively active U6 promoter. The apparent molecular weight of mature HA-hITGB1 in C6WT cells as a result of Vps29 knockdown decreased to the same apparent molecular weight as mature HA-hITGB1 in N5KD cells (Figure 4.4 F), in accordance with the results obtained from Retro-2 experiments (Figure 4.4 A). The size of mature HA-hITGB1 in N5KD cells expressing Vps29 shRNA also decreased slightly (Figure 4.4 F). The expression of NHE5 appeared to be increased by the depletion of Vps29 in N5KD cells, but not in C6WT cells (Figure 4.4 F). This could be due to the saturated signal intensity of NHE5 in C6 WT cells. Although these results are preliminary and need additional experiments, the results so far suggest that 'extra-sialylation' and retrograde trafficking of HA-hITGB1 occur via pathways involving NHE5 and Vps29.

4.6 A possible role of pH in 'extra-sialylation' of Intβ1

Previous studies showed that retrograde trafficking of TGN38 and Furin to the TGN is pH-dependent and NHE5 is a pH regulator in the recycling endosomes (Chapman and Munro, 1994; Fan et al., 2016). This prompted me to test whether the retrograde trafficking and 'extra-sialylation' of Intβ1 are pH-dependent. Thus, I performed synchronized trafficking of HA-hITGB1 experiments in the presence of Retro-2 and two other pharmacological drugs, bafilomycin A1 and chloroquine that elevate the pH of acidic organellar lumens. Bafilomycin A1 inhibits the activity of V-ATPases and prevents the acidification of the organellar lumens (Bowman et al., 1988; Johnson et al., 1993) whereas, chloroquine is a weak base that accumulates in the acidic organellar lumens and neutralizes therein. These acidic organelles include but not limited to early endosomes, lysosomes, and the Golgi apparatus (Axelsson et al., 2001; Chapman and Munro, 1994; de Duve et al., 1974). Alkalinization of organellar pH by chloroquine, not bafilomycin A1 decreased the apparent molecular weights of HA-hITGB1 in C6WT and N5KD cells, similar to Retro-2 treatment (Figure 4.5). In the presence of Retro-2, the apparent molecular weights of HA-hITGB1 in C6WT and N5KD cells were still partially sialylated (Figure 4.4 B). Therefore, future experiments are needed to investigate the sialylation status of HA-hITGB1 in chloroquine-treated cells by neuraminidase digestion and lectin pull-down assays to understand the role of endosomal lumen pH in the 'extra-sialylation' of Intβ1.

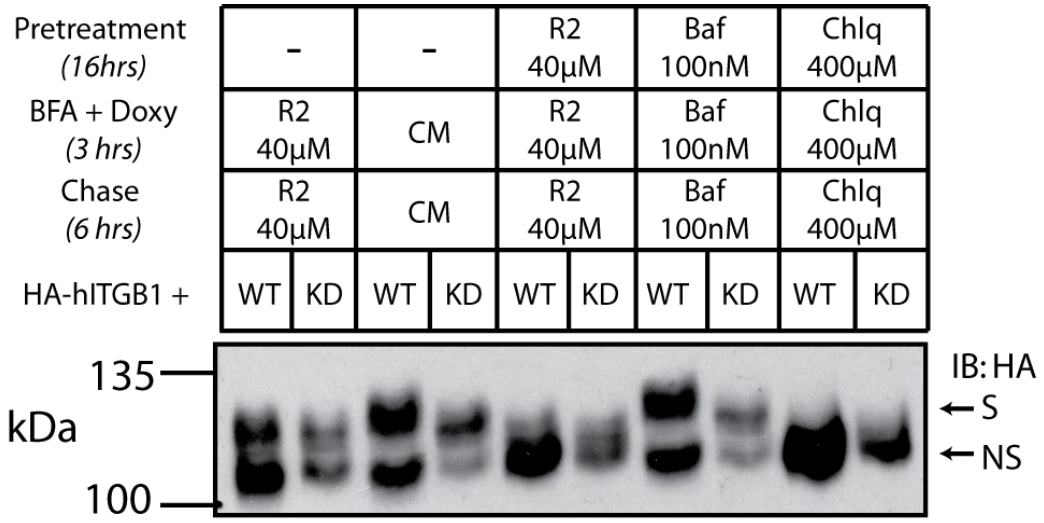

Figure 4.5 The decrease in the size of Intβ1 results from the knockdown of NHE5 and inhibition of retrograde trafficking.
C6 wildtype (WT) and NHE5-knockdown (KD) cells with inducible HA-hITGB1 were treated with 40 μM of Retro-2 (R2), 100 nM of bafilomycin A1 (Baf) or 400 μM of chloroquine (Chlq) for 16 hours (hrs) followed by an incubation with 200 ng/mL of doxycycline (Doxy) and 5 μg/mL of Brefeldin A (BFA) for three hours. In the control group, the cells were not pre-incubated with pharmacological inhibitors prior to treatment with Doxy and BFA for three hours. After Doxy and BFA treatment, the drugs were washed out and cells were chased in complete medium with and without inhibitors for six hours. HA-hITGB1 in the total cell lysates was detected by immunoblotting. This is a representative blot of three independent experiments. NS: Non-sialylated; S: Sialylated

4.7 Re-expression of rat NHE5 or overexpression of human ST6Gal-I did not rescue the molecular weight of Intβ1 in NHE5-knockdown cells.

To investigate whether the size of Intβ1 can be rescued by re-expressing rat NHE5 into N5KD cells, I generated N5KD cells stably expressing shRNA-resistant HA-tagged rat NHE5 under tetracycline-inducible promoter. Recombinant expression of rat NHE5 did not appear to rescue the apparent molecular weight of Intβ1 from N5KD cells to the same size as C6WT cells (Figure 4.6 A). I performed immunofluorescence microscopy to examine the subcellular localization of the exogenously expressed HA-tagged rat NHE5 after 6 hours and 48 hours of induction. Most of the proteins localized to the ER-like structure around the nucleus, while some were targeted to recycling endosomes-like puncta as indicated by the white arrows (Figure 4.6 B). Further experiments are required to define co-localization of HA-tagged rat NHE5 with appropriate organelle markers. Experiments with different Doxy concentrations or pulse and chase did not rescue the apparent molecular weight of Intβ1 in N5KD cells (data not shown). These preliminary observations suggest that the re-expression of NHE5 did not rescue the phenotype because the exogenously expressed NHE5 was not targeted to the correct subcellular localization. Future experiments to re-optimize the induction level of heterologously expressed NHE5 and measure the endosomal pH are needed to understand the functionality of the re-expression system.

Next, I asked whether overexpression of ST6Gal-I, the sialyltransferase that catalyzes α2-6 sialylation on Intβ1 (Kitazume, 2014), can increase the molecular weight of Intβ1 in N5KD cells. Previous studies showed that overexpression of ST6Gal-I increases the sialylation level of Intβ1 (Isaji et al., 2014; Seales et al., 2005a; Yu et al., 2013). Thus, I established C6WT and N5KD cells stably overexpressing flag-tagged human ST6Gal-I and immunoblotted for Intβ1. However, heterologous expression of flag-tagged human ST6Gal-I in N5KD cells did not increase the molecular weight of Intβ1 (Figure 4.6 C). Immunofluorescence microscopy revealed that the exogenously expressed human ST6Gal-I had a perinuclear staining which morphologically looked like the Golgi apparatus (Figure 4.6 D). To further verify the subcellular localization of the heterologously expressed flag-tagged human ST6Gal-I, colocalization experiments with the TGN markers should be performed (Nilsson et al., 1993). Since

overexpressing ST6Gal-I did not rescue the size of Intβ1 in NHE5-depleted cells, it is possible that NHE5 regulates α2-6 sialylation of Intβ1 through other factors besides ST6Gal-I activity.

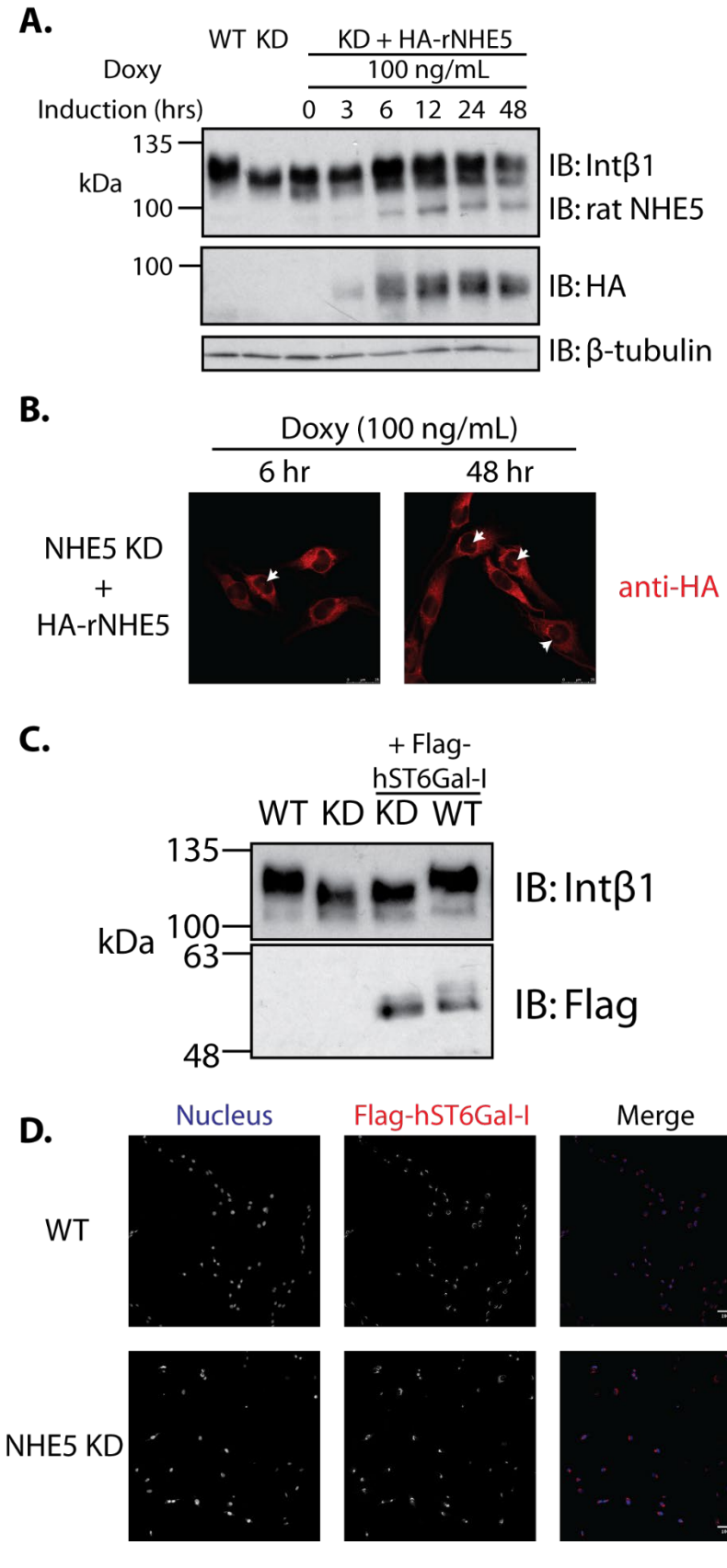
A.
WT KD
KD + HA-rNHE5
100 ng/mL
Doxy
Induction (hrs)
0 3 6 12 24 48
135
kDa
100
IB: Intβ1
IB: rat NHE5
100
IB: HA
IB: β-tubulin
B.
Doxy (100 ng/mL)
6 hr
48 hr
NHE5 KD
+
HA-rNHE5
anti-HA
C.
+ Flag-
hST6Gal-I
WT KD KD WT
135
kDa
100
63
48
IB: Intβ1
IB: Flag
D.
Nucleus
Flag-hST6Gal-I
Merge
WT
NHE5 KD

Figure 4.6 Re-expression of rat NHE5 or overexpression of human ST6Gal-I did not increase the molecular weight of Intβ1 in NHE5-knockdown cells.
(A) Protein expression of HA-tagged rat NHE5 were induced by 100 ng/mL of doxycycline (Doxy) for indicated times in NHE5-knockdown (KD) cells. The cell lysates were immunoblotted for Intβ1, endogenous NHE5, exogenous HA-tagged NHE5 and β-tubulin. This is a representative blot of two independent experiments.
(B) Protein expression of HA-tagged rat NHE5 was induced by 100 ng/mL of Doxy for indicated times in N5KD cells and cells were fixed with 3% PFA. The fixed cells were stained with anti-HA to visualize the subcellular localization of exogenously expressed HA-tagged rat NHE5. White arrows indicate the structure that resembles recycling endosomes. Scale bar= 25 μm. This is a representative image of two independent experiments
(C) C6 wildtype (WT) and N5KD cells stably expressing flag-tagged human ST6Gal-I and the respective parental cells were grown overnight in complete medium. The cell lysates were immunoblotted for Intβ1 and flag-tagged ST6Gal-I. This is a representative blot of three independent experiments.
(D) The subcellular localization of flag-tagged human ST6Gal-I is visualized. C6WT and N5KD cells stably expressing flag-tagged human ST6Gal-I were grown overnight and fixed with 3% PFA. The nucleus (blue) and the human ST6Gal-I (red) were stained with Draq5 and anti-Flag antibody, respectively. Scale bar = 100 μm. This is a preliminary result of one-time experiment

Chapter 5: Discussion

5.1 Summary

In this thesis, I found that NHE5, an acidifier of recycling endosomes (Diering, Numata, Fan, Church, & Numata, 2013; Fan, Numata, & Numata, 2016) regulates recycling and stability of Intβ1 in C6 glioma cells. Hence, depletion of NHE5 expression resulted in decreased expression of Intβ1 at the cell surface. Furthermore, knockdown of NHE5 reduced the apparent molecular weight of Intβ1, which is likely due to the decrease in α2-6 sialylation of the receptor. Thus, I established an inducible system with synchronized trafficking of HA-hITGB1 and showed, for the first time, that Intβ1 is further sialylated ('extra-sialylation') during its retrograde trafficking to the TGN. NHE5 is likely to regulate the 'extra-sialylation' of HA-hITGB1 by modulating the retrograde trafficking of HA-hITGB1. In summary, I present evidence suggesting that NHE5 plays a key role in integrin-mediated cell adhesion and spreading in C6 glioma cells by modulating endocytic recycling and retrograde trafficking of Intβ1, a major cell adhesion receptor expressed in glioma (Malek-Hedayat and Rome, 1992).

5.2 Intβ1 trafficking and sialylation regulate cell adhesion, spreading and migration.

Availability of Intβ1 at the cell surface regulates the extent of cell adhesion and spreading on its substrates. Studies showed that disruption of Intβ1 recycling or retrograde trafficking reduces the expression of Intβ1 at the plasma membrane, forms fewer focal adhesions and affects cell spreading (Ratcliffe et al., 2016; Riggs et al., 2012; Shafaq-Zadah et al., 2016). This is consistent with my findings, where knocking down of NHE5 impaired the recycling of Intβ1 (Figure 3.6) and reduced Intβ1 population at the cell surface (Figure 3.2). As a result, attachment and spreading of C6 glioma cells on collagen IV were reduced in N5KD cells (Figure 3.1). Previous studies also showed that NHE5 knockdown decreased the cell surface expression of c-Met and EGFR in C6 glioma cells and TrkA receptors in PC12 cells due to their defective recycling to the cell surface. (Diering et al., 2013; Fan et al., 2016). Therefore, it is likely that compromised cell attachment and spreading in N5KD cells are caused by the reduced availability of Intβ1 on the cell surface to engage with the ECM.

Dynamic turnover of focal adhesions (*i.e.* constant assembly, disassembly and reassembly) at the leading edge is critical for cell migration. It was shown that microtubule-

induced focal adhesion disassembly and the subsequent reassembly of focal adhesions are required for polarized formation of focal adhesions at the leading edge of migrating cells and their motility (Cleghorn et al., 2015; Ezratty et al., 2005; Nader et al., 2016). Integrins were shown to undertake endocytic recycling through Rab11-positive endosomes prior to the reassembly of the focal adhesions, and any perturbation in the reassembly process led to decreased integrin on the cell surface. Inhibition of focal adhesions reassembly caused integrins to accumulate in the Rab11-positive PNRC, leading to the formation of fewer focal adhesions on the cell surface (Nader et al., 2016). Similarly, depletion of NHE5 reduced the recycling of Intβ1, a component of the focal adhesion complex (Figure 3.6), and its expression on the cell surface (Figure 3.2). Given that NHE5 was shown to associate with Rab11-positive recycling endosomes (Fan et al., 2016), it is likely that re-targeting of Intβ1 to the cell surface to form new focal adhesions was impaired when the expression of NHE5 was depleted. Thus, there were fewer but bigger focal adhesions on the cell surface of N5KD cells (Figure 3.1 C). On the other hand, in C6 WT cells, there were many small focal adhesion complexes accompanied with lamellipodia formed at the cell periphery (Figure 3.1 C). This reflects the rapid recycling (turnover) of Intβ1 in C6WT cells (Figure 3.6). Therefore, one of the possible reasons for decreased migration of C6 glioma cells by NHE5 knockdown, as observed in the previous study (Fan et al., 2016), is reduced turnover of focal adhesions in N5KD cells, as indicated by the impaired recycling of Intβ1. Live-cell imaging and fluorescence recovery after photobleaching (FRAP) experiments can further deduce the rate of focal adhesion turnover in C6WT and N5KD cells.

Sialylation of Intβ1 also influences cell adhesion and migration. Several studies showed that adherent cells, such as human colorectal carcinoma cells, colon epithelial cells, and HeLa cells exhibited increased cell adhesion and migration along with increased sialylation of Intβ1 (Isaji et al., 2014; Lee et al., 2010a; Seales et al., 2005a). However, the opposite was observed with non-adherent cells, such as myeloid cells and lymphoid cells, where cell adhesion increased when Intβ1 was hyposialylated (Semel et al., 2002; Suzuki et al., 2015). Therefore, the effect of Intβ1 sialylation on cell adhesion and migration may be dependent on cell type. Given that C6 glioma cells are adherent cells, it is likely that the hyposialylation of Intβ1 as observed in N5KD cells (Figure 4.1) led to a decreased cell adhesion and spreading on Intβ1 substrates (Figure 1.5 & 3.1).

5.3 Sialylation influences Intβ1 activity

Sialylation of integrins may modulate ligand binding to the integrin heterodimers. A study using molecular modelling and dynamics found that sialic acids of the N-glycans could potentially form multiple hydrogen bonds with the I-like domain, therefore, affecting the conformations of key functional sites. Examples include the specificity-determining loop and MIDAS needed for ligand binding, as well as the conformation of the helices involved in the activation of I-like domain of β1 subunit (Liu et al., 2008). Moreover, a crystal structure of α5β1 heterodimer headpiece revealed multiple N-glycans surrounding the ligand binding site (Nagae et al., 2012). However, the effect of integrin sialylation on ligand binding is unclear. Some studies showed that de-sialylation of α5β1 leads to an increased adhesion to fibronectin (Seales et al., 2005b; Semel et al., 2002). On the other hand, other studies showed that increased sialylation on Intβ1 leads to an increased adhesion to collagen, laminin and fibronectin (Christie et al., 2008; Lee et al., 2010b; Seales et al., 2005a). In addition, another study using biophysical experiments and negative staining electron microscopy showed that N-glycosylation on α5β1 favoured the heterodimer to be in an extended and open (active) conformation, and this conformation was further stabilized by the presence of integrin lower legs (Li et al., 2017). The authors suggested that the presence of N-glycans on integrin creates a crowding and repulsion effect between the subunits, thereby stabilizes the heterodimer in an active conformation (Li et al., 2017). If this hypothesis holds true, then sialylation of integrin should stabilize the heterodimer in an extended-open confirmation and increase its affinity for the ligand. This is because the negatively-charged sialic acids may enhance the repulsion effect between the subunits and stabilize the active conformation. Based on the observation that NHE5-depletion has decreased cell spreading and attachment to Col IV, it is likely that the hyposialylation of Intβ1 in N5KD cells leads to an inactive conformation of Intβ1 and subsequently has lower ligand binding affinity.

Moreover, sialylation of Intβ1 can influence the activity and the stability of the heterodimer. Lee *et.al.* (2010a) showed that ionic radiation-induced ST6Gal-I activity increases α2-6 sialylation of Intβ1. The hypersialylated Intβ1 was shown to be more stable and constitutively active. Downstream effectors such as paxillin and Akt were phosphorylated regardless of the presence or absence of stimuli such as ionic radiation or fibronectin. However,

this constitutive phosphorylation was suppressed when the expression of ST6Gal-I was depleted, suggesting that sialylation of Intβ1 is responsible for the aberrant signaling (Lee et al., 2010a). In another study, hypersialylation of Intβ1 led to an increased association with talin (Seales et al., 2005a). This observation suggests that hypersialylated Intβ1 in colon epithelial cells are in an activated state since the binding of talin to Intβ1 is known to activate Intβ1 (Calderwood et al., 2002). It is likely that the increase in the α2-6 sialylation of Intβ1 stabilizes the heterodimer in an active conformation, leading to an increased activity of Intβ1. Therefore, it is probable that Intβ1 is in an inactive conformation in N5KD cells, since α2-6 sialylation and the stability of Intβ1 were decreased by the knockdown of NHE5 while the hypersialylated Intβ1 in C6WT cells is in an active conformation.

5.4 Involvement of NHE5 in retrograde trafficking of Intβ1

NHE5 has been shown for the first time to influence α2-6 sialylation of Intβ1 by regulating its retrograde trafficking. A recently developed inhibitor, Retro-2, was used to study the retrograde trafficking of Intβ1 (Stechmann et al., 2010). Retro-2 was shown to mislocalize SNARE proteins on the TGN such as syntaxin 5, syntaxin 6, and syntaxin 16 to the cytoplasm, and thus preventing fusion of vesicles from early endosomes to the TGN (Stechmann et al., 2010). Intβ1 was shown to be targeted from early endosomes to the TGN in vesicles containing VAMP3, a v-SNARE that interacts with syntaxin 6 and syntaxin 16 t-SNARE complexes at the TGN (Mallard et al., 2002; Riggs et al., 2012). Hence, retrograde trafficking of HA-hITGB1 is inhibited in the presence of Retro-2. When the cells were treated with Retro-2, the difference in the apparent molecular weight of HA-hITGB1 in C6WT and N5KD cells was abolished at 6 hours of chase (Figure 4.4 A-B). It was intriguing to observe a similar apparent molecular weight of HA-hITGB1 in Retro-2 treated C6WT cells and N5KD cells with no Retro-2 treatment (Figure 4.4 A-B). Given that HA-hITGB1 in Retro-2 treated C6WT was shown to be partially sialylated (Figure 4.4 B), it is likely that HA-hITGB1/Intβ1 is 'extra-sialylated' during its NHE5-mediated retrograde trafficking, in addition to the canonical sialylation in the secretory pathway.

NHE5 may regulate retrograde trafficking of Intβ1 by interacting with Vps29, a subunit of the heterotrimeric retromer complex (Haft et al., 2000). Vps29 is an important subunit for the assembly of retromer complex, and its knockdown has been shown to degrade the Vps26-Vps35 subcomplex (Fuse et al., 2015; McNally et al., 2017). Vps29 was previously shown to interact

with NHE5 by yeast two-hybrid and Co-IP experiments (unpublished data). In the current thesis study, I showed that the apparent molecular weight of HA-hITGB1 in Vps29-depleted C6WT cells decreased to the same apparent molecular weight as HA-hITGB1 in N5KD cells (Figure 4.4 F). This finding, together with a recent study showing that Intβ1 interacts with retromer subunits such as Vps35 and Vps26 (Shafaq-Zadah et al., 2016), collectively suggest that Intβ1 'extra-sialylation' is modulated by retromer-mediated retrograde trafficking in NHE5-dependent manner. Furthermore, it is possible that NHE5 regulates retrograde trafficking of a subset of Intβ1. The additional decrease in the apparent molecular weight of HA-hITGB1 in N5KD cells compared to C6WT cells when Vps29 was depleted or Retro-2 was added suggest that Intβ1 can be trafficked in retrograde manner and 'extra-sialylated' in a NHE5-independent manner as well.

Retromer complex and Vps29 have been shown to regulate additional trafficking processes other than retrograde trafficking from early endosomes to the TGN. For example, the retromer complex was shown to associate with sorting nexin 27 and regulate recycling of selective cargoes from endosomes to the plasma membrane (Steinberg et al., 2013). In another study, Vps29 was shown to form a newly discovered "retriever" complex that functions independently of the retromer complex (McNally et al., 2017). The retriever complex is recruited to endosomes and interacts with sorting nexin 17 that binds to the NPxY/NxxY-sorting motif containing receptors such as Intβ1, to recycle the receptors to the plasma membrane and prevent their degradation (Böttcher et al., 2012; McNally et al., 2017; Steinberg et al., 2012). Therefore, it is possible that NHE5-Vps29 participates in endocytic recycling and their interaction may not be limited to retrograde trafficking.

Retrograde trafficking of receptors plays a role in the directional migration of cells by mediating polarized trafficking of proteins to the leading edge of migrating cells. A study showed that the polarized targeting of ligand-unbound Intβ1 requires retrograde trafficking of the receptor to the TGN. It showed that the ligand-unbound Intβ1 is internalized and trafficked to the TGN upon stimulation, before being re-targeted to the leading edge (Shafaq-Zadah et al., 2016). A proteomic study showed that retrograde trafficking is not limited to integrin heterodimers. Interestingly, other transport proteins, such as zinc transporters, sodium potassium ATPase, and neutral amino acid transporter were also trafficked from the plasma membrane to the TGN (Shi, 2011). Furthermore, studies showed that perturbation in retrograde trafficking results in reduced

cell adhesion and migration (Riggs et al., 2012; Shafaq-Zadah et al., 2016). In our previous study, N5KD cells were shown to have impaired cell polarity and migration (Fan et al., 2016), and in my current thesis study, I showed that N5KD cells have impaired retrograde trafficking of Intβ1. The fact that the Golgi apparatus in polarized cells faces the leading edge of migrating cells suggests that cell polarity plays an important role in polarized trafficking of receptors through the TGN (Darido and Jane, 2013). Taken together, I propose that NHE5 regulates cell polarity and modulates retrograde trafficking of Intβ1 and potentially other receptors as well.

5.5 Endosomal pH regulates Intβ1 trafficking

Endosomal pH is crucial in determining the fate of endocytosed receptors. Previous studies showed that the disruption in endosomal pH affects recycling of the receptors (Diering et al., 2013; Fan et al., 2016; Johnson, Dunn, Pytowski, & McGraw, 1993). When the pH of endosomes was alkalinized by bafilomycin A1, recycling of the transferrin receptor was decreased, but not its internalization (Johnson et al., 1993). Depletion of NHE5 also led to alkalinization of recycling endosomes to the same extent as bafilomycin A1, and impaired the recycling of receptor tyrosine kinases (RTK) such as TrkA and c-Met (Diering et al., 2013; Fan et al., 2016). My finding that NHE5 knockdown reduced the recycling of Intβ1 and TfR is consistent with these results (Figure 3.6). Dissociation of ligands from receptors is a prerequisite for the recycling of these receptors back to the plasma membrane, and this process is highly dependent on endosomal pH (Harding et al., 1983; Kharitidi et al., 2015; Roepstorff et al., 2009). A study showed that the dissociation of fibronectin from Intβ1 requires acidic pH and approximately 70% of fibronectin disengaged from the cell surface integrins after a 10-minute incubation in a medium with pH ~6.1 compared to only 30% of fibronectin dissociated from the cell surface integrins when the pH of the medium is ~6.5 (Kharitidi et al., 2015). The pH of recycling endosomes in C6WT is ~6.0 and depleting NHE5 raises the pH to ~6.2 (Fan et al., 2016). Therefore, the dissociation of fibronectin from integrin heterodimer will be slower in N5KD cells than in C6WT cells, resulting in a slower recycling of Intβ1 as observed (Figure 3.6).

Endosomal pH may also modulate retrograde trafficking of cargoes. A study showed that neutralization of acidic luminal pH of endosomes with chloroquine relocalizes the TGN proteins such as TGN38 and Furin enzymes to early endosomal compartments instead of the TGN

(Chapman and Munro, 1994). Based on this study and my own experimental results, my working hypothesis is that retrograde trafficking of Intβ1 from early/recycling endosomes to the TGN is dependent on the acidic luminal pH of endosomes. To test this hypothesis, I tested the effect of chloroquine, a weak base that accumulates in and neutralizes acidic organelles in the cell (Homewood et al., 1972), and bafilomycin A1, an inhibitor of V-ATPase (Dröse and Altendorf, 1997; Dyve Lingelem et al., 2012), on the retrograde trafficking and 'extra-sialylation' of HA-hITGB1. A shift in the apparent molecular weight of HA-hITGB1 in C6WT to the same size as N5KD cells was seen when cells were treated with chloroquine, but not with bafilomycin A1 (Figure 4.5, section 4.6). One possible explanation is that the high concentration of bafilomycin A1 used in the experiment could have induced off-target effects such as apoptosis (Kinoshita et al., 1996). The effect of NHE5 knockdown is limited to recycling endosomes whereas bafilomycin A1 and chloroquine treatment indiscriminately affect virtual all the acidic organellar pH. It is possible that acidic pH of different organellar compartments have different roles in protein trafficking and degradation.

The pH along the endocytic recycling pathway is tightly regulated and understanding the effect of pH disruption on this pathway is challenging due to the existence of a heterogenous of endosomal population. For example, the heterogenous recycling endosomes in the cell are defined by different markers such as Rab11, Arf6, TfR, and cellubrevin (Kobayashi and Fukuda, 2013; Teter et al., 1998). Importantly, altering the luminal pH of different endosomal compartments along the endocytic pathway may cause different effects to the cell. For instance, both NHE5 and NHE9 are found in the endosomal compartments, but they are differentially localized; NHE9 localizes predominantly to Rab5-positive endosomes and NHE5 to Rab11-positive endosomes (Fan et al., 2016; Gomez Zubieta et al., 2017). Unlike NHE5, NHE9 has a higher binding affinity to K^+ over Na^+, meaning NHE9 activity likely to alkalinize the endosomal pH by its K^+/H^+ exchange module (Gomez Zubieta et al., 2017; Kondapalli et al., 2015). When the luminal pH of recycling endosomes was alkalinized by depleting NHE5, endocytic recycling of RTKs was impaired (Diering et al., 2013; Fan et al., 2016). On the other hand, alkalinization of luminal pH of sorting endosomes by NHE9 overexpression resulted in an enhanced endocytic recycling of EGFR (Kondapalli et al., 2015). Given that Intβ1 is recycled through multiple pathways (Arjonen et al., 2012; De Franceschi et al., 2015; Roberts et al., 2001; Shafaq-Zadah et

al., 2016), it is possible that a majority of retrograde trafficking and 'extra-sialylation' of Intβ1 occurs specifically through NHE5-positive recycling endosomes. Therefore, to understand the effect of NHE5-regulated acidic lumen of recycling endosomes on retrograde trafficking of Intβ1, pH of recycling endosomes must be disrupted using NHE5-specific inhibitors.

5.6 NHE5 regulates the recycling of Intβ1 and TfR

My initial discovery of the NHE5-dependent Intβ1 and TfR recycling was a surprise because previous findings showed that NHE5 does not regulate endocytic recycling of Intβ1 and TfR (Diering et al., 2013; Fan, 2015; Fan et al., 2016). This apparent discrepancy could be due to different incubation times used for internalizing and recycling the receptors. There are fast (short-loop) and slow (long-loop) recycling routes that are regulated by different GTPases (Arjonen et al., 2012; Maxfield and McGraw, 2004; Powelka et al., 2004). To define short- and long-recycling loops, recycling experiments were performed with two different incubation times, and termed short-incubation recycling assays and long-incubation recycling assays, respectively. There was less difference in the relative recycling percentage of Intβ1 and TfR between C6WT and N5KD cells in the long-incubation recycling assays than there was in the short-incubation recycling assays (Figure 3.6). This data indicates that the recycling of Intβ1 and TfR became less dependent on NHE5 in the long-incubation recycling assays. One of the factors that influence the outcome of these recycling assays is the recycling kinetics of receptors. Half-lives of integrin trafficking via short-loop and long-loop recycling pathways are approximately 3 minutes and 10 minutes, respectively (Caswell and Norman, 2006). While transferrin receptors are recycled back to the cell surface with a typical half-life of 5-10 minutes, it takes an average of approximately 5 minutes and up to 60 minutes for 50% of the RTK to recycle via short- and long-loop pathways, respectively (Ciechanover et al., 1983; Goh and Sorkin, 2013; Maxfield and McGraw, 2004; Mayor et al., 1993). As the recycling kinetics are faster for Intβ1 and TfR compared to RTKs, and thus, the effect of NHE5 on the recycling of Intβ1 and TfR might have been masked when the cells were incubated for an extended period. Thereby, explaining why NHE5-dependent recycling was only observed with RTKs, but not TfR or Intβ1, during long-incubation recycling assays in previous studies (Diering et al., 2013; Fan, 2015; Fan et al., 2016).

Also, the results of short- and long-incubation recycling assays indicate that NHE5 may mediate short-loop recycling of Intβ1 and TfR. However, this is not in agreement with previous

studies where NHE5 was shown to colocalize with Rab11-positive endosomes that are involved in the long-loop recycling, but not with Rab4-positive endosomes that are involved in the short-loop recycling (Diering et al., 2013; Fan et al., 2016, unpublished data). Both Intβ1 and TfR can be trafficked through the long-loop recycling pathways with a half-life of approximately 10 minutes (Caswell and Norman, 2006; Mayor et al., 1993), which is also the incubation period I used for receptor recycling in the short-incubation recycling assays. Thus, it is possible that the short-incubation recycling assays that I performed is not exclusive to short-loop recycling of Intβ1 and TfR. Therefore, by performing recycling assays after depleting the expression of Rab4 or Rab11 and immunofluorescence-based antibody feeding assays in C6WT and N5KD cells, it is possible to understand the relationship between NHE5 and the different recycling routes of Intβ1 and TfR.

Depletion of NHE5 affects trafficking of both Intβ1 and TfR. Recycling of both Intβ1 and TfR were decreased with NHE5 knockdown, resulting in an increased population of internalized receptors in the cells (Figure 3.5-3.6). The cell surface expression of TfR was also lowered by NHE5 knockdown (Figure 3.4 A), suggesting that Intβ1 and TfR follow NHE5-mediated trafficking pathways. Several studies indeed showed that TfR follows similar trafficking routes as Intβ1. For example, both Intβ1 and TfR were endocytosed via clathrin-mediated endocytosis, and accumulated at the perinuclear region upon knockdown of syntaxin 6, a t-SNARE at the TGN (Arjonen et al., 2012; Riggs et al., 2012). Moreover, Coppolino *et.al. (*1995) showed that α3 subunit of integrin can form a disulphide bond with one of the monomers of the TfR, which led to the formation of a 225 kDa protein complex. Interestingly, Intβ1 was immunoprecipitated together with this protein complex. This suggests that Intβ1 interacts with TfR through α3 subunit. Given that α3 is one of several α subunits expressed in C6 glioma cells, there is a possibility that Intβ1 and TfR interact together and are trafficked in an NHE5-dependent manner (Malek-Hedayat and Rome, 1992). Alternatively, NHE5 may regulate the recycling of Intβ1 and TfR independently, but in a similar manner. Besides Intβ1 and TfR, NHE5 was shown to downregulate recycling of receptor tyrosine kinases (RTKs) such as c-Met, EGFR and TrkA (Diering et al., 2013; Fan et al., 2016). These receptors are generally endocytosed upon ligand-binding and are recycled to the cell surface after ligand dissociation from the receptor (Harding et al., 1983; Roepstorff et al., 2009). Therefore, it is interesting to hypothesize that NHE5

contributes to the ligand-dissociation efficiency by modulating endosomal pH (see section 5.5), and preferentially facilitates recycling of ligand-bound receptors.

It is also possible that NHE5 be part of a previously unidentified endosomal compartment, where it sorts and mediates recycling and retrograde trafficking of various receptors. Interestingly, a study using single particle tracking and live-cell imaging showed that different cargoes were pre-sorted and endocytosed into two distinct populations of early endosomal compartments namely static early endosomes (SEE) and dynamic early endosomes (DEE). It also showed that transferrin was endocytosed non-selectively into both SEE and DEE, but cargoes such as LDL, EGF and influenza virus were selectively endocytosed into DEE despite high concentrations of cargoes were available. SEE was termed for slowly maturing early endosomes marked by Rab5, which then matures to Rab11-containing recycling endosomes, while DEE was termed for Rab5-marked early endosomes that associates with microtubule and rapidly matures into Rab7-containing late endosomes (Lakadamyali et al., 2006). Another study supported this hypothesis too, where using TIRF microscopy, it was found that EGF and transferrin bind to distinct regions of the plasma membrane and are endocytosed into distinct compartments (Leonard et al., 2008). Furthermore, transferrin was shown to form tubulation and recycle from both SEE and DEE, suggesting that recycling of receptors can occur from both SEE and DEE (Lakadamyali et al., 2006). Similarly, another study showed that recycling of transferrin was inhibited when the function of dynein, the minus end-directed microtubule motor protein, was disrupted (Driskell et al., 2007). These studies together suggest that different receptors can be endocytosed differently into different early endosomes and recycled back to the plasma membrane. However, it is unclear whether the recycling routes of the receptors from different early endosomes are distinct or they overlap with each other. Previous yeast two-hybrid screening of a human brain cDNA library suggested that various microtubule binding proteins as potential NHE5 interactors (unpublished observations). These observations led me to hypothesize that NHE5 to be involved with sorting/recycling of receptors endocytosed through DEE (SE/DEE) rather than SEE (SE/SEE). As a consequence, NHE5 determines the fate of a subset of receptors including RTKs, integrins and TfR. Recycling assays in the presence of nocodazole can be performed to test this hypothesis. Also, if NHE5 is forming a new

uncharacterized endosomal compartment, then future experiment such as proximity-labeling BioID assay can elucidate novel NHE5 interactors and endosomal markers.

Additionally, the conformation of Intβ1 regulates its recycling pathway. It was shown that inactive and active Intβ1 are recycled to the cell surface through different endocytic recycling routes (Arjonen et al., 2012). Inactive Intβ1 was shown to recycle rapidly to the plasma membrane via the Rab4-pathway, whereas active Intβ1 was shown to recycle slowly via the Rab11-pathway (Arjonen et al., 2012). It is probable that NHE5 regulates recycling of active Intβ1 only. A study showed that it takes about 20 minutes for fibronectin to dissociate from α5β1 before the heterodimers are recycled (Kharitidi et al., 2015). Therefore, in long-incubation recycling assays, it is likely that both active and inactive Intβ1 are recycled to the cell surface, thus masking the influence of NHE5 on the recycling of Intβ1.

5.7 Future directions

NHE5, which is abnormally expressed in C6 glioma cells, but not in astrocytes, may play a role in cancer progression. Dr. Basler, in her thesis dissertation, indeed found expression of NHE5 mRNA in human glioblastoma tissues. She found that there are higher NHE5 mRNA levels in samples from patients older than the median age and patients with shorter survival time than the median survival time (Basler, 2013. "*Studies on the expression and function of pH - regulatory transporters in Glioblastoma multiforme (German to English."* (Doctoral dissertation http://d-nb.info/1046071394/34). Moreover, through TCGA data analysis tools such as cBioPortal (http://www.cbioportal.org/?ref=labworm) and Genomic Data Commons Data Portal (https://portal.gdc.cancer.gov/), I found that the expression of neuron-enriched NHE5 to be amplified in pancreatic, colon, uterus and lung cancers to name a few. Further characterization of tumor samples from patients and bioinformatic analysis of these data sets can elucidate the correlation of NHE5 expression with different cancers, at different stages of cancer progression and the outcome of patients' survival.

Given that conformations of integrin heterodimers on the cell surface can affect the downstream signaling and trafficking of these receptors, understanding how NHE5-mediated 'extra-sialylation' of Intβ1 influences their conformation is important. One of the methods to study the conformations of Intβ1 in C6WT and N5KD cells is by using different monoclonal Intβ1 antibodies that recognize specific conformations of Intβ1. For example, the mAB13

antibody recognizes the inactive conformation of Intβ1 while the 12G10 or 9EG7 antibody recognizes the active Intβ1 (Byron et al., 2009). Conformation also influences Intβ1 recycling since Rab4 and Rab11 are suggested to associate with inactive and active Intβ1, respectively (Arjonen et al., 2012). To understand how NHE5 regulates the recycling of differentially sialylated Intβ1 in C6WT and N5KD, *i.e.* through Rab4-dependent pathway or Rab11-dependent pathway, cell-surface biotinylation-based recycling assays in combination with knocking down different Rabs will be a useful approach.

Furthermore, the newly established inducible HA-hITGB1 system that allows synchronization of Intβ1 trafficking will be a powerful method to understand the molecular mechanism of NHE5-mediated retrograde trafficking and 'extra-sialylation' of Intβ1. It is interesting to speculate that NHE5 regulates the recycling and retrograde trafficking of Intβ1 by modifying the activity of Rab11, which localizes at the pericentriolar recycling endosomes and regulates the slow recycling pathway of receptors (Ullrich et al., 1996). By overexpressing different mutants of Rab11 *i.e.* GTPase-deficient (Rab11Q70L) and dominant negative (Rab11S25N), it was shown that Rab11 regulates trafficking of TGN38 and STxB from early endosomes to the TGN in HeLa cells (Wilcke et al., 2000). Internalized STxB and surface-labelled TGN38 were shown to accumulate in an extensive tubular structure, instead of the TGN when the dominant negative Rab11 was overexpressed (Wilcke et al., 2000). Based on the observation that NHE5 associates with Rab11-positive recycling endosomes in C6WT cells, I hypothesize that NHE5 regulates the 'extra-sialylation' and retrograde trafficking of Intβ1 via Rab11 (Fan et al., 2016). To test this hypothesis, the synchronized trafficking of HA-hITGB1 assay can be performed by knocking down Rab11.

5.8 Conclusion/ Model

In summary, this study highlighted for the first time that Intβ1 is 'extra-sialylated' in addition to its canonical sialylation in the secretory pathway and that 'extra-sialylation' occurs during the retrograde trafficking of Intβ1. Results from this thesis together with previous studies suggest that NHE5 regulates endocytic recycling of a subset of receptors including RTKs, integrins and TfR. In addition, NHE5 is shown to regulate retrograde trafficking of Intβ1 and influence the 'extra-sialylation' of this cell adhesion receptor. By regulating the trafficking of Intβ1, NHE5 affects the stability and surface expression of Intβ1 in C6 glioma cells. As a result,

NHE5 plays a key role in regulating integrin-mediated cell spreading, adhesion, polarity and migration.

In the current thesis work, NHE5 is shown to regulate the recycling of Intβ1 and TfR, which was previously found to be NHE5-independent. This phenomenon as well as the involvement of NHE5 in the retrograde trafficking of Intβ1 suggests a model, where NHE5 localizes in a sorting endosomal compartment (SE/DEE) that is distinct from canonical early/sorting endosomes (SE/SEE), to sort and modulate the recycling and retrograde trafficking of a subset of Intβ1 (Figure 5.1). By modulating the pH of the endosomal compartment, NHE5 is likely to regulate the retrograde trafficking/recycling of various receptors including RTKs, and a subset of integrins and TfR via SE/DEE, the TGN and Rab11-postive recycling endosomes. Thus, the overexpression of NHE5 can be advantageous for cancer cells to promote their proliferation and invasion. Therefore, understanding the role of NHE5 in C6 rat glioma cells will provide insights on its role in cancer as well as a foundation for future application of this transporter as a new target for diagnosis and therapy against malignant tumors.

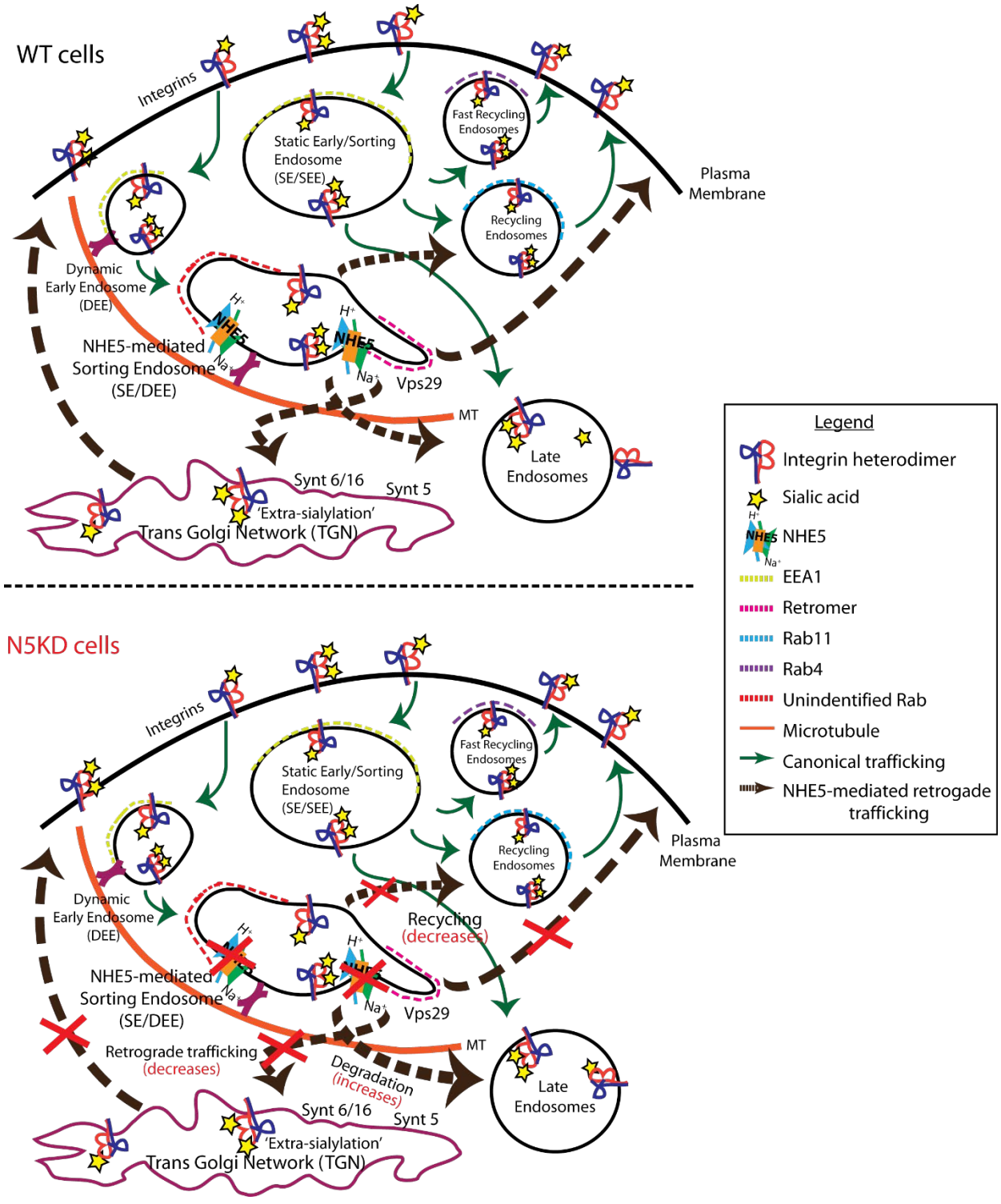
WT cells
Integrins
Static Early/Sorting Endosome (SE/SEE)
Fast Recycling Endosomes
Recycling Endosomes
Plasma Membrane
Dynamic Early Endosome (DEE)
NHE5-mediated Sorting Endosome (SE/DEE)
NHE5
Vps29
MT
Late Endosomes
Synt 6/16
Synt 5
'Extra-sialylation'
Trans Golgi Network (TGN)
N5KD cells
Integrins
Static Early/Sorting Endosome (SE/SEE)
Fast Recycling Endosomes
Recycling Endosomes
Plasma Membrane
Dynamic Early Endosome (DEE)
Recycling (decreases)
NHE5-mediated Sorting Endosome (SE/DEE)
Vps29
Retrograde trafficking (decreases)
Degradation (increases)
MT
Late Endosomes
Synt 6/16
Synt 5
'Extra-sialylation'
Trans Golgi Network (TGN)
Legend
Integrin heterodimer
Sialic acid
NHE5
EEA1
Retromer
Rab11
Rab4
Unindentified Rab
Microtubule
Canonical trafficking
NHE5-mediated retrogade trafficking

Figure 5.1 A model of the role of NHE5 in the retrograde trafficking and 'extra-sialylation' of Intβ1.
A model of Intβ1 trafficking in C6WT and N5KD cells. The brown dotted arrows indicate the newly proposed NHE5-mediated retrograde trafficking and 'extra-sialylation' pathways whereas the green arrows indicate the canonical trafficking pathways. NHE5 localizes in a previously unidentified sorting endosome that matures along microtubule (SE/DEE). By modulating the pH of the microtubule-associated sorting endosome (SE/DEE), NHE5 regulates the recycling and degradation of Intβ1.

Bibliography

Abraham, L., Lu, H.Y., Falcão, R.C., Scurll, J., Jou, T., Irwin, B., Tafteh, R., Gold, M.R., and Coombs, D. (2017). Limitations of Qdot labelling compared to directly-conjugated probes for single particle tracking of B cell receptor mobility. Sci. Rep. *7*, 11379.

Aebi, M. (2013). N-linked protein glycosylation in the ER. Biochim. Biophys. Acta - Mol. Cell Res. *1833*, 2430–2437.

Anthis, N.J., Wegener, K.L., Ye, F., Kim, C., Goult, B.T., Lowe, E.D., Vakonakis, I., Bate, N., Critchley, D.R., Ginsberg, M.H., et al. (2009). The structure of an integrin/talin complex reveals the basis of inside-out signal transduction. EMBO J. *28*, 3623–3632.

Arjonen, A., Alanko, J., Veltel, S., and Ivaska, J. (2012). Distinct recycling of active and inactive β1 integrins. Traffic *13*, 610–625.

Attaphitaya, S., Park, K., and Melvin, J.E. (1999). Molecular cloning and functional expression of a rat Na^+/H^+ exchanger (NHE5) highly expressed in brain. J. Biol. Chem. *274*, 4383–4388.

Attaphitaya, S., Nehrke, K., and Melvin, J.E. (2001). Acute inhibition of brain-specific Na^+/H^+ exchanger isoform 5 by protein kinases A and C and cell shrinkage. Am J Physiol Cell Physiol *281*, C1146-57.

Axelsson, M.A.B., Karlsson, N.G., Steel, D.M., Ouwendijk, J., Nilsson, T., and Hansson, G.C. (2001). Neutralization of pH in the Golgi apparatus causes redistribution of glycosyltransferases and changes in the O-glycosylation of mucins. Glycobiology *11*, 633–644.

Baird, N.R., Orlowski, J., Szabo, E.Z., Zaun, H.C., Schultheis, P.J., Menon, A.G., Shull, G.E., Szabó, E.Z., Zaun, H.C., Schultheis, P.J., et al. (1999). Molecular Cloning, Genomic Organization, and Functional Expression of Na^+/H^+ Exchanger Isoform 5 (NHE5) from Human Brain. J. Biol. Chem. *274*, 4377–4382.

Barczyk, M., Carracedo, S., and Gullberg, D. (2010). Integrins. Cell Tissue Res. *339*, 269–280.

Bartik, P., Maglott, A., Entlicher, G., Vestweber, D., Takeda, K., Martin, S., and Dontenwill, M. (2008). Detection of a hypersialylated β1 integrin endogenously expressed in the human astrocytoma cell line A172. Int. J. Oncol. *32*, 1021–1031.

Bellis, S.L. (2004). Variant glycosylation: an underappreciated regulatory mechanism for β1 integrins. Biochim. Biophys. Acta - Biomembr. *1663*, 52–60.

Bock, J.B., Klumperman, J., Davanger, S., and Scheller, R.H. (1997). Syntaxin 6 functions in trans-Golgi network vesicle trafficking. Mol. Biol. Cell *8*, 1261–1271.

Bock, J.B., Matern, H.T., Peden, A.A., and Scheller, R.H. (2001). A genomic perspective on membrane compartment organization. Nature *409*, 839–841.

Bonifacino, J.S., and Hierro, A. (2011). Transport according to GARP: Receiving retrograde cargo at the trans-Golgi network. Trends Cell Biol. *21*, 159–167.

Bonifacino, J.S., and Rojas, R. (2006). Retrograde transport from endosomes to the trans-Golgi network. Nat. Rev. Mol. Cell Biol. *7*, 568–579.

Böttcher, R.T., Stremmel, C., Meves, A., Meyer, H., Widmaier, M., Tseng, H.-Y., and Fässler, R. (2012). Sorting nexin 17 prevents lysosomal degradation of β1 integrins by binding to the β1-integrin tail. Nat. Cell Biol. *14*, 584–592.

Bowman, E.J., Siebers,A., and Altendorf, K. (1988). Bafilomycins: a class of inhibitors of membrane ATPases from microorganisms, animal cells, and plant cells. Proc. Natl. Acad. Sci. U. S. A. *85*, 7972–7976.

Braulke, T., and Bonifacino, J.S. (2009). Sorting of lysosomal proteins. Biochim. Biophys. Acta - Mol. Cell Res. *1793*, 605–614.

Brett, C.L., Donowitz, M., and Rao, R. (2005). Evolutionary origins of eukaryotic sodium / proton exchangers. Am. J. Physiol. - Cell Physiol. *288*, C223–C239.

Bröcker, C., Engelbrecht-Vandré, S., and Ungermann, C. (2010). Multisubunit tethering complexes and their role in membrane fusion. Curr. Biol. *20*, 943–952.

Burd, C., and Cullen, P.J. (2014). Retromer: A master conductor of endosome sorting. Cold Spring Harb. Perspect. Biol. *6*, 1–14.

Byron, A., Humphries, J.D., Askari, J.A., Craig, S.E., Mould, A.P., and Humphries, M.J. (2009). Anti-integrin monoclonal antibodies. J. Cell Sci. *122*, 4009–4011.

Calderwood, D.A., Zent, R., Grant, R., Rees, D.J., Hynes, R.O., and Ginsberg, M.H. (1999). The talin head domain binds to integrin beta subunit cytoplasmic tails and regulates integrin activation. J. Biol. Chem. *274*, 28071–28074.

Calderwood, D.A., Yan, B., de Pereda, J.M., Alvarez, B.G., Fujioka, Y., Liddington, R.C., and Ginsberg, M.H. (2002). The phosphotyrosine binding-like domain of talin activates integrins. J. Biol. Chem. *277*, 21749–21758.

Calderwood, D.A., Fujioka, Y., de Pereda, J.M., Garcia-Alvarez, B., Nakamoto, T., Margolis, B., McGlade, C.J., Liddington, R.C., and Ginsberg, M.H. (2003). Integrin β cytoplasmic domain interactions with phosphotyrosine-binding domains: A structural prototype for diversity in integrin signaling. Proc. Natl. Acad. Sci. *100*, 2272–2277.

Casey, J.R., Grinstein, S., and Orlowski, J. (2010). Sensors and regulators of intracellular pH. Nat. Rev. Mol. Cell Biol. *11*, 50–61.

Caswell, P.T., and Norman, J.C. (2006). Integrin trafficking and the control of cell migration. Traffic *7*, 14–21.

Caswell, P.T., Spence, H.J., Parsons, M., White, D.P., Clark, K., Cheng, K.W., Mills, G.B., Humphries, M.J., Messent, A.J., Anderson, K.I., et al. (2007). Rab25 associates with α5β1 integrin to promote invasive migration in 3D microenvironments. Dev. Cell *13*, 496–510.

Chadda, R., Howes, M.T., Plowman, S.J., Hancock, J.F., Parton, R.G., and Mayor, S. (2007). Cholesterol-sensitive Cdc42 activation regulates actin polymerization for endocytosis via the GEEC pathway. Traffic *8*, 702–717.

Chapman, R.E., and Munro, S. (1994). Retrieval of TGN proteins from the cell surface requires endosomal acidification. EMBO J. *13*, 2305–2312.

Chen, Y.A, and Scheller, R.H. (2001). SNARE-mediated membrane fusion. Nat. Rev. Mol. Cell Biol. *2*, 98–106.

Christie, D.R., Shaikh, F.M., Lucas, J.A IV, Lucas, J.A III, and Bellis, S.L. (2008). ST6Gal-I expression in ovarian cancer cells promotes an invasive phenotype by altering integrin glycosylation and function. J. Ovarian Res. *1*, 3.

Ciechanover, A., Schwartz, A.L., Dautry-Varsat, A., and Lodish, H.F. (1983). Kinetics of internalization and recycling of transferrin and the transferrin receptor in a human hepatoma cell line. Effect of lysosomotropic agents. J. Biol. Chem. *258*, 9681–9689.

Cleghorn, W.M., Branch, K.M., Kook, S., Arnette, C., Bulus, N., Zent, R., Kaverina, I., Gurevich, E. V, Weaver, A.M., and Gurevich, V. V (2015). Arrestins regulate cell spreading and motility via focal adhesion dynamics. Mol. Biol. Cell *26*, 622–635.

Collins, B.M., Skinner, C.F., Watson, P.J., Seaman, M.N.J., and Owen, D.J. (2005). Vps29 has a phosphoesterase fold that acts as a protein interaction scaffold for retromer assembly. Nat. Struct. Mol. Biol. *12*, 594–602.

Condon, K.H., Ho, J., Robinson, C.G., Hanus, C., and Ehlers, M.D. (2013). The Angelman syndrome protein Ube3a/E6AP is required for Golgi acidification and surface protein sialylation. J. Neurosci. *33*, 3799–3814.

Conibear, E., and Stevens, T.H. (2000). Vps52p, Vps53p, and Vps54p form a novel multisubunit complex required for protein sorting at the yeast late Golgi. Mol. Biol. Cell *11*, 305–323.

Conibear, E., Cleck, J.N., and Stevens, T.H. (2003). Vps51p mediates the association of the GARP (Vps52/53/54) Complex with the late Golgi t-SNARE Tlg1p. Mol. Biol. Cell *14*, 1610–1623.

Coppolino, M., Migliorini, M., Argravest, W.S., and Dedhar, S. (1995). Identification of a novel form of the α3 integrin subunit : covalent association with transferrin receptor. Biochem J *306*, 129–134.

D'Souza, S., Garcia-Cabado, A., Yu, F., Teter, K., Lukacs, G., Skorecki, K., Moore, H.P., Orlowski, J., and Grinstein, S. (1998). The epithelial sodium-hydrogen antiporter Na^+/H^+ exchanger 3 accumulates and is functional in recycling endosomes. J. Biol. Chem. *273*, 2035–2043.

Darido, C., and Jane, S.M. (2013). Golgi feels its own wound. Adv. Wound Care *2*, 87–92.

Demaurex, N., Furuya, W., D'Souza, S., Bonifacino, J.S., and Grinstein, S. (1998). Mechanism of acidification of the trans-Golgi network (TGN). J. Biol. Chem. *273*, 2044–2051.

Diering, G.H., Church, J., and Numata, M. (2009). Secretory carrier membrane protein 2 regulates cell-surface targeting of brain-enriched Na^+/H^+ exchanger NHE5. J. Biol. Chem. *284*, 13892–13903.

Diering, G.H., Mills, F., Bamji, S.X., and Numata, M. (2011). Regulation of dendritic spine growth through activity-dependent recruitment of the brain-enriched Na^+/H^+ exchanger NHE5. Mol. Biol. Cell *22*, 2246–2257.

Diering, G.H., Numata, Y., Fan, S., Church, J., and Numata, M. (2013). Endosomal acidification by Na^+/H^+ exchanger NHE5 regulates TrkA cell-surface targeting and NGF-induced PI3K signaling. Mol. Biol. Cell *24*, 3435–3448.

Donowitz, M., Ming Tse, C., and Fuster, D. (2013). SLC9/NHE gene family, a plasma membrane and organellar family of Na^+/H^+ exchangers. Mol. Aspects Med. *34*, 236–251.

Dozynkiewicz, M.A., Jamieson, N.B., MacPherson, I., Grindlay, J., vandenBerghe, P.V.E., vonThun, A., Morton, J.P., Gourley, C., Timpson, P., Nixon, C., et al. (2012). Rab25 and CLIC3 collaborate to promote integrin recycling from late endosomes/lysosomes and drive cancer progression. Dev. Cell *22*, 131–145.

Driskell, O.J., Mironov, A., Allan, V.J., and Woodman, P.G. (2007). Dynein is required for receptor sorting and the morphogenesis of early endosomes. Nat. Cell Biol. *9*, 113–120.

Dröse, S., and Altendorf, K. (1997). Bafilomycins and concanamycins as inhibitors of V-ATPases and P-ATPases. J. Exp. Biol. *200*, 1–8.

Dubin-Thaler, B., Gianonne, G., Döbereiner, H.-G., and Sheetz, M.P. (2004). Nanometer analysis of cell spreading on matric-coated surfaces reveals two distinct cell states and STEPs. Biophys. J. *86*, 1794–1806.

de Duve, C., de Barsy, T., Poole, B., Trouet, A., Tulkens, P., and Van Hoof, F. (1974). Commentary. Lysosomotropic agents. Biochem. Pharmacol. *23*, 2495–2531.

Dyve Lingelem, A.B., Bergan, J., and Sandvig, K. (2012). Inhibitors of intravesicular acidification protect against shiga toxin in a pH-independent manner. Traffic *13*, 443–454.

Edwards, J.C., and Kahl, C.R. (2010). Chloride channels of intracellular membranes. FEBS Lett. *584*, 2102–2111.

Emsley, J., Knight, C.G., Farndale, R.W., Barnes, M.J., and Liddington, R.C. (2000). Structural basis of collagen recognition by integrin α2β1. Cell *101*, 47–56.

Ezratty, E.J., Partridge, M.A., and Gundersen, G.G. (2005). Microtubule-induced focal adhesion disassembly is mediated by dynamin and focal adhesion kinase. Nat. Cell Biol. *7*, 581–590.

Ezratty, E.J., Bertaux, C., Marcantonio, E.E., and Gundersen, G.G. (2009). Clathrin mediates integrin endocytosis for focal adhesion disassembly in migrating cells. J. Cell Biol. *187*, 733–747.

Fabbri, M., Di Meglio, S., Gagliani, M.C., Consonni, E., Molteni, R., Bender, J.R., Tacchetti, C., and Pardi, R. (2005). Dynamic partitioning into lipid rafts controls the endo-exocytic cycle of the αL/β 2 integrin, LFA-1, during leukocyte chemotaxis. Mol. Biol. Cell *16*, 5793–5803.

Fan, H. (2015). The role of Na^+/H^+ exchanger isoform 5 (NHE5) in glioma. MSc thesis (Vancouver, Canada: Univeristy of British Columbia).

Fan, S.H.-Y., Numata, Y., and Numata, M. (2016). Endosomal Na^+/H^+ exchanger NHE5 influences MET recycling and cell migration. Mol. Biol. Cell *27*, 702–715.

Fang, Z., Takizawa, N., Wilson, K.A., Smith, T.C., Delprato, A., Davidson, M.W., Lambright, D.G., and Luna, E.J. (2010). The membrane-associated protein, supervillin accelerates F-Actin-dependent rapid integrin recycling and cell motility. Traffic *11*, 782–799.

Fellmann, C., Hoffmann, T., Sridhar, V., Hopfgartner, B., Muhar, M., Roth, M., Lai, D.Y., Barbosa, I.A.M., Kwon, J.S., Guan, Y., et al. (2013). An optimized microRNA backbone for effective single-copy RNAi. Cell Rep. *5*, 1704–1713.

Forgac, M. (2007). Vacuolar ATPases: Rotary proton pumps in physiology and pathophysiology. Nat. Rev. Mol. Cell Biol. *8*, 917–929.

De Franceschi, N., Hamidi, H., Alanko, J., Sahgal, P., and Ivaska, J. (2015). Integrin traffic - the update. J. Cell Sci. *128*, 1–14.

Furtak, V., Hatcher, F., and Ochieng, J. (2001). Galectin-3 mediates the endocytosis of β1 integrins by breast carcinoma cells. Biochem. Biophys. Res. Commun. *289*, 845–850.

Fuse, A., Furuya, N., Kakuta, S., Inose, A., Sato, M., Koike, M., Saiki, S., and Hattori, N. (2015). Vps29-Vps35 intermediate of retromer is stable and may be involved in the retromer complex assembly process. FEBS Lett. *589*, 1430–1436.

Fuster, D.G., and Alexander, R.T. (2014). Traditional and emerging roles for the SLC9 Na^+/H^+ exchangers. Pflugers Arch. *466*, 61–76.

Ganley, I.G., Espinosa, E., and Pfeffer, S.R. (2008). A syntaxin 10-SNARE complex distinguishes two distinct transport routes from endosomes to the trans-Golgi in human cells. J. Cell Biol. *180*, 159–172.

Giancotti, F.G., and Ruoslahti, E. (1999). Integrin signaling. Science *285*, 1028–1032.

Ginsberg, M.H. (2014). Integrin activation. BMB Rep. *47*, 655–659.

Goh, L.K., and Sorkin, A. (2013). Endocytosis of receptor tyrosine kinases. Cold Spring Harb. Perspect. Biol. *5*, a017459–a017459.

Gomez, T.S., and Billadeau, D.D. (2009). A FAM21-Containing WASH complex regulates retromer-dependent sorting. Dev. Cell *17*, 699–711.

Gomez Zubieta, D.M., Hamood, M.A., Beydoun, R., Pall, A.E., and Kondapalli, K.C. (2017). MicroRNA-135a regulates NHE9 to inhibit proliferation and migration of glioblastoma cells. Cell Commun. Signal. *15*, 1–12.

Gu, Z., Noss, E.H., Hsu, V.W., and Brenner, M.B. (2011). Integrins traffic rapidly via circular dorsal ruffles and macropinocytosis during stimulated cell migration. J. Cell Biol. *193*, 61–70.

Gumbiner, B.M. (1996). Cell adhesion: The molecular basis of tissue architecture and morphogenesis. Cell *84*, 345–357.

Guo, H., Lee, I., Kamar, M., Akiyama, S.K., and Pierce, M. (2002). Aberrant N-glycosylation of β1 integrin causes reduced α5β1 integrin clustering and stimulates cell migration. Cancer Res. 6837–6845.

Haft, C.R., de la Luz Sierra, M., Bafford, R., Lesniak, M.A., Barr, V.A., and Taylor, S.I. (2000). Human orthologs of yeast vacuolar protein sorting proteins Vps26, 29, and 35: Assembly into multimeric complexes. Mol. Biol. Cell *11*, 4105–4116.

Hara-Chikuma, M., Yang, B., Sonawane, N.D., Sasaki, S., Uchida, S., and Verkman, A.S. (2005). ClC-3 chloride channels facilitate endosomal acidification and chloride accumulation. J. Biol. Chem. *280*, 1241–1247.

Harding, C., Heuser, J., and Stahl, P. (1983). Receptor-mediated endocytosis of transferrin and of the transferrin receptor in rat reticulocytes recycling. J. Cell. Biol. *97*, 329–339.

Hay, J.C., Klumperman, J., Oorschot, V., Steegmaier, M., Kuo, C.S., and Scheller, R.H. (1998). Localization, dynamics, and protein interactions reveal distinct roles for ER and Golgi SNAREs. J Cell Biol *141*, 1489–1502.

Hisamitsu, T., Ben Ammar, Y., Nakamura, T.Y., and Wakabayashi, S. (2006). Dimerization is crucial for the function of the Na^+/H^+ exchanger NHE1. Biochemistry *45*, 13346–13355.

Homewood, C.A, Warhurst, D.C., Peters, W., and Baggaley, V.C. (1972). Lysosomes, pH and the anti-malarial action of chloroquine. Nature *235*, 50–52.

Hong, W.J., and Lev, S. (2014). Tethering the assembly of SNARE complexes. Trends Cell Biol. *24*, 35–43.

Howes, M.T., Kirkham, M., Riches, J., Cortese, K., Walser, P.J., Simpson, F., Hill, M.M., Jones, A., Lundmark, R., Lindsay, M.R., et al. (2010). Clathrin-independent carriers form a high capacity endocytic sorting system at the leading edge of migrating cells. J. Cell Biol. *190*, 675–691.

Huet-Calderwood, C., Rivera-Molina, F., Iwamoto, D. V., Kromann, E.B., Toomre, D., and Calderwood, D.A. (2017). Novel ecto-tagged integrins reveal their trafficking in live cells. Nat. Commun. *8*, 570.

Hunte, C., Screpanti, E., Venturi, M., Rimon, A., Padan, E., and Michel, H. (2005). Structure of a Na^+/H^+ antiporter and insights into mechanism of action and regulation by pH. Nature *435*, 1197–1202.

Hynes, R.O. (1987). Integrins: A family of cell surface receptors. Cell *48*, 549–554.

Hynes, R.O. (1992). Integrins: Versatility, modulation, and signaling in cell adhesion. Cell *69*, 11–25.

Hynes, R.O. (2002). Integrins: Bidirectional, allosteric signaling machines. Cell *110*, 673–687.

Ilić, D., Furuta, Y., Kanazawa, S., Takeda, N., Sobue, K., Nakatsuji, N., Nomura, S., Fujimoto, J., Okada, M., and Yamamoto, T. (1995). Reduced cell motility and enhanced focal adhesion contact formation in cells from FAK-deficient mice. Nature *377*, 539–544.

Isaji, T., Sato, Y., Zhao, Y., Miyoshi, E., Wada, Y., Taniguchi, N., and Gu, J. (2006). N-glycosylation of the β-propeller domain of the integrin α5 subunit is essential for α5β1 heterodimerization, expression on the cell surface, and its biological function. J. Biol. Chem. *281*, 33258–33267.

Isaji, T., Sato, Y., Fukuda, T., and Gu, J. (2009). N-glycosylation of the I-like domain of β1 integrin is essential for β1 integrin expression and biological function. Identification of the minimal N-glycosylation requirement for α5β1. J. Biol. Chem. *284*, 12207–12216.

Isaji, T., Im, S., Gu, W., Wang, Y., Hang, Q., Lu, J., Fukuda, T., Hashii, N., Takakura, D., Kawasaki, N., et al. (2014). An oncogenic protein Golgi phosphoprotein 3 up-regulates cell migration via sialylation. J. Biol. Chem. *289*, 20694–20705.

Janik, M.E., Lityńska, A., and Vereecken, P. (2010). Cell migration - The role of integrin glycosylation. Biochim. Biophys. Acta - Gen. Subj. *1800*, 545–555.

Jinadasa, T., Szabó, E.Z., Numata, M., and Orlowski, J. (2014). Activation of AMP-activated protein kinase regulates hippocampal neuronal pH by recruiting Na^+/H^+ exchanger NHE5 to the cell surface. J. Biol. Chem. *289*, 20879–20897.

Johannes, L., and Popoff, V. (2008). Tracing the retrograde route in protein trafficking. Cell *135*, 1175–1187.

Johnson, L.S., Dunn, K.W., Pytowski, B., and McGraw, T.E. (1993). Endosome acidification and receptor trafficking: Bafilomycin A1 slows receptor externalization by a mechanism involving the receptor's internalization motif. Mol. Biol. Cell *4*, 1251–1266.

Kagami, T., Chen, S., Memar, P., Choi, M., Foster, L.J., and Numata, M. (2008). Identification and biochemical characterization of the SLC9A7 interactome. Mol. Membr. Biol. *25*, 436–447.

Kaushik, S., Ravi, A., Hameed, F.M., and Low, B.C. (2014). Concerted modulation of paxillin dynamics at focal adhesions by deleted in liver cancer-1 and focal adhesion kinase during early cell spreading. Cytoskeleton *71*, 677–694.

Kawasaki-Nishi, S., Nishi, T., and Forgac, M. (2001a). Arg-735 of the 100-kDa subunit a of the yeast V-ATPase is essential for proton translocation. Proc. Natl. Acad. Sci. U. S. A. *98*, 12397–12402.

Kawasaki-Nishi, S., Nishi, T., and Forgac, M. (2001b). Yeast V-ATPase complexes containing different isoforms of the 100-kDa a-subunit differ in coupling efficiency and in vivo dissociation. J. Biol. Chem. *276*, 17941–17948.

Kharitidi, D., Apaja, P.M., Manteghi, S., Suzuki, K., Malitskaya, E., Roldan, A., Gingras, M.-C.C., Takagi, J., Lukacs, G.L., and Pause, A. (2015). Interplay of endosomal pH and ligand occupancy in integrin α5β1 ubiquitination, endocytic sorting, and cell migration. Cell Rep. *13*, 599–609.

Kim, J.H., Johannes, L., Goud, B., Antony, C., Lingwood, C.A, Daneman, R., and Grinstein, S. (1998). Noninvasive measurement of the pH of the endoplasmic reticulum at rest and during calcium release. Proc. Natl. Acad. Sci. U. S. A. *95*, 2997–3002.

Kinoshita, K., Waritani, T., Noto, M., Takizawa, K., Minemoto, Y., Nishikawa, Y., and Ohkuma, S. (1996). Bafilomycin A1 induces apoptosis in PC12 cells independently of intracellular pH. FEBS Lett. *398*, 61–66.

Kirkham, M., Fujita, A., Chadda, R., Nixon, S.J., Kurzchalia, T. V., Sharma, D.K., Pagano, R.E., Hancock, J.F., Mayor, S., and Parton, R.G. (2005). Ultrastructural identification of uncoated caveolin-independent early endocytic vehicles. J. Cell Biol. *168*, 465–476.

Kitazume, S. (2014). ST6 beta-galactoside alpha-2,6-sialyltranferase 1 (ST6GAL1). In Handbook of Glycosyltransferases and Related Genes, (Tokyo: Springer Japan), pp. 693–703.

Klanke, C. A, Su, Y.R., Callen, D.F., Wang, Z., Meneton, P., Baird, N., Kandasamy, R.A, Orlowski, J., Otterud, B.E., and Leppert, M. (1995). Molecular cloning and physical and genetic mapping of a novel human Na^+/H^+ exchanger (NHE5/SLC9A5) to chromosome 16q22.1. Genomics *25*, 615–622.

Klock, H.E., and Lesley, S.A. (2009). The polymerase incomplete primer extension (PIPE) method applied to high-throughput cloning and site-directed mutagenesis. Methods Mol. Biol. *498*, 91–103.

Kobayashi, H., and Fukuda, M. (2013). Arf6 , Rab11, and transferrin receptor define distinct populations of recycling endosomes. 10–13.

Kondapalli, K.C., Llongueras, J.P., Capilla-Gonzalez, V., Prasad, H., Hack, A., Smith, C., Guerrero-Cazares, H., Quinones-Hinojosa, A., and Rao, R. (2015). A leak pathway for luminal protons in endosomes drives oncogenic signalling in glioblastoma. Nat Commun *6*, 6289.

Kowarz, E., Löscher, D., and Marschalek, R. (2015). Optimized sleeping beauty transposons rapidly generate stable transgenic cell lines. Biotechnol. J. *10*, 647–653.

Lakadamyali, M., Rust, M.J., and Zhuang, X. (2006). Ligands for clathrin-mediated endocytosis are differentially sorted into distinct populations of early endosomes. Cell *124*, 997–1009.

Lakshminarayan, R., Wunder, C., Becken, U., Howes, M.T., Benzing, C., Arumugam, S., Sales, S., Ariotti, N., Chambon, V., Lamaze, C., et al. (2014). Galectin-3 drives glycosphingolipid-dependent biogenesis of clathrin-independent carriers. Nat. Cell Biol. *16*, 592–603.

Lauffenburger, D.A., and Horwitz, A.F. (1996). Cell migration: A physically integrated molecular process. Cell *84*, 359–369.

Lebbink, R.J., Lowe, M., Chan, T., Khine, H., Wang, X., and McManus, M.T. (2011). Polymerase II promoter strength determines efficacy of microrna adapted shRNAs. PLoS One *6*.

Lee, J.O., Bankston, L.A., Arnaout, M.A., and Liddington, R.C. (1995). Two conformations of the integrin A-domain (I-domain): A pathway for activation? Structure *3*, 1333–1340.

Lee, M., Park, J.-J., and Lee, Y.-S. (2010a). Adhesion of ST6Gal I-mediated human colon cancer cells to fibronectin contributes to cell survival by integrin β1-mediated paxillin and AKT activation. Oncol. Rep. *23*, 757–761.

Lee, M., Lee, H.J., Seo, W.D., Park, K.H., and Lee, Y.S. (2010b). Sialylation of integrin β1 is involved in radiation-induced adhesion and migration in human colon cancer cells. Int. J. Radiat. Oncol. Biol. Phys. *76*, 1528–1536.

Leonard, D., Hayakawa, A., Lawe, D., Lambright, D., Bellve, K.D., Standley, C., Lifshitz, L.M., Fogarty, K.E., and Corvera, S. (2008). Sorting of EGF and transferrin at the plasma membrane and by cargo-specific signaling to EEA1-enriched endosomes. J. Cell Sci. *121*, 3445–3458.

Li, J., Su, Y., Xia, W., Qin, Y., Humphries, M.J., Vestweber, D., Cabañas, C., Lu, C., and Springer, T.A. (2017). Conformational equilibria and intrinsic affinities define integrin activation. EMBO J. *36*, 629–645.

Lippincott-Schwartz, J., Yuan, L.C., Bonifacino, J.S., and Klausner, R.D. (1989). Rapid redistribution of Golgi proteins into the ER in cells treated with brefeldin A: Evidence for membrane cycling from Golgi to ER. Cell *56*, 801–813.

Lis, H., and Sharon, N. (1998). Lectins: Carbohydrate-specific proteins that mediate cellular recognition. Chem. Rev. *98*, 637–674.

Liu, H., and Naismith, J.H. (2008). An efficient one-step site-directed deletion, insertion, single and multiple-site plasmid mutagenesis protocol. BMC Biotechnol. *8*, 91.

Liu, L., Liao, H., Castle, A., Zhang, J., Casanova, J., Szabo, G., and Castle, D. (2005). SCAMP2 interacts with Arf6 and phospholipase D1 and links their function to exocytotic fusion pore formation in PC12 cells. Mol. Biol. Cell *16*, 4463–4472.

Liu, Y., Pan, D., Bellis, S.L., and Song, Y. (2008). Effect of altered glycosylation on the structure of the I-like domain of β1 integrin: A molecular dynamics study. Proteins Struct. Funct. Bioinforma. *73*, 989–1000.

Lobert, V.H., Brech, A., Pedersen, N.M., Wesche, J., Oppelt, A., Malerød, L., Stenmark Harald, H., Stenmark, H., and Stenmark Harald, H. (2010). Ubiquitination of α5β1 integrin controls fibroblast migration through lysosomal degradation of fibronectin-integrin complexes. Dev. Cell *19*, 148–159.

Lu, L., and Hong, W. (2014). From endosomes to the trans-Golgi network. Semin. Cell Dev. Biol. *31*, 30–39.

Lu, M., Sautin, Y.Y., Holliday, L.S., and Gluck, S.L. (2004). The glycolytic enzyme aldolase mediates assembly, expression, and activity of vacuolar H^+-ATPase. J. Biol. Chem. *279*, 8732–8739.

Macia, E., Ehrlich, M., Massol, R., Boucrot, E., Brunner, C., and Kirchhausen, T. (2006). Dynasore, a cell-permeable inhibitor of dynamin. Dev. Cell *10*, 839–850.

Maeda, Y., Ide, T., Koike, M., Uchiyama, Y., and Kinoshita, T. (2008). GPHR is a novel anion channel critical for acidification and functions of the Golgi apparatus. Nat. Cell Biol. *10*, 1135–1145.

Malek-Hedayat, S., and Rome, L.H. (1992). Expression of multiple integrins and extracellular matrix components by C6 glioma cells. J. Neurosci. Res. *31*, 470–478.

Mallard, F., Tang, B.L., Galli, T., Tenza, D., Saint-Pol, A., Yue, X., Antony, C., Hong, W., Goud, B., and Johannes, L. (2002). Early/recycling endosomes-to-TGN transport involves two SNARE complexes and a Rab6 isoform. J. Cell Biol. *156*, 653–664.

Mammoto, A., Mammoto, T., and Ingber, D.E. (2012). Mechanosensitive mechanisms in transcriptional regulation. J. Cell Sci. *125*, 3061–3073.

Marshansky, V., and Futai, M. (2008). The V-type H^+-ATPase in vesicular trafficking: targeting, regulation and function. Curr. Opin. Cell Biol. *20*, 415–426.

Marsico, G., Russo, L., Quondamatteo, F., and Pandit, A. (2018). Glycosylation and integrin regulation in cancer. Trends in Cancer *4*, 537–552.

Maxfield, F.R., and McGraw, T.E. (2004). Endocytic recycling. Nat. Rev. Mol. Cell Biol. *5*, 121–132.

Mayor, S., and Pagano, R.E. (2007). Pathways of clathrin-independent endocytosis. Nat. Rev. Mol. Cell Biol. *8*, 603–612.

Mayor, S., Presley, J.F., and Maxfield, F.R. (1993). Sorting of membrane-components from endosomes and subsequent recycling to the cell-surface occurs by a bulk flow process. J. Cell Biol. *121*, 1257–1269.

McMahon, H.T., and Boucrot, E. (2011). Molecular mechanism and physiological functions of clathrin-mediated endocytosis. Nat. Rev. Mol. Cell Biol. *12*, 517–533.

McNally, K.E., Faulkner, R., Steinberg, F., Gallon, M., Ghai, R., Pim, D., Langton, P., Pearson, N., Danson, C.M., Nägele, H., et al. (2017). Retriever is a multiprotein complex for retromer-independent endosomal cargo recycling. Nat. Cell Biol. *19*, 1214–1225.

Mohammad-Panah, R., Harrison, R., Dhani, S., Ackerley, C., Huan, L.J., Wang, Y., and Bear, C.E. (2003). The chloride channel ClC-4 contributes to endosomal acidification and trafficking. J. Biol. Chem. *278*, 29267–29277.

Nader, G.P.F., Ezratty, E.J., and Gundersen, G.G. (2016). FAK, talin and PIPKIγ regulate endocytosed integrin activation to polarize focal adhesion assembly. Nat. Cell Biol. *18*, 491–503.

Nagae, M., Re, S., Mihara, E., Nogi, T., Sugita, Y., and Takagi, J. (2012). Crystal structure of α5β1 integrin ectodomain: atomic details of the fibronectin receptor. J. Cell Biol. *197*, 131–140.

Nguyen, O.N.P., Grimm, C., Schneider, L.S., Chao, Y.K., Atzberger, C., Bartel, K., Watermann, A., Ulrich, M., Mayr, D., Wahl-Schott, C., et al. (2017). Two-pore channel function is crucial for the migration of invasive cancer cells. Cancer Res. *77*, 1427–1438.

Nilsson, T., Pypaert, M., Hoe, M.H., Slusarewicz, P., Berger, E.G., and Warren, G. (1993). Overlapping distribution of two glycosyltransferases in the Golgi apparatus of HeLa cells. J. Cell Biol. *120*, 5–13.

Nishi, T., and Forgac, M. (2002). The vacuolar (H^+)-ATPases - Nature's most versatile proton pumps. Nat. Rev. Mol. Cell Biol. *3*, 94–103.

Onishi, I., Lin, P.J.C., Diering, G.H., Williams, W.P., and Numata, M. (2007). RACK1 associates with NHE5 in focal adhesions and positively regulates the transporter activity. Cell. Signal. *19*, 194–203.

Orlowski, J., and Grinstein, S. (2004). Diversity of the mammalian sodium/proton exchanger SLC9 gene family. Pflugers Arch. *447*, 549–565.

Orlowski, J., and Grinstein, S. (2011). Na^+/H^+ exchangers. Compr. Physiol. *1*, 2083–2100.

Padan, E., Kozachkov, L., Herz, K., and Rimon, A. (2009). NhaA crystal structure: functional-structural insights. J. Exp. Biol. *212*, 1593–1603.

Park, J.G., Kahn, J.N., Tumer, N.E., and Pang, Y.-P. (2012). Chemical structure of Retro-2, a compound that protects cells against ribosome-inactivating proteins. Sci. Rep. *2*, 631.

Paul, N.R., Jacquemet, G., and Caswell, P.T. (2015). Endocytic trafficking of integrins in cell migration. Curr. Biol. *25*, R1092-105.

Picollo, A., and Pusch, M. (2005). Chloride/proton antiporter activity of mammalian CLC proteins ClC-4 and ClC-5. Nature *436*, 420–423.

Pocheć, E., Bubka, M., Rydlewska, M., Janik, M., Pokrywka, M., and Lityńska, A. (2015). Aberrant glycosylation of αVβ3 integrin is associated with melanoma progression. Anticancer Res. *35*, 2093–2103.

van der Poel, S., Wolthoorn, J., van den Heuvel, D., Egmond, M., Groux-Degroote, S., Neumann, S., Gerritsen, H., van Meer, G., and Sprong, H. (2011). Hyperacidification of trans-Golgi network and endo/lysosomes in melanocytes by glucosylceramide-dependent V-ATPase activity. Traffic *12*, 1634–1647.

Powelka, A.M., Sun, J., Li, J., Gao, M., Shaw, L.M., Sonnenberg, A., and Hsu, V.W. (2004). Stimulation-dependent recycling of integrin β1 regulated by Arf6 and Rab11. Traffic *5*, 20–36.

del Pozo, M.A., Balasubramanian, N., Alderson, N.B., Kiosses, W.B., Grande-García, A., Anderson, R.G.W., and Schwartz, M.A. (2005). Phospho-caveolin-1 mediates integrin-regulated membrane domain internalization. Nat. Cell Biol. *7*, 901–908.

Priya, A., Kalaidzidis, I. V., Kalaidzidis, Y., Lambright, D., and Datta, S. (2015). Molecular insights into Rab7-mediated endosomal recruitment of core Retromer: Deciphering the role of Vps26 and Vps35. Traffic *16*, 68–84.

Radhakrishna, H., and Donaldson, J.G. (1997). ADP-ribosylation factor 6 regulates a novel plasma membrane recycling pathway. J. Cell Biol. *139*, 49–61.

Raley-Susman, K.M., Cragoe, E.J., Sapolsky, R.M., and Kopito, R.R. (1991). Regulation of intracellular pH in cultured hippocampal neurons by an amiloride-insensitive Na^+/H^+ exchanger. J. Biol. Chem. *266*, 2739–2745.

Ratcliffe, C.D.H., Sahgal, P., Parachoniak, C.A., Ivaska, J., and Park, M. (2016). Regulation of cell migration and β1 integrin trafficking by the endosomal adaptor GGA3. Traffic *17*, 670–688.

Ridley, A.J., Schwartz, M. a, Burridge, K., Firtel, R. a, Ginsberg, M.H., Borisy, G., Parsons, J.T., and Horwitz, A.R. (2003). Cell migration: integrating signals from front to back. Science *302*, 1704–1709.

Riggs, K.A., Hasan, N., Humphrey, D., Raleigh, C., Nevitt, C., Corbin, D., and Hu, C. (2012). Regulation of integrin endocytic recycling and chemotactic cell migration by syntaxin 6 and VAMP3 interaction. J. Cell Sci. *125*, 3827–3839.

Roberts, M., Barry, S., Woods, A., Van der Sluijs, P., and Norman, J. (2001). PDGF-regulated rab4-dependent recycling of αvβ3 integrin from early endosomes is necessary for cell adhesion and spreading. Curr. Biol. *11*, 1392–1402.

Roberts, M.S., Woods, A.J., Dale, T.C., Van Der Sluijs, P., and Norman, J.C. (2004). Protein kinase B/Akt acts via glycogen synthase kinase 3 to regulate recycling of αvβ3 and α5β1 integrins. Mol. Cell. Biol. *24*, 1505–1515.

Roepstorff, K., Grandal, M.V., Henriksen, L., Knudsen, S.L.J., Lerdrup, M., Grøvdal, L., Willumsen, B.M., and Van Deurs, B. (2009). Differential effects of EGFR ligands on endocytic sorting of the receptor. Traffic *10*, 1115–1127.

Sabharanjak, S., Sharma, P., Parton, R.G., and Mayor, S. (2002). GPI-anchored proteins are delivered to recycling endosomes via a distinct cdc42-regulated clathrin-independent pinocytic pathway. Dev. Cell *2*, 411–423.

Saint-Pol, A., Yélamos, B., Amessou, M., Mills, I.G., Dugast, M., Tenza, D., Schu, P., Antony, C., McMahon, H.T., Lamaze, C., et al. (2004). Clathrin adaptor epsinR is required for retrograde sorting on early endosomal membranes. Dev. Cell *6*, 525–538.

Sautin, Y.Y., Lu, M., Gaugler, A., Zhang, L., and Gluck, S.L. (2005). Phosphatidylinositol 3-kinase-mediated effects of glucose on vacuolar H^+-ATPase assembly, translocation, and acidification of intracellular compartments in renal epithelial cells. Mol. Cell. Biol. *25*, 575–589.

Schultz, M.J., Swindall, A.F., and Bellis, S.L. (2012). Regulation of the metastatic cell phenotype by sialylated glycans. Cancer Metastasis Rev. *31*, 501–518.

Scott, C.C., and Gruenberg, J. (2011). Ion flux and the function of endosomes and lysosomes: pH is just the start: The flux of ions across endosomal membranes influences endosome function not only through regulation of the luminal pH. BioEssays *33*, 103–110.

Seales, E.C., Jurado, G.A., Singhal, A., and Bellis, S.L. (2003). Ras oncogene directs expression of a differentially sialylated, functionally altered β1 integrin. Oncogene *22*, 7137–7145.

Seales, E.C., Jurado, G.A., Brunson, B.A., Wakefield, J.K., Frost, A.R., and Bellis, S.L. (2005a). Hypersialylation of beta1 integrins, observed in colon adenocarcinoma, may contribute to cancer progression by up-regulating cell motility. Cancer Res. *65*, 4645–4652.

Seales, E.C., Shaikh, F.M., Woodard-Grice, A. V., Aggarwal, P., McBrayer, A.C., Hennessy, K.M., and Bellis, S.L. (2005b). A protein kinase C/Ras/ERK signaling pathway activates myeloid fibronectin receptors by altering β1 integrin sialylation. J. Biol. Chem. *280*, 37610–37615.

Semel, A.C., Seales, E.C., Singhal, A., Eklund, E.A., Colley, K.J., and Bellis, S.L. (2002). Hyposialylation of integrins stimulates the activity of myeloid fibronectin receptors. J. Biol. Chem. *277*, 32830–32836.

Seol, J.H., Shevchenko, A., Shevchenko, A., and Deshaies, R.J. (2001). Skp1 forms multiple protein complexes, including RAVE, a regulator of V-ATPase assembly. Nat. Cell Biol. *3*, 384–391.

Shafaq-Zadah, M., Gomes-Santos, C.S., Bardin, S., Maiuri, P., Maurin, M., Iranzo, J., Gautreau, A., Lamaze, C., Caswell, P., Goud, B., et al. (2016). Persistent cell migration and adhesion rely on retrograde transport of β1 integrin. Nat. Cell Biol. *18*, 54–64.

Shi, G. (2011). Development of functional proteomics approaches for studying retrograde transport. PhD thesis (Paris, France: École normale supérieure de Paris).

Shi, F., and Sottile, J. (2008). Caveolin-1-dependent β1 integrin endocytosis is a critical regulator of fibronectin turnover. J. Cell Sci. *121*, 2360–2371.

Shi, G., Azoulay, M., Dingli, F., Lamaze, C., Loew, D., Florent, J.C., and Johannes, L. (2012). SNAP-tag based proteomics approach for the study of the retrograde route. Traffic *13*, 914–925.

Shi, H., Rojas, R., Bonifacino, J.S., and Hurley, J.H. (2006). The retromer subunit Vps26 has an arrestin fold and binds Vps35 through its C-terminal domain. Nat. Struct. Mol. Biol. *13*, 540–548.

Smardon, A.M., Tarsio, M., and Kane, P.M. (2002). The RAVE complex is essential for stable assembly of the yeast V-ATpase. J. Biol. Chem. *277*, 13831–13839.

Snider, M.D., and Rogers, O.C. (1985). Intracellular movement of cell surface receptors after endocytosis: Resialylation of asialo-transferrin receptor in human erythroleukemia cells. J. Cell Biol. *100*, 826–834.

Söllner, T., Whiteheart, S.W., Brunner, M., Erdjument-Bromage, H., Geromanos, S., Tempst, P., and Rothman, J.E. (1993). SNAP receptors implicated in vesicle targeting and fusion. Nature *362*, 318–324.

Stechmann, B., Bai, S.-K.K., Gobbo, E., Lopez, R., Merer, G., Pinchard, S., Panigai, L., Tenza, D., Raposo, G., Beaumelle, B., et al. (2010). Inhibition of retrograde transport protects mice from lethal ricin challenge. Cell *141*, 231–242.

Steinberg, F., Heesom, K.J., Bass, M.D., and Cullen, P.J. (2012). SNX17 protects integrins from degradation by sorting between lysosomal and recycling pathways. J. Cell Biol. *197*, 219–230.

Steinberg, F., Gallon, M., Winfield, M., Thomas, E.C., Bell, A.J., Heesom, K.J., Tavaré, J.M., and Cullen, P.J. (2013). A global analysis of SNX27–retromer assembly and cargo specificity reveals a function in glucose and metal ion transport. Nat. Cell Biol. *15*, 461–471.

Suzuki, O., Abe, M., and Hashimoto, Y. (2015). Sialylation and glycosylation modulate cell adhesion and invasion to extracellular matrix in human malignant lymphoma: Dependency on integrin and the Rho GTPase family. Int. J. Oncol. *47*, 2091–2099.

Szabó, E.Z., Numata, M., Lukashova, V., Iannuzzi, P., and Orlowski, J. (2005). β-Arrestins bind and decrease cell-surface abundance of the Na^+/H^+ exchanger NHE5 isoform. Proc. Natl. Acad. Sci. U. S. A. *102*, 2790–2795.

Szászi, K., Paulsen, A., Szabó, E.Z., Numata, M., Grinstein, S., and Orlowski, J. (2002). Clathrin-mediated endocytosis and recycling of the neuron-specific Na^+/H^+ exchanger NHE5 isoform: Regulation by phosphatidylinositol 3'-kinase and the actin cytoskeleton. J. Biol. Chem. *277*, 42623–42632.

Tagawa, A., Mezzacasa, A., Hayer, A., Longatti, A., Pelkmans, L., and Helenius, A. (2005). Assembly and trafficking of caveolar domains in the cell: Caveolae as stable, cargo-triggered, vesicular transporters. J. Cell Biol. *170*, 769–779.

Tai, G., Lu, L., Wang, T.L., Tang, B.L., Goud, B., Johannes, L., and Hong, W. (2004). Participation of the syntaxin 5/Ykt6/GS28/GS15 SNARE complex in transport from the early/recycling endosome to the trans-Golgi network. Mol. Biol. Cell *15*, 4011–4022.

Takagi, J., Petre, B.M., Walz, T., and Springer, T.A. (2002). Global conformational rearrangements in integrin extracellular domains in outside-in and inside-out signaling. Cell *110*, 599–611.

Takashima, S., and Tsuji, S. (2011). Functional diversity of mammalian sialyltransferases. Trends Glycosci. Glycotechnol. *23*, 178–193.

Taniguchi, Y., Li, S., Takizawa, M., Oonishi, E., Toga, J., Yagi, E., and Sekiguchi, K. (2017). Probing the acidic residue within the integrin binding site of laminin-511 that interacts with the metal ion-dependent adhesion site of α6β1 integrin. Biochem. Biophys. Res. Commun. *487*, 525–531.

Tarentino, A.L., and Plummer Jr, T.H. (1993). Deglycosylation of asparagine-linked glycans by PNGase F. Trends Glycosci. Glycotechnol. *5*, 163–170.

Teter, K., Chandy, G., Quiñones, B., Pereyra, K., Machen, T., and Moore, H.P.H. (1998). Cellubrevin-targeted fluorescence uncovers heterogeneity in the recycling endosomes. J. Biol. Chem. *273*, 19625–19633.

Tseng, H.Y., Thorausch, N., Ziegler, T., Meves, A., Fässler, R., and Böttcher, R.T. (2014). Sorting nexin 31 binds multiple β integrin cytoplasmic domains and regulates β1 integrin surface levels and stability. J. Mol. Biol. *426*, 3180–3194.

Tycko, B., and Maxfield, F.R. (1982). Rapid acidification of endocytic vesicles containing α2-macroglobulin. Cell *28*, 643–651.

Ullrich, O., Reinsch, S., Urbé, S., Zerial, M., and Parton, R.G. (1996). Rab11 regulates recycling through the pericentriolar recycling endosome. J. Cell Biol. *135*, 913–924.

Upla, P., Marjomäki, V., Kankaanpää, P., Ivaska, J., Hyypiä, T., van der Goot, F.G., and Heino, J. (2004). Clustering induces a lateral redistribution of α2β1 integrin from membrane rafts to caveolae and subsequent protein kinase C-dependent internalization. Mol. Biol. Cell *15*, 625–636.

Wakabayashi, S., Shigekawa, M., and Pouyssegur, J. (1997). Molecular physiology of vertebrate Na^+/H^+ exchangers. Physiol. Rev. *77*, 51–74.

Wang, P.H., Lee, W.L., Lee, Y.R., Juang, C.M., Chen, Y.J., Chao, H.T., Tsai, Y.C., and Yuan, C.C. (2003). Enhanced expression of α2,6-sialyltransferase, ST6Gal I in cervical squamous cell carcinoma. Gynecol. Oncol. *89*, 395–401.

Wei, Y., Yang, X., Liu, Q., Wilkins, J.A., and Chapman, H.A. (1999). A role for caveolin and the urokinase receptor in integrin-mediated adhesion and signaling. J. Cell Biol. *144*, 1285–1294.

Wilcke, M., Johannes, L., Galli, T., Mayau, V., Goud, B., and Salamero, J. (2000). Rab11 regulates the compartmentalization of early endosomes required for efficient transport from early endosomes to the trans-Golgi network. J. Cell Biol. *151*, 1207–1220.

Wu, M.M., Grabe, M., Adams, S., Tsien, R.Y., Moore, H.P.H., and Machen, T.E. (2001). Mechanisms of pH regulation in the regulated secretory pathway. J. Biol. Chem. *276*, 33027–33035.

Xiong, J.-P., Stehle, T., Zhang, R., Joachimiak, A., Frech, M., Goodman, S.L., and Arnaout, M.A. (2002). Crystal structure of the extracellular segment of integrin αVβ3 in complex with an Arg-Gly-Asp ligand. Science *296*, 151–155.

Yamashiro, D.J., and Maxfield, F.R. (1987). Kinetics of endosome acidification in mutant and wild-type Chinese hamster ovary cells. J. Cell Biol. *105*, 2713–2721.

Yamashiro, D.J., Tycko, B., Fluss, S.R., and Maxfield, F.R. (1984). Segregation of transferrin to a mildly acidic (pH 6.5) para-Golgi compartment in the recycling pathway. Cell *37*, 789–800.

Yoshimura, M., Nishikawa, A., Ihara, Y., Taniguchi, S., and Taniguchi, N. (1995). Suppression of lung metastasis of B16 mouse melanoma by N-acetylglucosaminyltransferase III gene transfection. Proc. Natl. Acad. Sci. U. S. A. *92*, 8754–8758.

Yu, C., Law, J.B.K., Suryana, M., Low, H.Y., and Sheetz, M.P. (2011). Early integrin binding to Arg-Gly-Asp peptide activates actin polymerization and contractile movement that stimulates outward translocation. Proc. Natl. Acad. Sci. U. S. A. *108*, 20585–20590.

Yu, S., Fan, J., Liu, L., Zhang, L., Wang, S., and Zhang, J. (2013). Caveolin-1 up-regulates integrin α2,6-sialylation to promote integrin α5β1-dependent hepatocarcinoma cell adhesion. FEBS Lett. *587*, 782–787.

Zaidel-Bar, R., Ballestrem, C., Kam, Z., and Geiger, B. (2003). Early molecular events in the assembly of matrix adhesions at the leading edge of migrating cells. J. Cell Sci. *116*, 4605–4613.

Zhao, Y., Nakagawa, T., Itoh, S., Inamori, K.I., Isaji, T., Kariya, Y., Kondo, A., Miyoshi, E., Miyazaki, K., Kawasaki, N., et al. (2006). N-Acetylglucosaminyltransferase III antagonizes the effect of N-acetylglucosaminyltransferase V on α3β1 integrin-mediated cell migration. J. Biol. Chem. *281*, 32122–32130.

Zheng, M., Fang, H., and Hakomori, S.I. (1994). Functional role of N-glycosylation in α5β1 integrin receptor: De-N-glycosylation induces dissociation or altered association of α5 and β1 subunits and concomitant loss of fibronectin binding activity. J. Biol. Chem. *269*, 12325–12331.